Institut für Hydrologie, Albert-Ludwigs Universität Freiburg i. Br.

Application of electrical resistivity tomography (ERT) together with tracer data to identify hydrological process areas at a surface water / groundwater test site

St. Wilhelm, Black Forest Mountains, Germany

Kristof Michael Koch

Referent: PD Dr. Stefan Uhlenbrook

Koreferent: Dr. Jens Lange

Betreuer: Dipl. Hyd. Jochen Wenninger

Diplomarbeit unter Leitung von PD Dr. S. Uhlenbrook

Freiburg i. Br., August 2004

Contents

List of figures in the text

List of tables in the text

Contents of the appendix

Notations

a	[m]	electrode spacing
a.s.l.	[m]	above see level
A		current electrode
B		current electrode
DFG		Deutsche Forschungsgemeinschaft
E.C.	[µS/cm]	electrical conductivity
ERT		electrical resistivity tomography
GWMH		groundwater monitoring hole
HHQ	[$m^3 * s^{-1}$]	highest discharge recorded
HOF		Hortonian overland flow
I	[A]	current
IHF		Institute for Hydrology, Freiburg
min.		minutes
MHQ	[$m^3 * s^{-1}$]	mean highest discharge
MHq	[$l * s^{-1} * km^{-2}$]	mean flood yield
MQ	[$m^3 * s^{-1}$]	mean discharge
Mq	[$l * s^{-1} * km^{-2}$]	mean yield
MNQ	[$m^3 * s^{-1}$]	mean low flow discharge
MNq	[$l * s^{-1} * km^{-2}$]	mean low flow yield
na	[m]	multiple electrode spacing
NNQ	[$m^3 * s^{-1}$]	lowest discharge recorded
P	[mm/d]	precipitation
pH	[-]	value of pH
ρ	[Ωm]	resistivity
R	[Ωm]	resistivity
Res2Dinv		resistivity-2D-inversion programme
RMS	[%]	root-mean-squared
SOF		saturated overland flow
SSF		subsurface stormflow
V, U	[V]	voltage
ΔV	[V]	difference in voltage
x	[m]	distance

Summary

This work was supported by the German Research Foundation (DFG) project "Runoff generation processes and catchment modelling".

The research site is located in the Black Forest Mountains in Germany at 800 m elevation, where snow is an important form of precipitation, but rain is still decisive. Forest-covered steep slopes, which occupy three quarters of the catchment area, and strong Pleistocene influences, determine present hydrological processes to a high degree. Well-conductive boulder fields alternate with poorly conductive boulder clay as well as solifluction debris and moraine deposits. The latter three consist of a wide range of grain sizes and are well mixed by glacial transport.

Based on the importance of subsurface structures for hydrological processes, electrical resistivity tomography was applied to investigate the areas where these processes mostly take place. A total number of 111 measurements have been conducted using Wenner and dipole – dipole array with electrode spacing from half a meter to five meters. The two-dimensional images of electrical resistivity display the differences between subsurface zones in water content, water conductivity or changes in materials or material's grain sizes.

The poor resolution of the displayed image makes the interpretation of an ERT difficult, as colours and vague forms are recognizable, but are not detailed enough to be interpreted correctly. This can be compared to looking through frosted glass, where a grey silhouette might be a van or an elephant. It is the knowledge of the context which enables the interpreter to choose between the alternative associations. This simple image also illustrates the approach to the interpretation of the conducted electrical resistivity surveys. As precise information from drillings was not available, knowledge about the region's geology and morphology, the present understanding of hydrological processes and facts from hydrometric and environmental tracer data provided the background for the interpretation of ERT.

It was recognized that a more impervious layer is distributed all over the test site. In general, the thickness of this layer was previously underestimated and at some places reaches below the depth of the groundwater monitoring holes. Thus, a re-interpretation of the collected hydrometric data was necessary, as effects of a possible pressure wave that passes in deeper parts of the aquifer might be detected only marginally or not at all. Moreover, weaker parts of this layer could be identified as the possible flowpath supplying saturated areas. In line with the identification of poorly permeable structures an improved understanding of the behaviour of water flux under pressure within such structures was achieved.

ERT results further indicate that the stream channel is embedded in the more impervious layer. Comparison of electrical conductivity with silica values as well as hydrometric data from both the stream channel and from groundwater monitoring holes combine to further support the idea that the stream is hardly draining the aquifer at the research site. However, this contradicts the general perception described in any hillslope concept. In these concepts, the centre of water flux in mountainous regions is a persistently receiving stream channel.

The assumption of a perched stream implies greater importance of water transport in deeper and deep parts of the aquifer than previously thought. This hypothesis is supported by findings from the test site’s deeper layer where zones of assumed better transmissivity exist and are possibly connected with each other, perhaps forming a natural drainage network.

Keywords:

hydrological concept
piston flow
tracer
saturated area
electrical resistivity tomography
surface water – groundwater interface
hydrological process
natural drainage

Zusammenfassung

Die vorliegende Diplomarbeit wurde im Rahmen des DFG-Verbundprojektes „Abflussbildung und Einzugsgebietsmodellierung“ gefördert.

Die Versuchsfläche befindet sich im südlichen Schwarzwald etwa 20 km östlich von Freiburg i. Br. in einer Höhe von 800 m ü.NN. Ein bedeutender Teil des Niederschlags fällt als Schnee in dem zu drei vierteln bewaldeten Einzugsgebiet. Steile Hänge und der glaziale Ursprung des Gebietes bestimmen die hydrologischen Prozesse. Gut durchlässige Blockschutthalden finden sich im Wechsel mit schlecht durchlässigem Geschiebelehm, periglazialen Fließerden und Moränenmaterial.

Basierend auf der Bedeutung von unterirdischen Strukturen für Prozesse in der Hydrologie wird die elektrische Widerstands Tomographie (ERT) angewandt um Einblick in diese hydrologischen Prozessgebiete zu ermöglichen. Es wurden 111 Messungen mit den Methoden Wenner und Dipole – Dipole mit Abständen zwischen 0.5 und 5 m zwischen den einzelnen Elektroden ausgeführt. Die zwei-dimensionalen Abbilder der elektrischen Widerstände zeigen Unterschiede zwischen den verschiedenen Strukturen im Untergrund, sei es Wassergehalt, elektrische Leitfähigkeit des Wassers und / oder Wechsel in der Material Zusammensetzung und / oder veränderte Korngrößenanteile des gleichen Materials.

Schwierigkeiten bei der Interpretation von Tomographien liegen in der schlechten bildlichen Auflösung im Vergleich zur Photographie. Eine ERT ist vergleichbar mit dem Blick durch eine Milchglasscheibe. Zum Beispiel kann ein grauer Schemen zu erkennen sein, doch kann dieser entweder als grauer Transporter oder als Elefant interpretiert werden. Mit Hilfe der Kenntnis der Umwelt in welcher man sich befindet ist es möglich sich klar für eine der Alternativen zu entscheiden. Dieser einfache Vergleich erklärt die beschrittene Vorgehensweise in dieser Arbeit. Da eindeutige Erkenntnisse über Materialien des Untergrundes aus Bohrkernuntersuchungen nicht zu Verfügung standen, musste Wissen über den allgemeinen hydrologischen, geologischen und morphologischen Kontext, zur Interpretation der elektrischen Widerstandsbilder angewandt werden. Die Einbeziehung von natürlichen Tracer-Daten, vor allem

aus vorherigen Untersuchungen (WENNINGER 2002, SCHEIDLER 2002), lieferte notwendige Indizien bzw. Beweise für die aufgestellten Hypothesen.

So war es möglich zu zeigen, dass eine schlechter durchlässige Schicht über die gesamte Fläche des Testfeldes ausgebreitet ist, welche früher in ihrer Mächtigkeit unterschätzt wurde. Die neuen Erkenntnisse ermöglichten ein verbessertes Verständnis der gesammelten hydrometrischen Daten. Der perforierte Teil befand sich teilweise noch innerhalb des schlecht durchlässigen Horizontes, was die Beobachtung vermuteter Druckwellen im tieferen Aquiferbereich stark beeinflusst. Des Weiteren konnten Schwachstellen innerhalb dieser Schicht als wahrscheinlicher Zustromsweg von Grundwasser zu verschiedenen Sättigungsflächen identifiziert werden. Zusammen mit dem Wissen über die Ausdehnung von unterirdischen Strukturen konnte das Verständnis über das Verhalten von Wasserfluss unter Einfluss von Druck erweitert werden.

Zusätzlich liefert die ERT Hinweise, dass der örtliche Bachlauf in dieser kaum durchlässigen Schicht eingebettet ist und nur in schlechter Verbindung mit dem Aquifer ist. Dies widerspricht jedoch den gängigen Konzepten zur Hydrologie im Oberlauf von Einzugsgebieten, in welchen der Fluss als Vorfluter das Ende aller Fließwege beschreibt.

Als logische Konsequenz muss dem unterirdischen Transport von Wasser eine größere Bedeutung zukommen. Diese Hypothese wird durch die Entdeckung von teilweise miteinander verbundenen Zonen mit vermutlich höherer hydraulischer Leitfähigkeit unterstützt. Dies unterstützt die Vorstellung der Existenz eines natürlichen Drainage – Netzwerkes im Untergrund.

1 Introduction

Application of electrical resistivity tomography (ERT) to the field of hydrology is almost as old as the technique itself, due to the important influence of water on electrical resistivity of structures. However, recent development of this technique from one dimensional sounding to the recording of cross-sections via easy to use measuring devices in connection with improved data processing increased its usefulness for hydrological questions tremendously. The investigated area, the surface water / groundwater test site St. Wilhelm, Black Forest, Germany, two consecutive studies (WENNINGER 2002; SCHEIDLER 2002) have already been carried out. Their main focus was on possible occurrence of the piston flow effect and to identify the origin of water at saturated areas in particular during events. Reasoning was established on the basis of natural tracer data (deuterium, dissolved silica, and major anions and cations) and the dynamics in piezometric heads but with regards to the observed heterogeneity knowledge of subsurface structures was assumed insufficient to provide evidence for possible piston flow. In this study over one hundred electrical resistivity tomographies were conducted using dipole – dipole as well as Wenner array in combination with electrode spacing in the range of half a meter to five meters in order to increase understanding of the role of hydrological process areas such as interfaces between zones of different hydrological properties (stream channel – phreatic zone, phreatic zone – saturated areas, hillslope – valley bottom). The results from electrical resistivity data could be analysed with help of new and previously collected data on hydrometric and especially tracer data.

1.1 Objectives

Possible applications of electrical resistivity tomography (ERT) for hydrological research are examined.

The main focus of this study is to asses the valley bottom's filling in order to gain knowledge on specific subsurface structures, which are responsible for the observed hydrological processes, existing hydrologic landscape units and groundwater – surface water interaction (namely at saturated areas and the stream channel).

For the interpretation of electrical resistivity plots it is not possible to revert to geological borehole data from the test site as such. Instead, it is attempted to establish an alternative, process-orientated approach to minimize possible interpretations of electrical resistivity tomography. Thus, the discussion of results is based on a combination of general hydrological expertise, known geological background (genesis as well as structures found today) and in particular on tracer data (which give information about possible flowpaths, assumably related to subsurface structures visualised by ERT). In the framework of two previously conducted diploma theses, tracer and hydrometric data were collected on site. The idea of piston flow at the test site was established due to fast response in the groundwater monitoring holes and a high content of relatively old water in the regions streams during events. Assuming piston flow is only conceivable under very particular subsurface conditions. Through the use of electrical resistivity tomography it is attempted to verify existence and extent of subsurface structures which might enable piston flow.

Finally, the produced image of the valley bottom's subsurface is supposed to allow improved identification and understanding of hydrological process areas and their link among themselves as well as to the surface.

1.2 Perception of hydrologic processes

"The nature of the soil surface is the key factor in deciding how rainfall will infiltrate and move through the soil, i.e. whether water will move downwards or sideways. Surface soil hydraulic properties control the rate of entry (i.e. infiltration) but, if unimpeded vertically, incoming water will move through the regolith as percolation to reach the water table. More commonly, however, there is a reduction in the permeability in the upper soil horizons at various points because of the presence of more impervious soil layers. These deflect water laterally, either at the surface (as *infiltration excess (Hortonian) overland flow, HOF* (HORTON, 1933;

> 1945)) or subsurface (as *subsurface stormflow*, *SSF*, or *interflow*) (CHORLEY, 1978). This SSF can emerge at the surface as *return flow* and combine with precipitation falling on saturated soils to produce *saturation* (or *saturation-excess*) *overland flow*, *SOF*. This is also known as the Dunne mechanism (DUNNE and BLACK, 1970a,b)." (BONELL 2004a)

As illustrated by BONELL 2004a, properties of surface and subsurface structures are the key factors to explain distribution and dominance of specific hydrologic processes.
One of the objectives of this study is to evaluate whether subsurface conditions can provoke *piston flow*. In the following, *piston flow* describes the movement of water forced by a pressure gradient through uninterrupted saturated flowpaths. These pathways are confined to all sides by more impermeable structures (UHLENBROOK & LEIBUNDGUT, 1997), or by respectively stronger forces, as it will be outlined in the next paragraphs.

In general, like every matter, water moves due to the imbalance of forces, as described by Newton's equation of motion (VOGEL, 1995, p. 115; KOCH, personal communication, 2004). The forces taking effect on a fluid's movement are:

- Volume forces, i.e. forces attacking from outside, proportional to volume, respectively masses (e.g. gravity)
- Forces related to gradients of pressure
- Frictional forces

For instance water percolates when gravity exceeds the sum of all other forces, capillary rise is observed when adhesion and cohesion surpass gravity and a gradient of pressure between a stream channel and an aquifer create influent or effluent conditions. Other examples for the effect of the different forces are water table stagnation after a pressure gradient is balanced, which means that pressure equals gravity. Moreover, stagnation in pores, where pressure gradient might still exceed gravity but friction compensates this discrepancy between the two other forces and creates equilibrium. In this case, reducing frictional force (e.g. pores with greater diameter) would result in a rising water table until again a balance of forces is reached.

Consequently, different hydrological conditions produce a change in power of forces, as gravity can be regarded as constant whereas both gradient of pressure and frictional forces change. This may result in a modification of the relative significance of each flowpath to the total volume transported.
For example, under pressure certain flowpaths get available, while other forces were making them inefficient before. As a result, new pathways are activated and at the same time existing pathways may show increased capacity of water transport.
(compare roughly to a picture collapsible tube: more pressure → more tooth paste and no pressure → no tooth paste)

The forces above listed are rather easy to assess, as gravity can be assumed almost constant at a specific place in space and a gradient in pressure is well monitored by piezometers theoretically. However, in contrast, variation of frictional forces remain difficult to evaluate, as there can be large local variations in pore (macropore) diameter and other characteristics which can be regarded as key parameters to the value of frictional force. Thus the difficulty in correctly understanding subsurface fluxes is in truly understanding the nature of the subsurface. For example, in nature the existence of purely and permanently impervious structures can be doubted (except for solid bedrock) instead the interplay of forces determines a structure’s quality of fluxes. Accordingly, in this understanding of flux, it is domination of frictional forces which confines the water’s pathways.

2 Study area

2.1 Location

The valley bottom research site “Hintere Matte” is part of the meso-scale (40km²) Brugga catchment, located 20 km south-west of Freiburg (48° N, 7°51’ E) in the southern Black Forest in Germany. Elevation ranges between 1493 m a.s.l. at Feldberg and 434 m a.s.l. at gauge Oberried, the basin’s outlet. The elevation averages 945 m a.s.l., the elevation range is 1059 m.

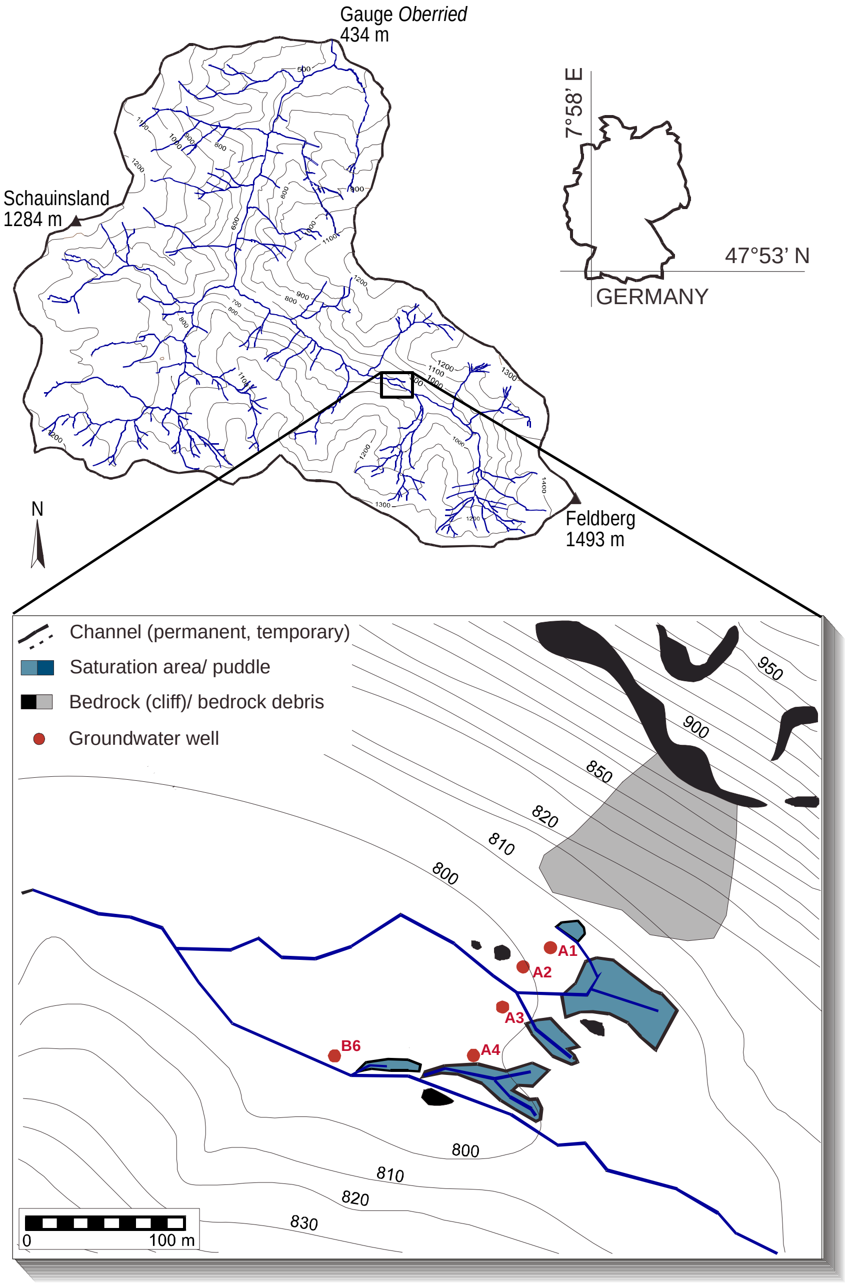

Figure 2.1: Geographical position of the research area.

2.2 Climate and hydrology

The southern Black Forest region is situated in temperate-clime, at the southern outskirts of the west wind zone.

Unsettled atmospheric conditions due to interacting hot sub – tropic and cold sub – polar air masses are common as in mid-latitudes in general. Thus precipitation is dominated by cyclonal weather systems, where prevailing west winds bear maritime influence on weather conditions. When the westerlies shift northward during summer, convective cells become the main factor in precipitation. (For a detailed description of the regional climate see REKLIP (1995)).

In general, precipitation is sufficient all over the year with maxima in May and December as displayed in the climatic chart (Figure 2.2). At 765 m a.s.l. the mean annual rainfall is 1750 mm. However, precipitation is highly dependent on the altitude as described in UHLENBROOK (1999).

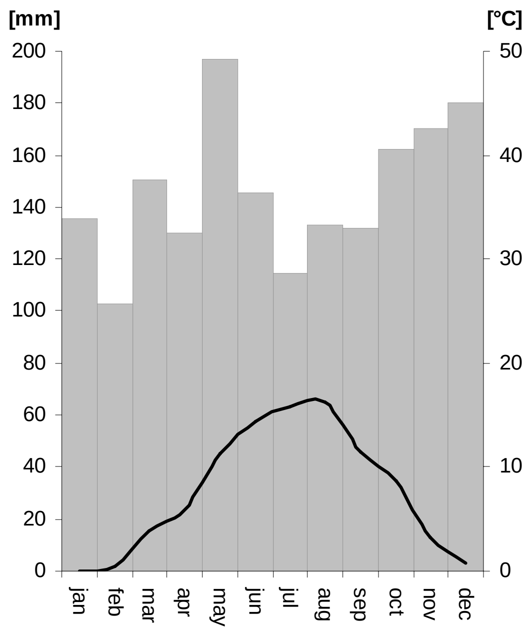

Figure 2.2: Climatic chart of *Katzensteig* meteorological station situated in the *Brugga* catchment at 765 m a.s.l. 1994 – 2004; precipitation is not corrected.

The temperature's annual average is 7.7 °C and varies from -15 °C to 25 °C (Katzensteig meteorological station, 1994 – 2004, IHF).

The runoff regime is nivo-pluvial, coherent with the influence of snowmelt on runoff generation (see peak in April Figure 2.3). The significance of snow is also shown in snow heights of 20 cm at 900 m a.s.l. throughout 85 to 95 days a year.

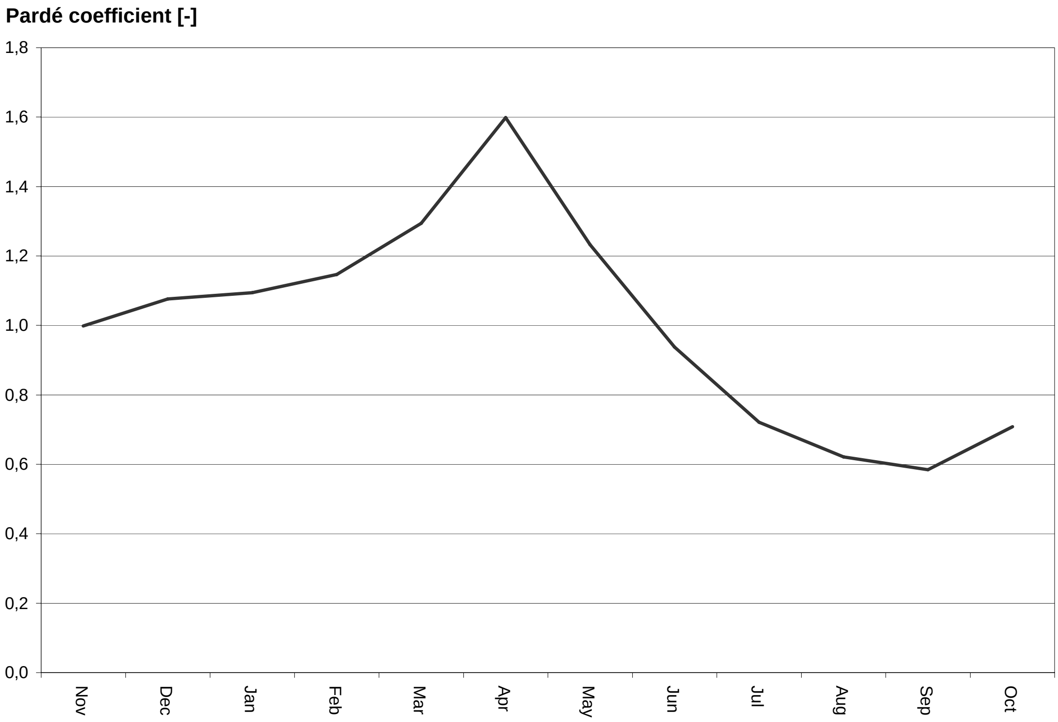

Figure 2.3: Runoff regime of the Brugga River (1934 – 1994).

Characteristic water discharges at different hydrologic conditions are listed in (Table 2.1). In case of the Brugga basin the significant difference between mean discharge (1.56 m³/s) and mean highest discharge (17.6 m³/s) hints at an important influence of fast runoff components (UHLENBROOK 1999) on discharge. Rainfall is relatively persistent throughout the year (Figure 2.2) and thus cannot be the source of those variations.

Table 2.1: Characteristic water discharges of the Brugga River (1934-1979) (UHLENBROOK 1999).

		Brugga Basin, 40 km²
HHQ	(highest discharge recorded)	51.0 [m^3 s^{-1}] (23.11.1944)
MHQ	(mean highest discharge)	17.6 [m^3 s^{-1}]
MQ	(mean discharge)	1.56 [m^3 s^{-1}]
MNQ	(mean low flow discharge)	0.36 [m^3 s^{-1}]
NNQ	(lowest discharge recorded)	0.10 [m^3 s^{-1}] (03.09.1964)
MHq	(mean flood yield)	442 [l s^{-1} km^{-2}]
Mq	(mean yield)	39.1 [l s^{-1} km^{-2}]
MNq	(mean low flow yield)	9.03 [l s^{-1} km^{-2}]

2.3 Topography, morphology and geology

Glacial influence is evident all over the basin. Especially the U-shaped valley of *St. Wilhelm* (Figure 2.4) shows several characteristic morphologic forms such as cirques and moraines. Alluvial fans and slide-rocks partly superpose the shallow soils at the valley bottoms. Three morphologic units can be distinguished in the catchment (Figure 2.4):

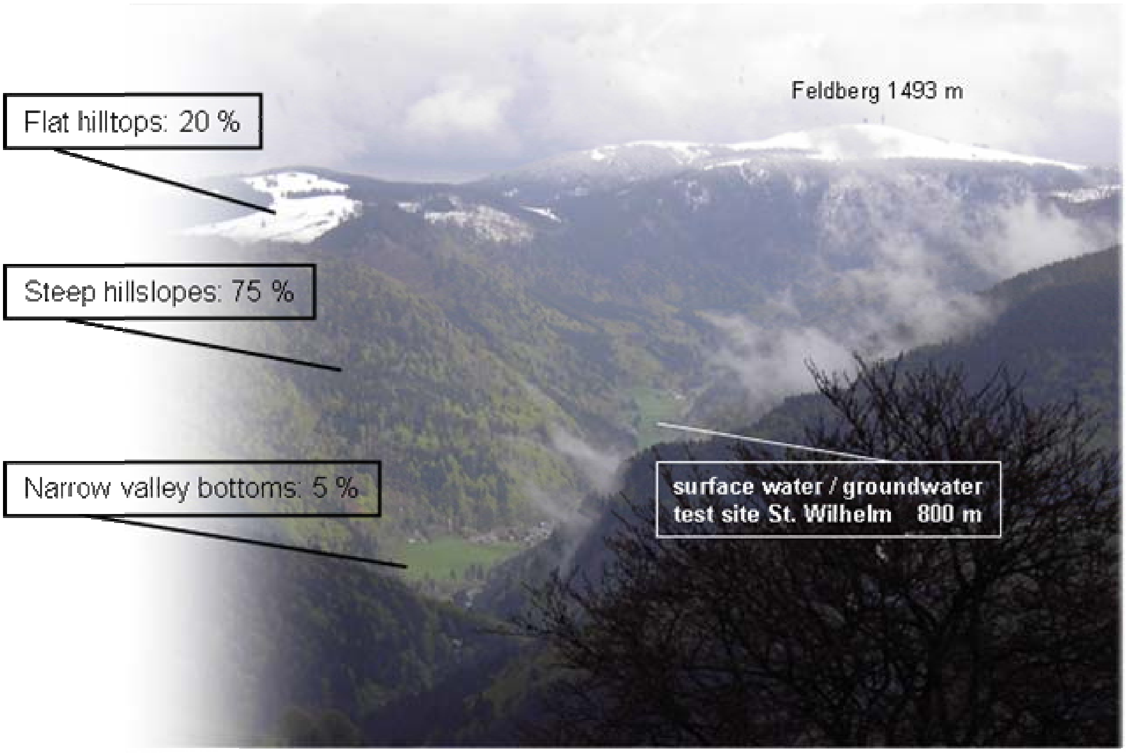

Figure 2.4: View from Schauinsland Mountain to Feldberg Mountain, May 7th 2004, together with main morphologic classes and their percentage of the total catchment area.

Crystalline bedrock is underlying the surface's morphology. Figure 2.5 shows the transformation steps the southern Black Forest crystalline bedrock underwent over time. An important part of today's southern Black Forest bedrock originated from sandy and clayey material, which was deposited during Precambrian period around 600 million years ago. An early metamorphosis transformed these sediments into (Para-) Gneiss.

During the "First Anatexis" which took place in the Cambrium period, the intrusions of magma lead to the formation of (Ortho-) Gneiss through metamorphic activity. As a result of the "Second Anatexis" (Ordovician, Silur), Metatexite and Diatexite emerged. Porphyry rocks such as Granite mainly date back to the Carbon (about 300 million years ago), when the Variscian orogenesis (Devon, Carbon and Perm) took place.

In Triassic and Jurassic times sedimentation occurred on top of the crystalline rocks. Tectonic uplifting and thus enhanced exposure of these sediments at cretacious and tertiary periods resulted in their complete removal at the southern Black-Forest area (depicted at the bottom left corner of Figure 2.5).

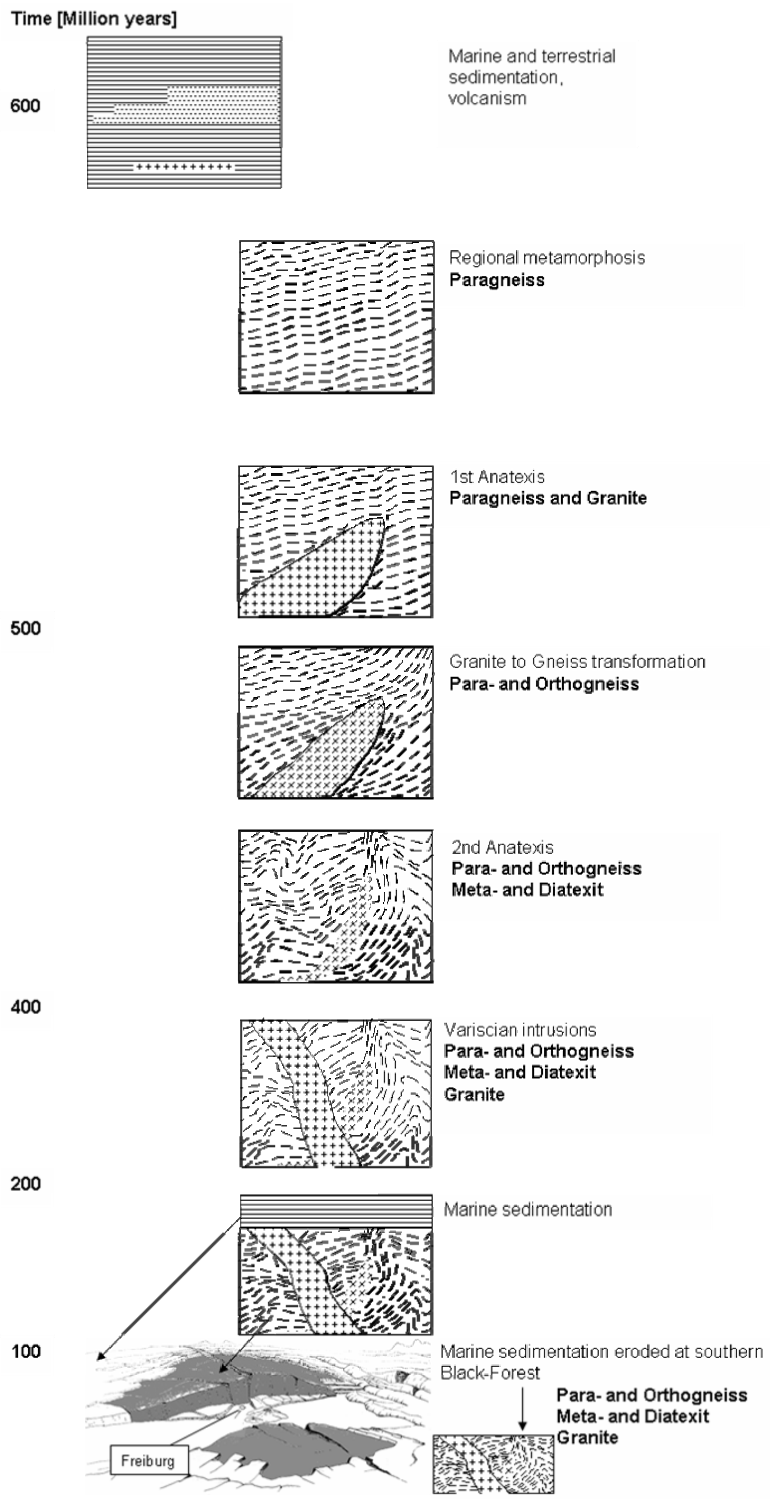

Figure 2.5: Genesis of southern Black Forest bedrock (simplified and compiled after WIMMENAUER & SCHREINER 1981 and GROSCHOPF et *al*. 1981 reviewed in FRIEG 1987).

While the Black Forest bedrock is relatively old, the current relief developed in younger times. The present landscape developed due to the most recent uplifting at the end of Pliocene period about two to three million years ago and was shaped by glaciers and the two river-systems of Rhine and Danube since then.

2.4 Sediments and soils

In the course of periglacial climate, regoliths and solifluction detritus developed. These sediments fill the valleys together with moraine material at the valley bottoms. However, some exceptions such as partially active boulder fields and young floodplain sediments (e.g. from medieval deforestation) do exist.

Evolving from the extreme climatic conditions of the glacial epoch, solifluction detritus and moraines heavily mix different components of clastic rock. The sediment material in the research area mainly consists of unsorted grains of all sizes (from clay to boulders). Single layers almost only vary in proportions of grading, but not in material type.

In contrast to this, sediments transported by melt water are sorted. They originate in the soil, when the ice-soil mixture heated up and the melting ice caused a drainage effect. As well as on the surface where melt water lakes and meandering streams were landscape forming factors.

Due to chemical weathering of the bedrock, no abrupt occurrence of solid rock can be found underneath the sediments. Instead an isomorphic (due to lack of transport) layer of weathered rock (*Gruss*) exists. Along tectonic fissures the metamorphic Gneiss bedrock degrades easily to fine-grained material. In comparison, porphyry rocks weather to coarser and sandier substrates.

Soil formation was favoured by the large surface of shattered rock and the resulting accelerated degradation. In the test site’s case, albic umbrisols developed on top of skeletic glacial material.

2.5 Vegetation and land use

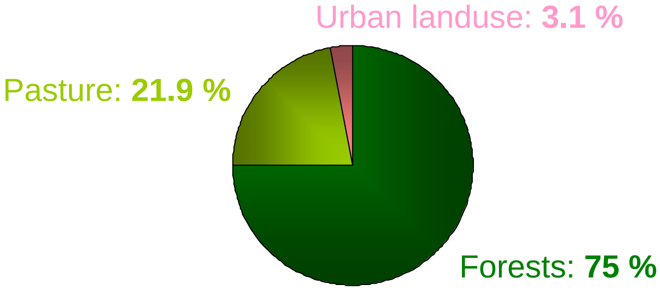

Figure 2.6: Landuse at Brugga basin.

The Brugga catchment is dominated by coniferous and mixed forests as shown in Figure 2.6. The study site itself is used as a pasture and the vegetation is cut two to three times a year by tractor.

2.6 Summary

The Black-Forest is a typical low mountain range situated in the mid-latitudes where snow is an important part of precipitation but rain is still decisive.

The glacial epoch’s strong impacts on the crystalline bedrock determine the present hydrological processes to a high degree. Well conductive boulder fields alternate with poorly conductive boulder clay as well as solifluction debris and moraine deposits. The latter three consist of a wide range of grain sizes and are well mixed through glacial transport.

The steep slopes are forest-covered while the remaining part of the Brugga catchments area is characterised by pasture land and few settlements.

3 Methods

3.1 Climate data

Precipitation and air temperature used to evaluate the test sites time-variation curves are provided by IHFs Katzensteig climate station. Its position about 700 m west and 35 m below (at 765 m a.s.l.) the test site is sufficient for the purpose of giving qualitative information on climatic parameters at the study site. Rainfall is measured at a temporal resolution of 10 min. using tipping bucket technique. No correction factor was applied.

3.2 Ground water and stream data

3.2.1 Permanent site equipment

The field site was equipped with five groundwater monitoring holes along one transect. Moreover, stream-water data was recorded as indicated in Table 3.1.

Table 3.1: Different data recorded at the test site in 10 minute intervals throughout the study period.

	Water level	Electric conductivity	pH	Water temperature	Soil-air temperature
Stream-water monitoring					
Groundwater monitoring					

The groundwater monitoring holes were previously implemented (WENNINGER 2002). Their access depth is approximately two meters. The last meter is equipped with a filter element.

3.2.2 Tracer data

In the past, water from drainage trenches of saturated areas, groundwater monitoring holes, sources and stream water was sampled and analysed (deuterium, dissolved silica, and major anions and cations) by WENNINGER (2002) and SCHEIDLER (2002). During this work electrical conductivity, pH and temperature were recorded as described in the previous chapter.

3.3 Soil moisture data

Four dialectric aquameters (ECH_2O) measuring soil moisture have been installed in the third study month. Their implementation was marked by adverse conditions, as a strong event took place the time aquameters were available. Probe placement was immediately executed. Due to the high water table, the dialectric aquameters were placed not deeper than 50 cm (Figure 3.1, a)).

The data was compared to electric resistivity tomographies placed at the same soil profile. Thus massive disruption of soil-structure due to whole digging did not pose a problem to the consecutively planed treatment of soil moisture data. It was planed to enable allocation of relative water content to electric resistivity values obtained from the ERTs (Figure 3.1, b), Figure 3.2). Problems mentioned in the previous paragraph together with data-logger malfunction during the ERT observation period were the final reason for no further application in the cause of studies.

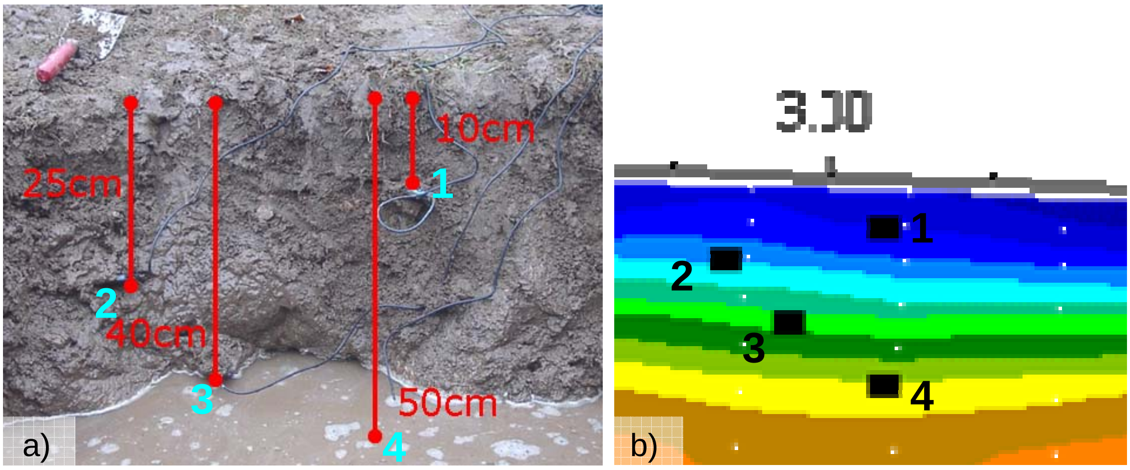

Figure 3.1: a) Implementation of diaelectric aquameters (1-4) in different depth b) Electrical resistivity tomography with diaelectric aquameters (1-4) positions indicated.

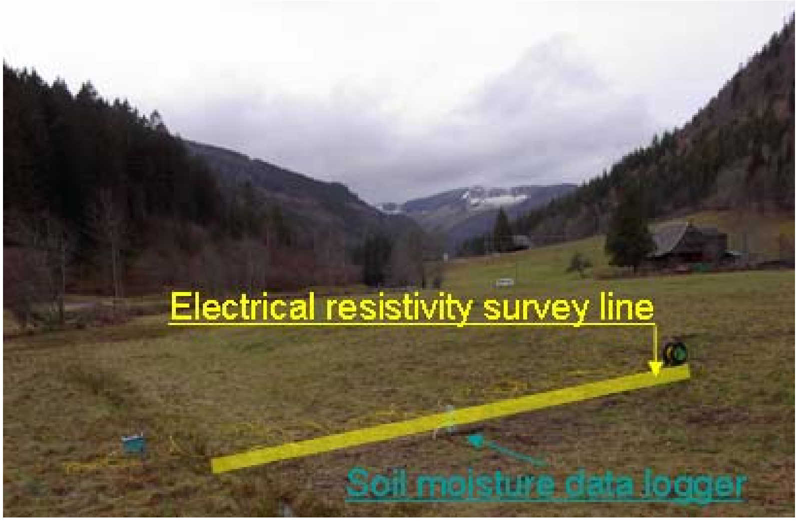

Figure 3.2: Coupling of electrical resistivity tomography with dialectric aquameters in the field.

3.4 Soil probing

Soil probing at 50 spots to a depth of ~100 cm and at some locations to a maximal depth of 200 cm, was performed by WENNINGER (2002). Supplementary soil samples were taken at specific spots during this work according to consulted ERT results.

3.5 *Electrical Resistivity Tomography*

3.5.1 Physical background

Electrical resistivity ρ is the inverse of electrical conductivity and describes how well the flow of electrical current is retarded by a material. Therefore bodies of different material (e.g. copper vs. iron or solid bedrock vs. open water), or bodies composed of diverse materials in different proportions (e.g. soil with 10 vol. % water vs. soil with 35 vol. % water or water with a low concentration of ions vs. water with a high concentration of ions) as well as bodies of the same material but in different phase or temperature (e.g. water vs. ice) possess a different electrical resistivity.

Flow of electrical current behaves in a certain way similar to the flow of water. Both follow a gradient in potential. Water follows gravity and always takes the fastest way to a lower level of potential energy, which can be seen in every topographic map, where the river-network strictly follows the steepest incline. In case of electrical current, flow is perpendicular to the contour lines of electric equipotential instead of gravimetric equipotential. In Figure 3.3, current flow from the positive potential at electrode B to the negative potential at electrode A is displayed in combination with equipotential lines. The potential gradients or “voltage drops” between the lines of equipotential drive the electric current according to the simple scalar form of Ohm’s law given by $\boldsymbol{I} = \boldsymbol{V} / \boldsymbol{R}$ (see next page for details)(HERMAN 2001). Furthermore it can be seen that current follows circular paths which is why resistivity measurements yield information on the deeper subsurface material, although electrodes through which current is injected only penetrate the first few centimeter.

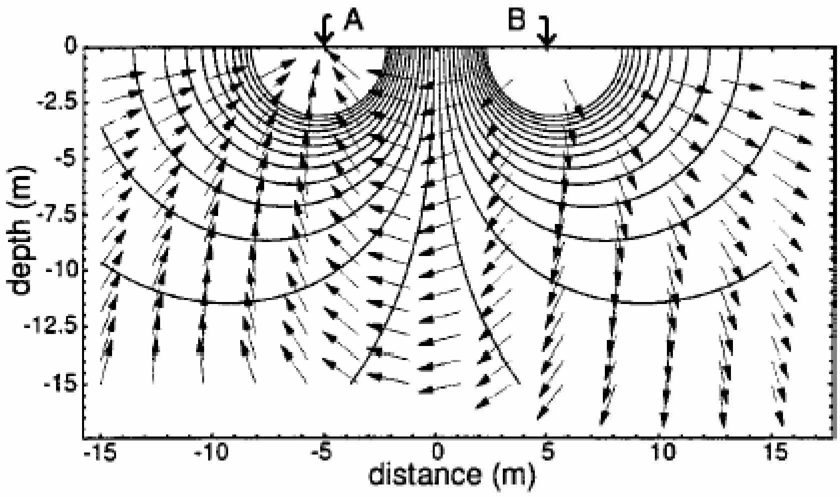

Figure 3.3: Current flow and equipotential lines (surfaces) between the two current electrodes A and B in a level field with homogeneous subsurface structure (HERMAN 2001).

Figure 3.3 illustrates that current penetrates the entire body in which it is induced. However, the cycles of current flow are dependent on the injecting electrodes position. With increasing distance between the electrodes the cycles get wider and therefore greater depth is penetrated. At the same time current flow close to the surface decreases. As a result, wider spacing of electrodes has greater “effective depth” but yields less information on upper regions. This fact is unimportant when penetrating homogeneous structures such as displayed in Figure 3.3, where resistivity is consistent. Yet, it is the reason why layers or structures with differing properties may be identified and associated to a certain depth.

A layer with high resistivity on top of material with low resistivity is displayed in Figure 3.4. In consequence of current flowing orthogonal to equipotential lines, current flow alters its way when meeting the layer with lower resistivity (Figure 3.4, Figure 3.6). To discern the presence of the two layers, the current electrodes need to be placed in different distances from one to another. Placing them close to each other only a shallow part will be reached by the current and unless the borderline between the layers is within that reach the deeper layer will not be encountered. Accordingly the resistivity measured will be due to the material of the upper layer (HERMAN 2001). With an increasing distance between the current electrodes, the “effective depth” is increasing as well. The current therefore is influenced to a growing extent by the material placed deeper underneath the surface. Once the current electrodes spacing vastly exceeds the depth of the borderline, current is bridging the gap in-between poles essentially by passing through the deeper layer. Thus resistivity primarily showing the properties of the deeper layer's material will be measured.

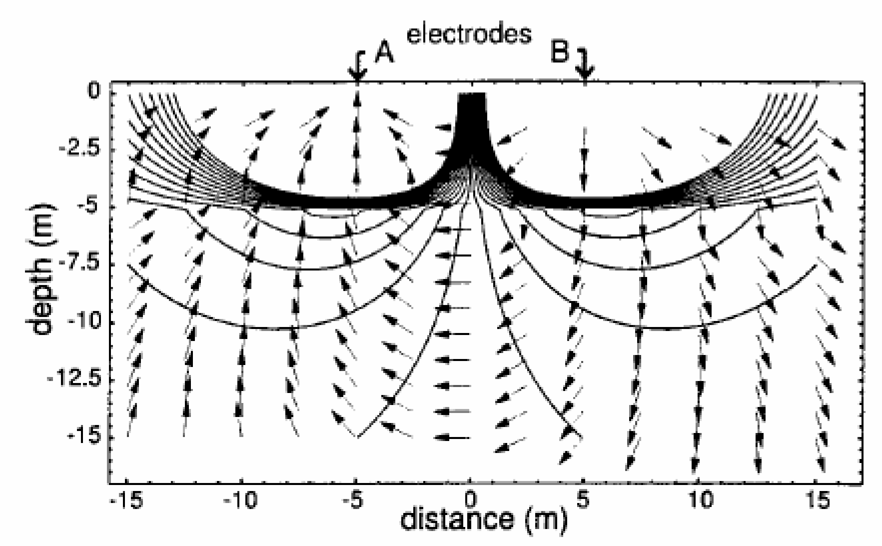

Figure 3.4: Current flow and equipotential lines (surfaces) between electrodes in a level field with inhomogeneous subsurface structure. The boundary between the two materials in this example is at a depth of 5 m (HERMAN 2001).

Measurements on resistivity are obtained on the basis of Ohm's law given by:

$$\boldsymbol{I} = \boldsymbol{V} / \boldsymbol{R} \qquad (1.1)$$

, where $\boldsymbol{I}$ is the current induced through the current electrodes A and B and $\boldsymbol{V}$ is the voltage measured between electrodes M and N (or in other words: $\boldsymbol{V}$ is the difference between the equipotential line at electrode M to the equipotential line at electrode N). Transformation of Ohm's law provides resistivity $\boldsymbol{R}$ as $\boldsymbol{R} = \boldsymbol{V} / \boldsymbol{I}$.

In order to simplify the physics of resistivity surveys, the image of a two dimensional space is shown (Figure 3.5, a). In reality however, space is three dimensional (Figure 3.5, b) which is of utmost importance for further treatment and interpretation of the obtained resistivities. Chapter 3.5.4 "Tomography interpretation" consequences of this will be taken into account.

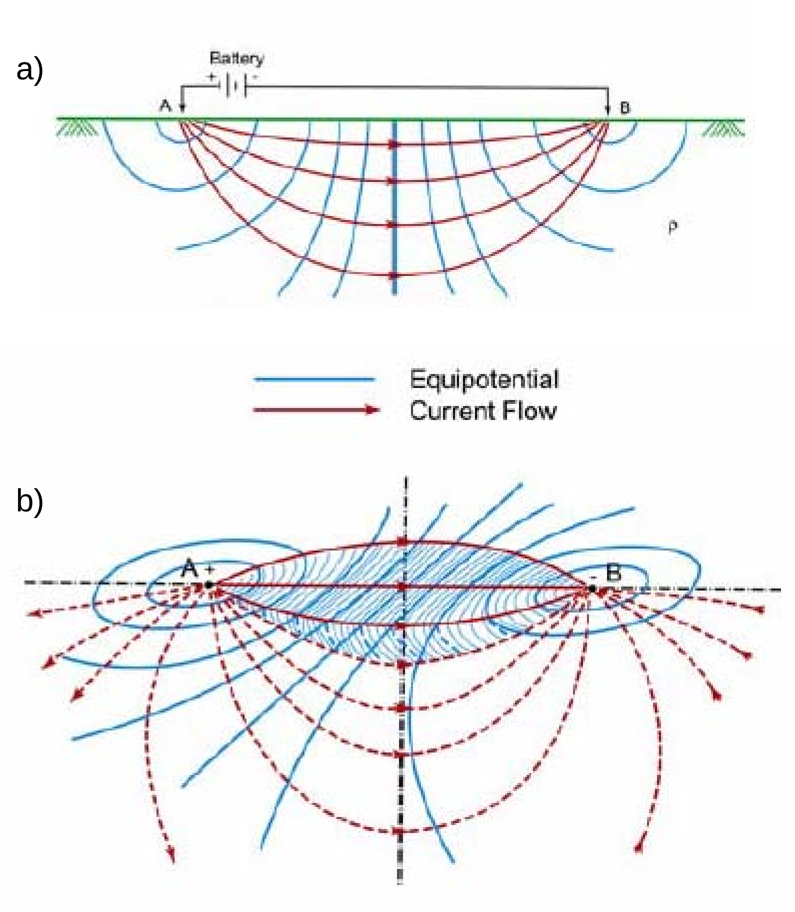

Figure 3.5: Schematic diagram of the distribution of current flow and equipotential lines in a homogeneous soil: a) 2D picture b) 3D picture (Damiata 2001).

3.5.2 Mathematical treatment of resistivity data

The accurate mathematical formulation of resistivity surveys is based on the physics described in the previous chapter but is dependent on the details of the measurement design. Several types of electrode arrays exist and will be in part explained in the chapter 5.1. Their complexity of calculation varies. In terms of calculation the most simple electrode set-up is the Wenner array. This manifests also in the possibility to do first interpretation of its data already before further processing has been executed. The mathematical processing of this array on a one dimensional basis may be reviewed in HERMAN (2001), where true resistivity and depth are calculated by means of a well defined experimental arrangement. In general, the complex mathematical treatment of resistivity data is performed by commercial inversion software and therefore only explained in a conceptual way in the frame of this work.

As described in the previous chapter, current does not flow in well distinguished paths. Consequently, the collected field-data does not monitor the actual subsurface facts on resistivity in combination with depth. True depth and true resistivity are associated with one another. For instance, a given spacing between A and B, on the one hand applied to a homogeneous one layer structure and on the other hand applied to a two layer structure of different resistivity, would result in the current penetrating to dissimilar depths on each structure (see chapter 3.5.1). In both cases the same current is injected and the same voltage is recorded on the surface but due to the difference in subsurface structure not the same penetration depth may be obtained (Figure 3.6). Thus the raw data implies only an apparent depth as information on the different resistivity layers is not integrated. Due to varying electrode spacing, information on various depths is gained enabling the calculation of the true depth for each layer. For this purpose, a top-down approach is used as the first layer is assumed to be not affected by more than one resistivity. Together with the "true" information on this first layer, the second layer may be calculated etcetera, until finally the effective penetration from the widest spacing is calculated and true depth obtained.

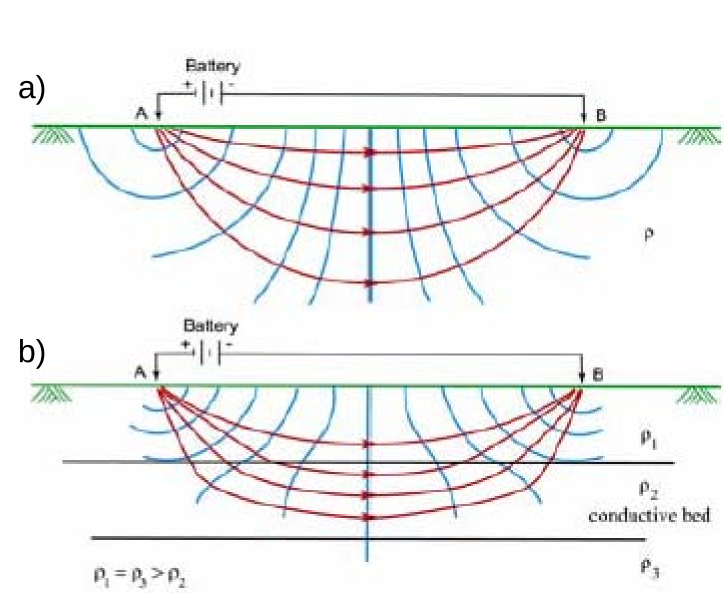

Figure 3.6: Schematic diagram of the distribution of current flow and equipotential lines for different cases of layered conductive and resistive beds: a) Homogeneous soil with uniform distribution. b) A more conductive bed between two resistive beds. The current prefers to flow in the conductive bed. As a consequence, the equipotential lines become distorted at the ground surface. The result is a smaller effective depth and a lower measured apparent resistivity (after Damiata 2001).

In the same manner true resistivity is calculated. However, true resistivity is a delicate matter and probably can never be attained. For example a close spacing of current electrodes in order to measure the top layer's resistivity would still have a small quantity of current penetrating the deeper layer with its disparate resistivity. Accordingly, resistivity measured is a weighted mean of the range of resistivities current comes across while passing different soil structures (BURGER 1992; ROBINSON & CORUH 1988). In the field, all measures taken are influenced by multiple structures with diverse resistivities. This influence is increasing with wider spacing respectively greater penetration depth.

From the previous two chapters one can derive that the calculation of true resistivities and depth depends on one another. To calculate true resistivity from apparent resistivity knowledge about the true depth is necessary, likewise calculating the true depth, information about the true resistivity is required. Usually neither true depth nor true resistivity is at hand. To overcome this problem various inversion-software-programmes are available. They perform several steps of iterative calculation to achieve the conditioning of calculated and measured resistivities and depths. Depending on the raw data (e.g. high heterogeneity, signal to noise ratio (see next chapter on arrays)), a close match may be achieved producing an image of “true” resistivities assigned to “true” depth.
As this inversion-software-programmme actually tries to minimize the calculated models difference to the measured apparent resistivity values, a measure of this difference is provided by the root-mean-squared (RMS) error. However, a mathematically best fit does not necessarily best describe the true subsurface structures.

3.5.2.1 Data processing

Data on electrical resistivity collected with the Syscal kid switch 24 needs to be transformed using Prosys software to allow further treatment. Therefore the raw data files (*.bin) are read in Prosys and first steps of quality audit can be performed. Assortment of bad datum points with exceptionally large deviations can be excluded from the continuing process. After the pre-selection of reliable datum points, the raw data file is converted to *.dat format. In *.dat format topographical information of the profile may be added and different datasets on the same profile (but at different timepoints) may be combined. The combination of multiple datasets from the same transect (timelaps option) allows to study the temporal changes in resistivity. As subsurface material stays the same changes can be interpreted as changes in fluids or temperature. This step of processing, the actual calculation of inversion images (*.inv) via iteration is of course also performed on single datasets. In this study the inversion software Res2Dinv was applied.

In Res2Dinv inversion settings can be changed. Nevertheless, regular settings give good and comparable results. Those alternative settings may simplify interpretation of tomography images, as for example layer boundaries may be sharpened. However, being based on the same raw data, changes in the inversion settings mainly result in a change of the visual perception of the resistivity data previously recorded. Changes in settings for the computation of data need to be well labeled, to avoid misinterpretation when comparing multiple tomographies. Therefore this work sets aside multi setting use in order to facilitate full visual comparison of the total of profiles studied.

3.5.3 Experimental set – up

In the following paragraph the set up for a two dimensional survey is explained with the Wenner switch as an example because of its simple alignment. As mentioned above, the electrode's spacing determines the penetration depth. To receive information along a single, imaginary line vertically in the ground, one varies the electrodes distance towards this imaginary line. The resolution of the measurement is merely depending on the number of measurements taken in different spacing and therefore depends on the time available. This one dimensional survey can be expanded along a chosen profile, adding datum points to the left and right. However, in practice the time-consuming set up of several one dimensional surveys is infeasible. Therefore 2D resistivity apparatus have the ability to switch between not only four but multiple connected electrodes. Those electrodes are strung with constant spacing, building a catena on the profiles surface (Figure 3.7). In addition to the resistivity measurement itself, 2D resistivity measuring devices are able to switch between the connected electrodes independently to perform several single measurements in a row. The information about the spacing (effective depth) and resistivity recorded of each single measurement is gathered and forms the information on the whole profile. The way electrodes are switched is according to the array previously chosen by the user.

Figure 3.7: Lign up of electrodes for an electrical resistivity survey.

3.5.4 Tomography interpretation

In analogy with the physical background given in section 3.5.1, electrical resistivity tomography is not a one-to-one picture of the subsurface. This chapter outlines the principles of electrical resistivity imagery interpretation by means of actual examples, as the character of current flow leaves some uncertainties in interpretation of ERT. Essential for correct interpretation is knowledge about the nature of data interpreted. In the case of ERT there are values from three dimensional resistivity measurements (Figure 3.8, a) which are transformed to point data (Figure 3.8, b) interpolated to two dimensional images (Figure 3.8, c).

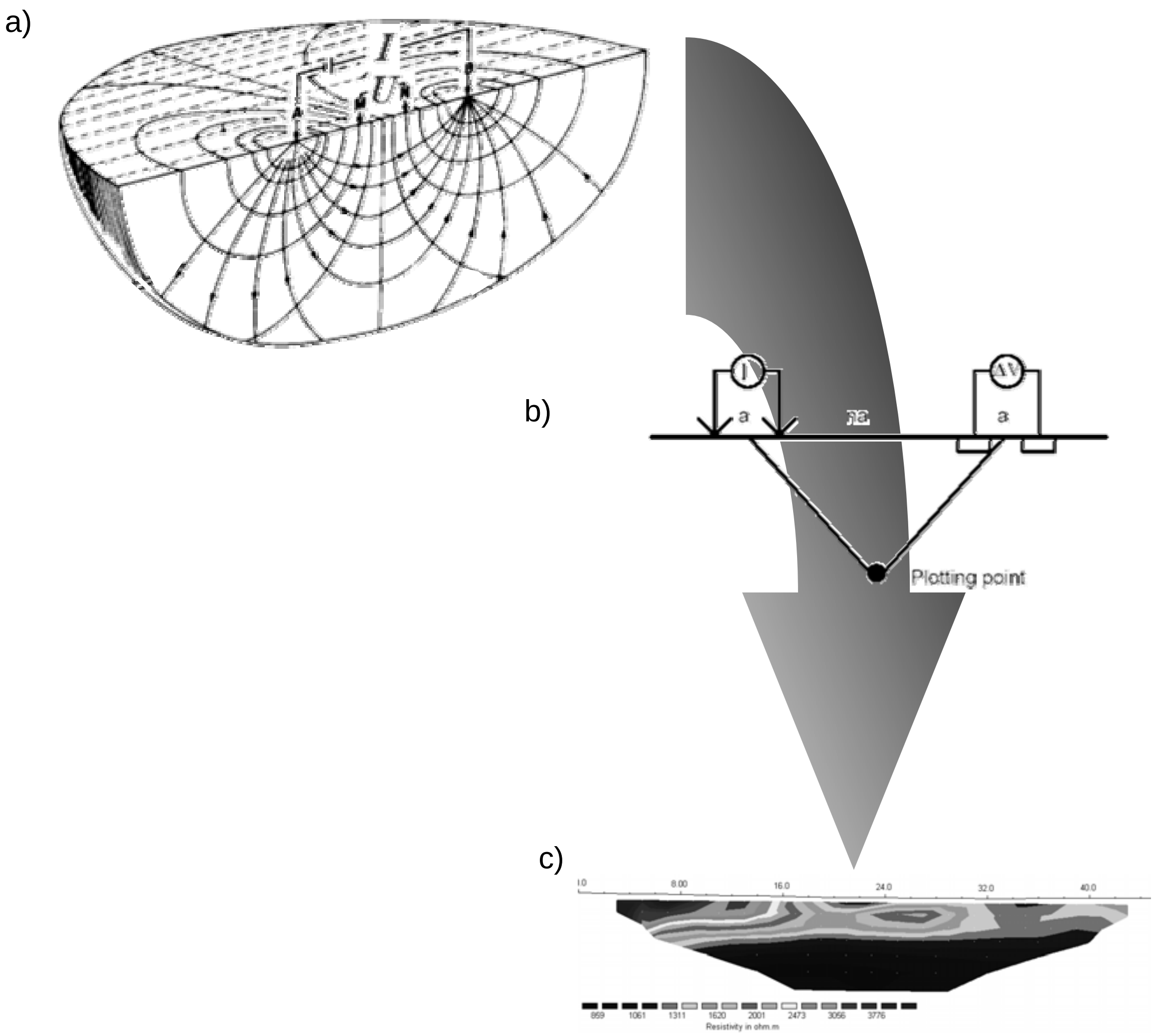

Figure 3.8: Basis of ERT; a) 3D picture of current flow and equipotential surfaces b) Geometry of the dipole-dipole array (CARDIMONA 2002) c) Electrical resistivity tomography.

Example 1:

The three dimensional quality of resistivity data is monitored in the following example, where a boulder is enclosed by sediments. By chance the cross-section shown in Figure 3.9 (left side) could directly cut the boulder in two and consequently illustrates its true dimension. Though more likely the profiles' position is only in neighborhood of the boulder or may cut part of it. This would mean on the one hand underestimating the boulders size, on the other hand seeing a boulder in a profile where there is none. A couple of profiles from different angels however, permit to determine the boulders' position.

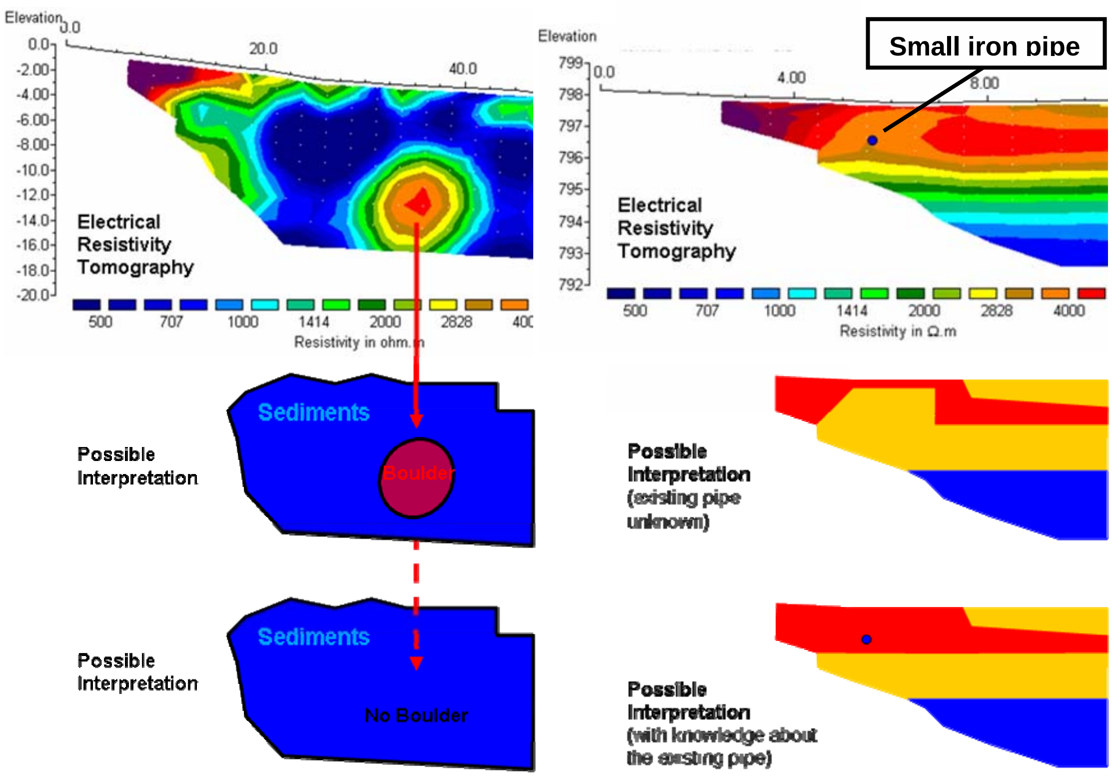

Figure 3.9: Two cases of problems in ERT interpretation. Left side: A structure which is not layer like can not be precisely grasped with a single tomography. Right side: Small structures, very different in resistivity can lead to misinterpretation of bigger structures.

Example 2:

Another important point is the resolution of electrical resistivity tomography, for small subjects may not be correctly displayed, but still do influence the overall image (presented in Figure 3.9 at the top of the right side) with their resistivity properties.

4 Results

In the following, electrical resistivity and hydrometric data as well as observations at the field site (see soft information) are described. For description of data previously collected (notably tracer data), see WENNINGER (2002) and SCHEIDLER (2002).

4.1 Soft information

Throughout the field work the research site could be observed under the influence of various conditions, which is in some cases illustrated by photo evidence. In the following, pictures from a period with a high volume of precipitation are presented and shortly explained. The rainfall data from that period is given in Figure 4.28. The eleventh of January no overland flow was observed.

12.1.: Small puddles at zones with probable soil compaction from tractor wheels (Figure 4.1 c)).

Pond filled from overland flow which originated from a source at the contact point of the boulder field with the valley bottom (Figure 4.1 a-b)).

Surface water can be seen at several micro-topographic depressions.

Water ascents directly from grass covered soil (Figure 4.1 d)).

Figure 4.1: Test site (12.1.2004).

13.1.: Water is still at areas of soil compaction (Figure 4.2 a)) and filling the pond.

Water discharges from molehills as well as directly out of the soil at several areas (Figure 4.2 b)).

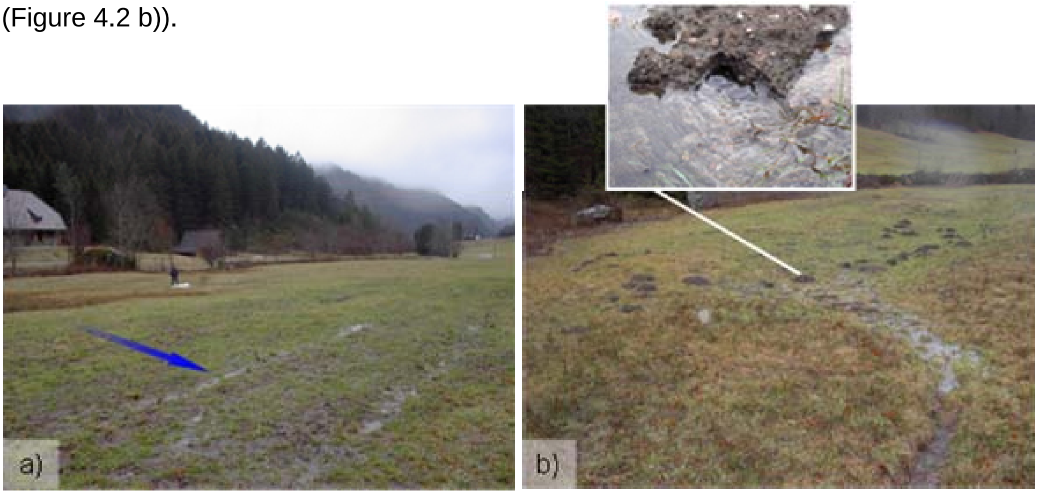

Figure 4.2: Test site (13.1.2004).

14.1: Surface water at areas of soil compaction has vanished (Figure 4.3 a)).

Water discharges from molehills (Figure 4.3 b)) as well as from other macro-pores located a few meters from the 80 cm deeper stream channel (Figure 4.3 c)).

Areas where water ascents directly from the soil increase (Figure 4.3 b-d)).

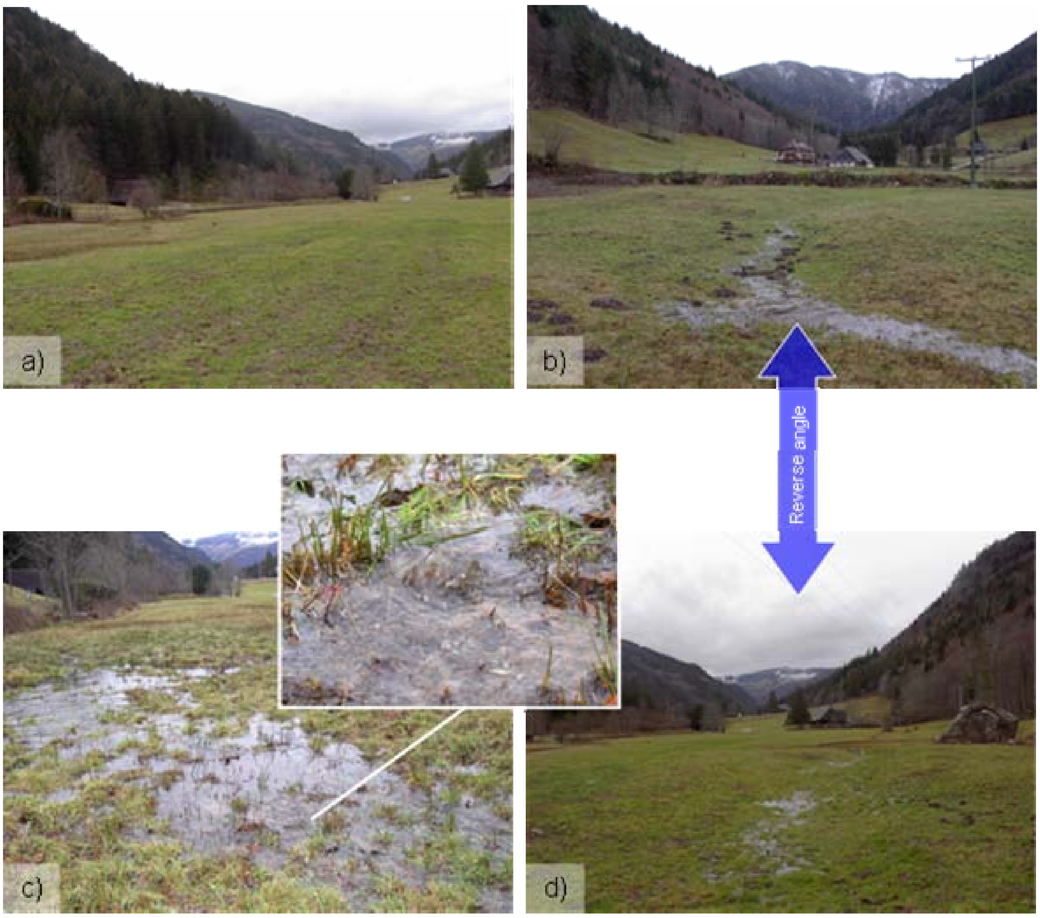

Figure 4.3: Test site (14.1.2004).

15.1.: Precipitation falls as snow.

Water flows from molehills as well as straight out of the soil at almost the same extend as the day before (Figure 4.4 a & b)).

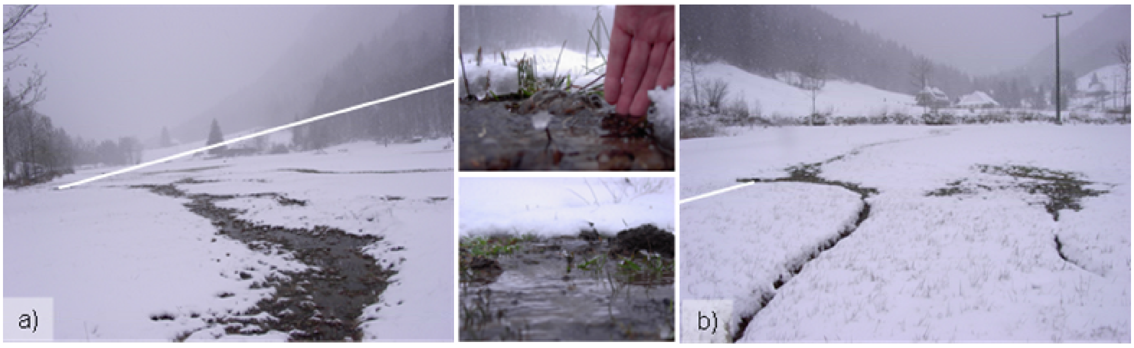

Figure 4.4: Test site (15.1.2004).

17.1.: Water discharge from molehills continues as before (Figure 4.5 a)).

Soil discharge is much less pronounced (Figure 4.5 b)) and the pond is not recharged by the boulder field source anymore.

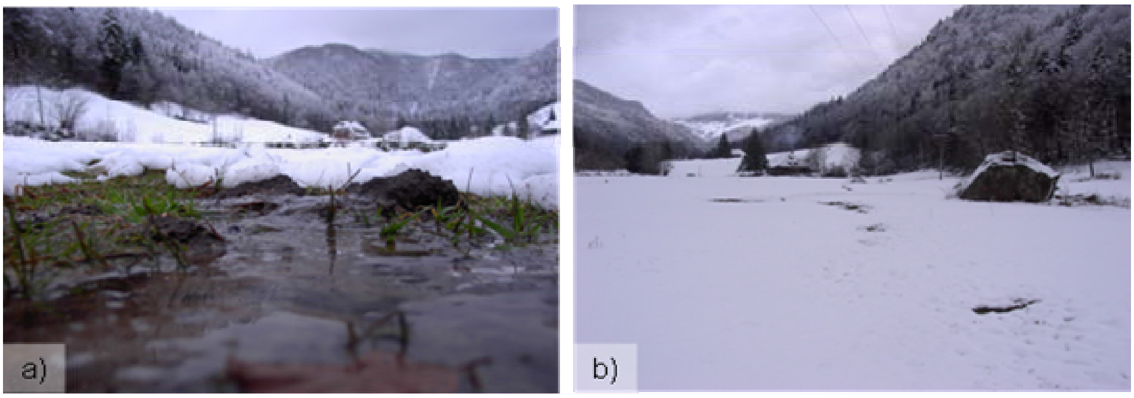

Figure 4.5: Test site (17.1.2004).

19.1.: Flow from molehills decreased significantly (Figure 4.6 a)).

Water ascending directly from the soil is rarely observed.

The pond is almost empty (Figure 4.6 b)).

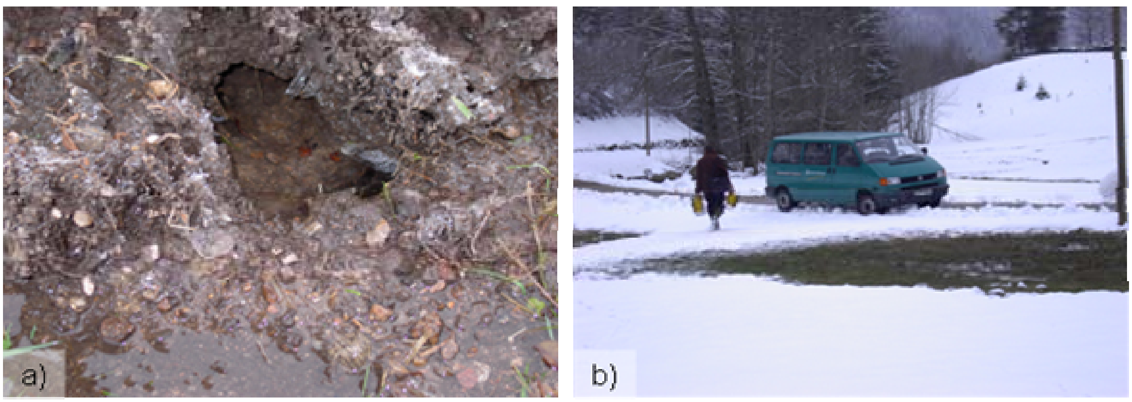

Figure 4.6: Test site (19.1.2004).

21.1: The pond and all other areas which previously showed surface water are covered by snow except for some molehills where discharge may still be observed (Figure 4.7).

Figure 4.7: Test site (21.1.2004).

24.1.: No liquid surface water is observed (Figure 4.8).

Figure 4.8: Test site (24.1.2004).

5.2.: After no additional precipitation but warmer temperature, snowmelt occurred. Some molehills re-discharged. One of them close to the hillslope did so relatively intense while a bit further away from the slope smaller amounts of water ascended, which actually descended in another channel (Figure 4.9).

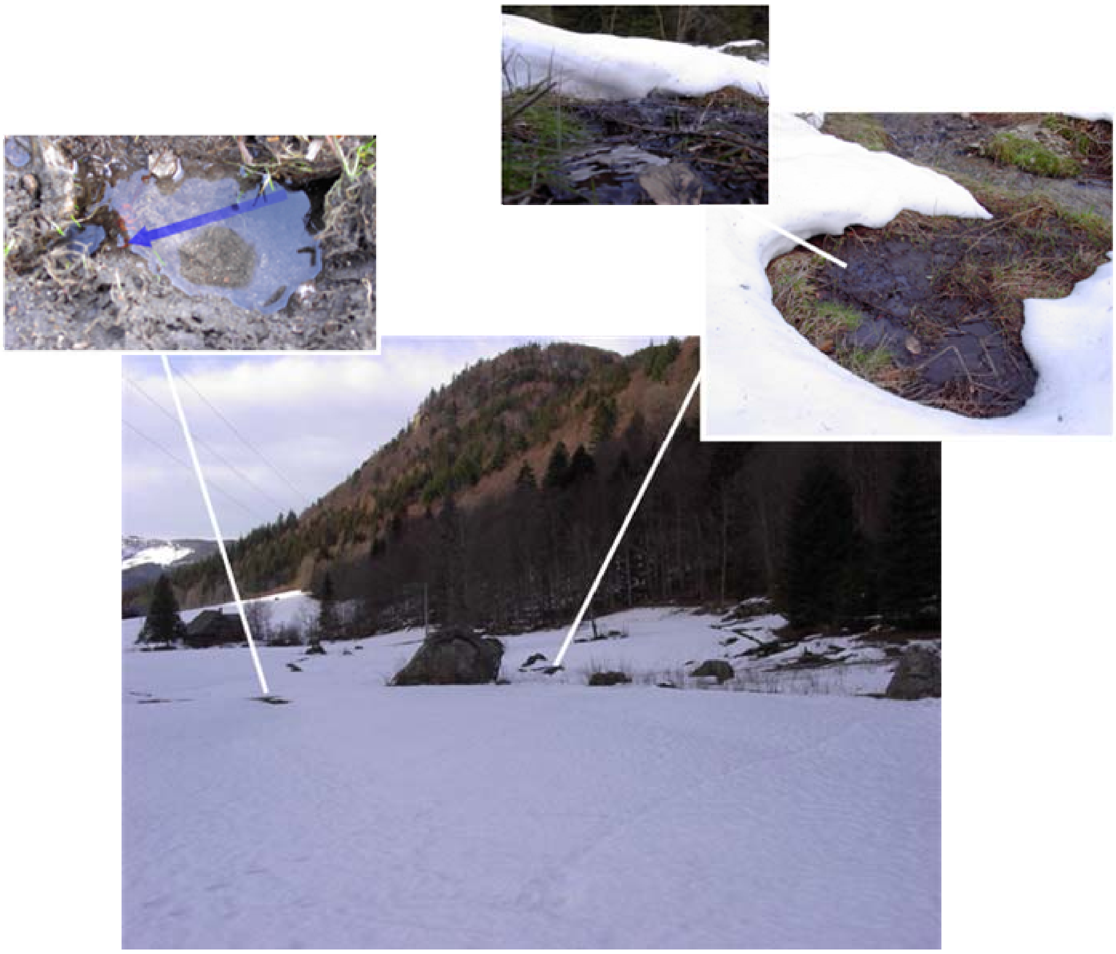

Figure 4.9: Test site (2.5.2004).

A local resident told that this kind of situation appears normally once or twice a year, but did not do so during the previous year.

Another important observation at the field site was made when soil probing was performed half a meter from an artesian source. Water was ascending from the source but did not “bubble”. After pulling the stake of two centimetres diameter back out of a depth of ~60 cm, water was bubbling to a height of two to three centimetres from the hole for at least 20 minutes.

4.2 *Hydrometric data*

4.2.1 Groundwater

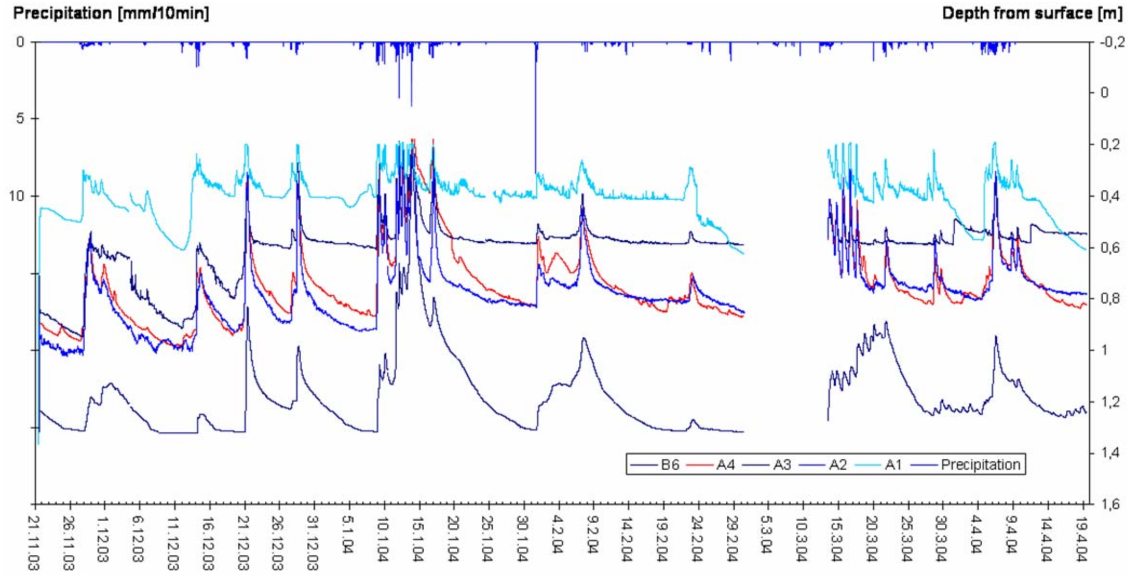

Figure 4.10: Graphic display of recorded piezometric heads in groundwater monitoring holes A1, A2, A3, A4 and B6.

The piezometric heads from the groundwater monitoring holes at the test site are displayed in Figure 4.10. Differences in the time durations curves can be depicted amongst the different monitoring holes. A1 located closest to the hillslope in vicinity of a saturated area shows the smallest distance between surface and water level. For long periods a constant level is maintained. Sometimes peaks may surpass the limit of measurement at about 25 cm in depth, which at other groundwater monitoring holes was only the case during the mid-January event. A3 shows the most similar curve, although being placed further away than A2 (see Figure 4.13). No such temporary constancy is shown in the curves of groundwater monitoring holes A2 and A4. These two monitoring holes however show a strong similarity among each other.

Overall, many analogies according to the groundwater monitoring holes timing towards the precipitation input is visible. Differences can be depicted in the quality of reaction to a particular event. The rising and descending of the measured groundwater table is not persistent between different monitoring holes as well as events. Here groundwater monitoring hole B6 shows the strongest discrepancies.

4.2.2 Stream water

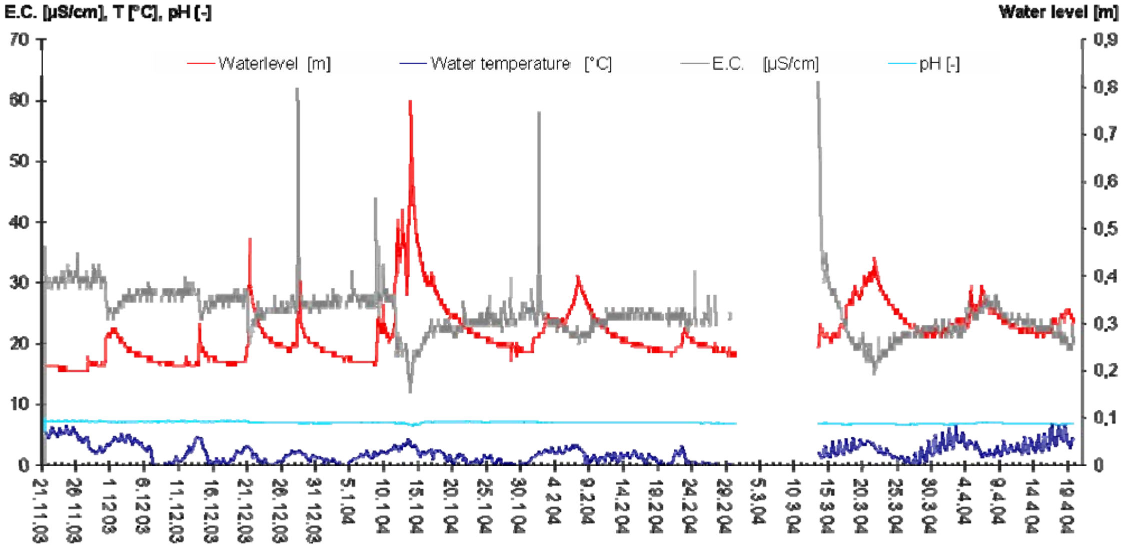

Figure 4.11: Graphic display of recorded stream data.

In Figure 4.11 the course of water temperature, electric conductivity, pH and water levels in the stream are displayed. Values of pH are constantly around seven with minor lowering throughout storm-events. With its day-night-variation, clearly visible for example at the end of May, the stream's temperature shows strong dependence from air temperature. In addition, temperatures around freezing point are common. Electrical conductivity and water level show almost perfect negative correlation, except for some events in winter, which are related to snowmelt. These snowmelt events show conductivities of about 60 µS / cm whereas in general, electrical conductivity varies between 30 µS / cm in the beginning to 23 µS / cm in March and April. Lowest electrical resistivity recorded was 13 µS / cm on January the 14th and 15 µS / cm on March the 21st, 2004.

4.2.3 Comparative study

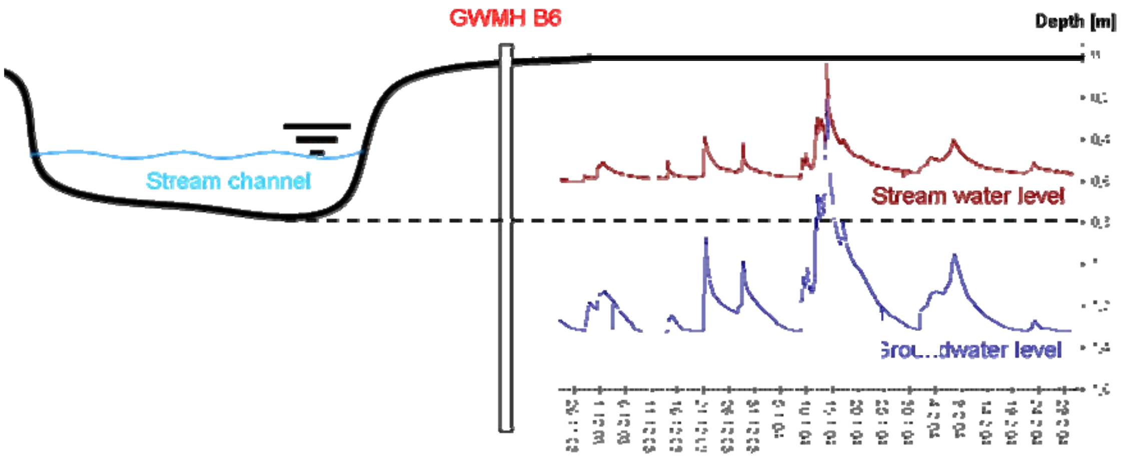

Figure 4.12: Relation between water level at groundwater monitoring hole B6 and stream water hydrograph.

The given excerpt on groundwater and stream water level (Figure 4.12) illustrates similar reactions of the two systems monitored. Nevertheless, proportion in reaction to the different events is not consistent.

Bringing stream and groundwater height on the same basis, demonstrates that groundwater is without exception beneath stream water level. In addition, the comparison of peak dates and the dates that mark the beginning of rise before a peak showed that only two of the 23 clearly definable events were recorded to rise in the groundwater monitoring hole before they rise in the stream. All peaks appear first in the stream and later in the monitoring hole.

4.3 Electrical resistivity tomography

From the 111 conducted electrical resistivity tomographies only some are presented. The cross-sections shown in this chapter are based on at least two measurements each. As an example ERT *a* – *d* (Figure 4.14 to Figure 4.17) feature two transects monitored and described with Wenner as well as dipole – dipole array. In the case of ERT *g* (Figure 4.20) and the stream channel profile only dipole – dipole data is displayed although Wenner data is also available. Partly recorded with dipole – dipole as well as Wenner array are the hillslope profile and the transversal profile, where only the first 120 m (92 m) were recorded twice in exactly the same manner but with the two array types, while the consecutive range can be compared to recordings made in its vicinity.

Raster grid's profiles and ERT *e* and *f* (Figure 4.18, Figure 4.19) are monitored only with dipole – dipole array.

It can be stated that no contradictory results between displayed and non displayed data occurred and that subsurface structures which are discussed in chapter five are always depicted in all measurements from the discussed profile, though in different quality.

4.3.1 Spatial resolution: small spacing (= penetration depth < 4 m)

Small electrode spacing is necessary to achieve higher resolution of structures close to the surface. A number of measurements were carried out in order to allow distinction mainly of possible impervious materials and for example their significance towards the location of saturated areas.

Four of the five surveys illustrated (Figure 4.13), are part of the time-lapse set up covered in chapter 4.3.3 and are situated at the limit between saturated – non – saturated – areas. The main properties of all measurements, also not-shown time-lapse tomographies, are combined in Table 4.1. The fifth electrical resistivity profile (ERT *g*) cuts the stream channel diagonally. It is, combined with a wide spacing ERT described in chapter 4.3.2, designed to gain knowledge on the groundwater – stream water interface.

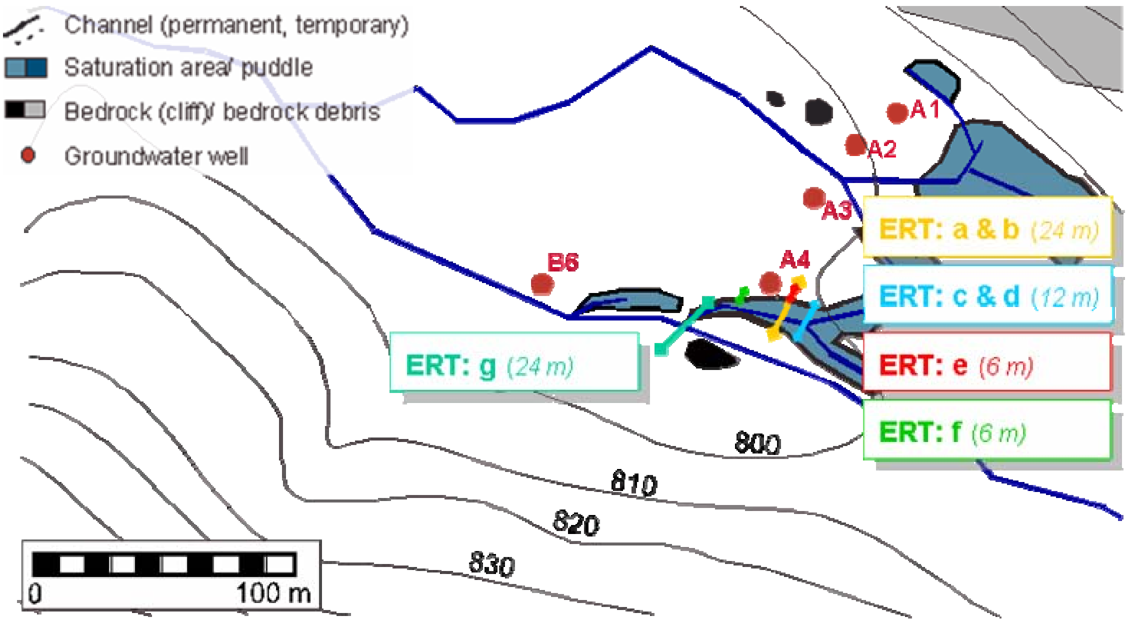

Figure 4.13: Location of conducted electrical resistivity tomographies.

Table 4.1: Properties of conducted electrical resistivity tomographies.

ERT	Array type	Spacing *(profile length)*	Number of electrodes	RMS error	Date
a (1, 2)	Wenner	1 m *(24 m)*	24	1.3, 1.4 %	12. & 14.12.03
b (1)	dipole – dipole	1 m *(24 m)*	24	1.2 %	14.12.03
c (1)	dipole – dipole	0.5 m *(12 m)*	24	1.5 %	14.12.03
d (1)	Wenner	0.5 m *(12 m)*	24	1.5 %	14.12.03
e (1 – 12)	dipole – dipole	0.5 m *(6 m)*	12	1.4–5.0 %	11. – 24.01.04
f (1 – 6)	dipole – dipole	0.5 m *(6 m)*	12	0.9–2.5 %	14. – 24.0104
g (1)	dipole – dipole	1 m *(24 m)*	24	5.9 %	12.12.03
a (3 – 16)	Wenner	1 m *(24 m)*	24	1.2–2.0 %	10. – 24.01.04
b (2 – 4)	dipole – dipole	1 m *(24 m)*	24	0.9–2.8 %	10.,12.,24.01.04

In Figure 4.14 the electrical resistivity tomography 15*a* is displayed. It was recorded using Wenner array on a 24 m profile with a spacing of one meter between electrodes. Resistivity values range from 700 Ωm to 6500 Ωm. The maximal values of 6500 Ωm are found at the left and right marginal position at 1.3 m underneath the surface. These regions of strong resistivity taper towards the centre of the transect. Across the entire tomography vertically highest resistivity values are recorded at the same level, while the distance to the surface is varying due to the change in surface topography.

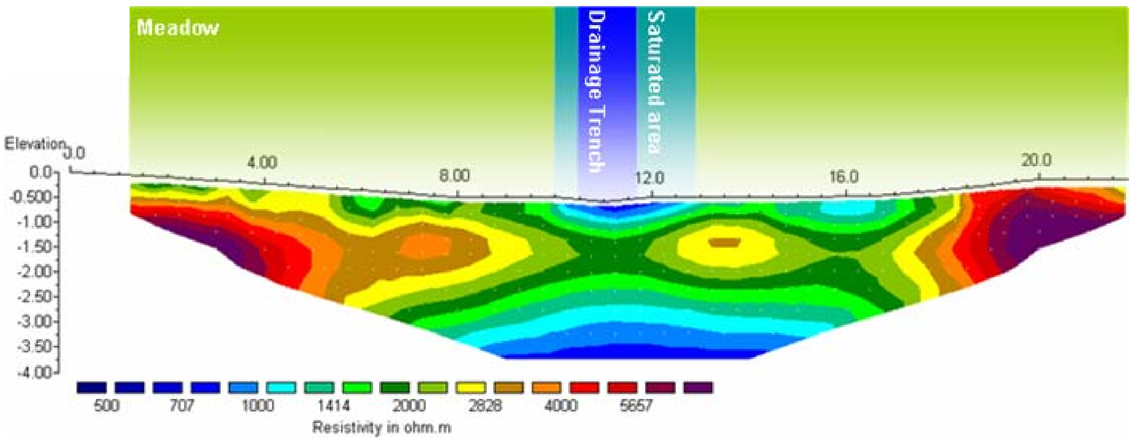

Figure 4.14: ERT *15 a* (Wenner | 1 m spacing | 24 electrodes | RMS error 1.5 % | 21.01.04) with surface facts.

At the left and right side this line of strongest resistivity has a depth of 1.3 m, whereas in the centre beneath the drainage trench the distance to the surface is 0.9 m. Along this line, the above mentioned decline of resistivity from margin to centre is not constant but shows secondary maxima (at x = 7.5 & 13.5 m) and minima (at x = 6 &16 m).

Areas of weak resistivity from 1200 to 700 Ωm exist in depths greater than 2.2 m as well as close to the surface. The lowest resistivity value is displayed in proximity of the drainage trench. Additionally, all along the surface-line of the transect small pockets relatively weaker in resistivity reach from the surface down to approximately 20 cm of depth (e.g. at x = 3, 4, 6 or 16 m).

The results in Figure 4.15 display the same transect, though at different date and dipole – dipole instead of Wenner array is employed. According to depth and position the described structures are similar in the two pictures. Changes in resistivity are to some degree more distinct and the surface pockets show a larger extent.

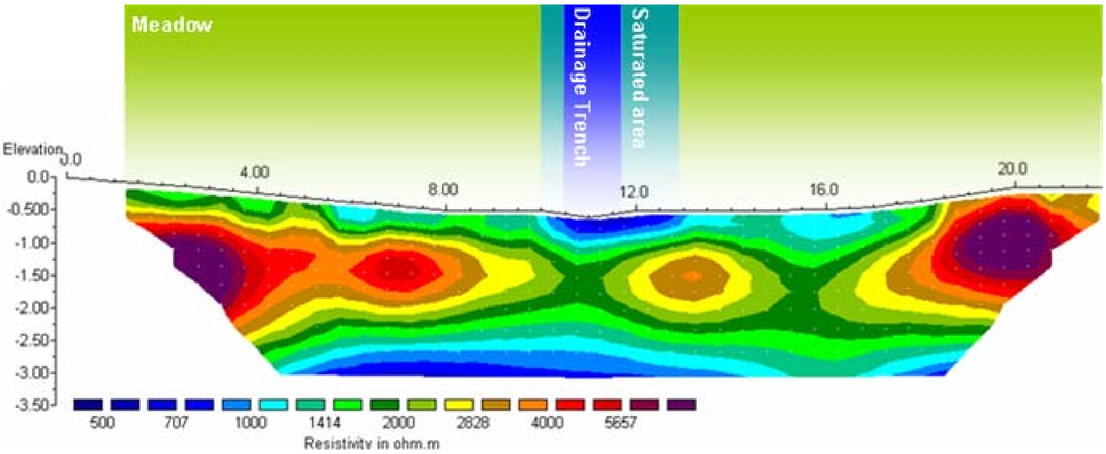

Figure 4.15: ERT *3b* (dipole – dipole | 0.5 m spacing | 24 electrodes | RMS error 1.1 % | 12.01.04) with surface facts.

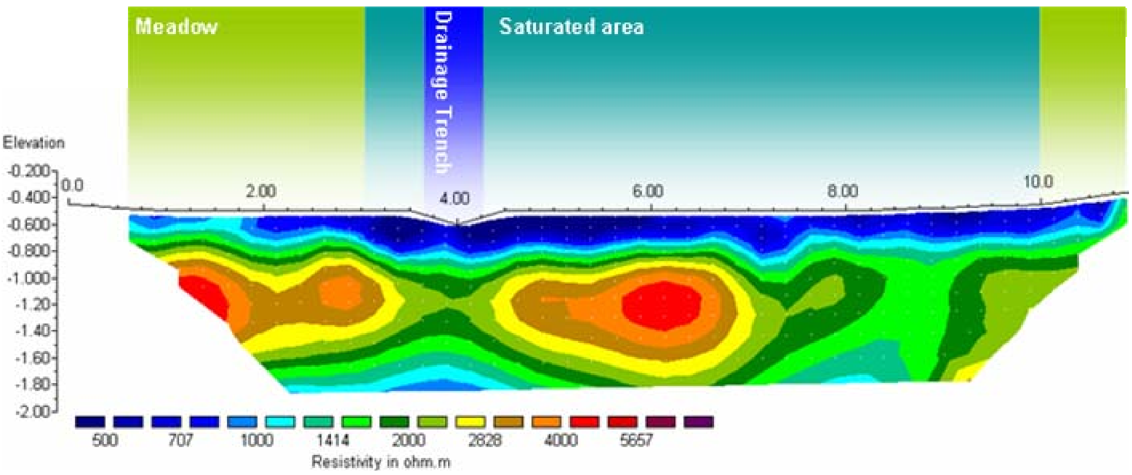

Figure 4.16: ERT *1c* (dipole – dipole | 0.5 m spacing | 24 electrodes | RMS error 1.5 % | 14.12.03) with surface facts.

The result from the electrical resistivity tomography 1*c* presented in Figure 4.16 can be organised in three main sections. The entire profile is marked by a close to surface band of 20 to 30 cm depth with resistivities of 500 to 1200 Ωm. The lowest resistivity is found in proximity of the drainage trench at x = 4 m, whilst the higher resistivities are recorded at the left as well as the very right outskirts of the profile.

Further from the surface, resistivity rises and a sector with 1500 to 4500 Ωm can be marked out. This zone reaches depths of 100 to 130 cm. Throughout the profile the highest resistivity is constantly found in a depth of 70 cm except for x = 9 m, where highest resistivity is at 130 cm of depth. This vertical line of strongest resistivity is characterized by eminent horizontal variation. High resistivity values of more than 4000 Ωm at x = 1.5 or 6 m alternate with values of 2000 Ωm underneath the trench (at x = 4 m) or 1500 Ωm at x = 8.75 m. Compared to its upper limit the zone's lower limit is less sharp, meaning shifts in resistivity take more space. Anyhow, resistivity drops down to 1200 at x = 8 m or even below 1000 Ωm underneath the trench at x = 4 m at depths of 1.5 m.

The ERT 1*d* (Figure 4.17) shows the same transect at the same time but was recorded using Wenner switch instead of dipole – dipole switch. Horizontal alternation in resistivity values is less pronounced (single exception is the upper left corner at x = 1.6 with a stronger shift in resistivity in the ERT 1*d*). In addition, resistivity at 1.8 m beneath the surface is illustrated and shows values down to 750 Ωm underneath the drainage trench.

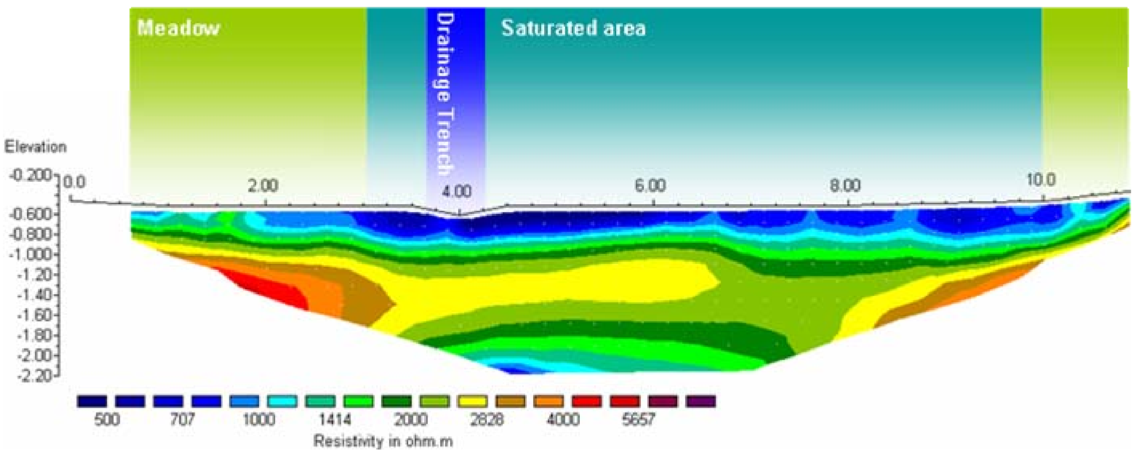

Figure 4.17: ERT *1d* (Wenner | 0.5 m spacing | 24 electrodes | RMS error 1.5 % | 14.12.03) with surface facts.

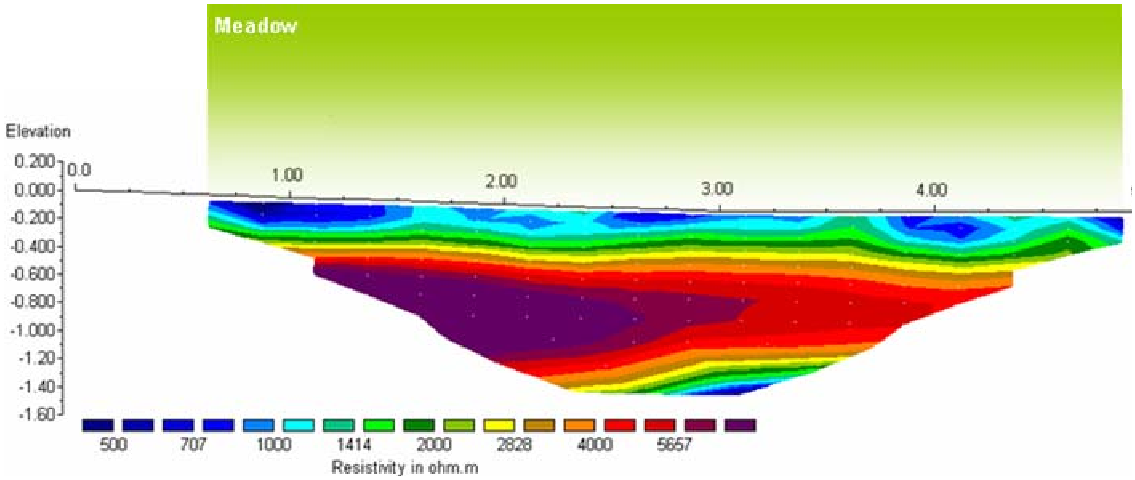

Figure 4.18: ERT *10e* (dipole –dipole | 0.5 m spacing | 12 electrodes | RMS error 2.3 % | 19.01.04) with surface facts.

In Figure 4.18 three differing structures are drawn. The first structure is located in the upper 20 cm of the profile and shows resistivities varying from pockets of 500 Ωm to 1000 Ωm separated by regions of up to 1400 Ωm.

The largest proportion of the recorded transect is distinguished by resistivities of over 2000 Ωm. The top edge of this section is constantly bordering the first structure at a depth of 20 cm. This deeper structure is triangularly shaped were depth and resistivity are diminishing from the left to the right. At 80 cm beneath the surface, the resistivity maximum of 6500 Ωm at the left side drops to roughly 5000 Ωm at the right side of the transect. The bottom line rises from 150 cm at the left of the profile to 130 cm below the surface at its right. At a depth of 150 cm in the bottom right corner, resistivity attributes drop down to 500 Ωm.

ERT 4*f* (Figure 4.19) illustrates similar patterns as described above, though departure from ERT 10*e* (Figure 4.18) crops up in the central structure with resistivities above 2000 Ωm. No diminishment from the left to the right can be depicted, as electrical resistivity shows two maxima of roughly 5500 Ωm at 80 cm beneath surface. The first is located at x = 1.8 m and the second x = 4.0 m. The area in-between these maxima at x = 3 m reaches only 3000 Ωm. The bottom line however, rises like in ERT 10*e* from the left to the right but in the case of ERT 4*f*, from 120 cm to 110 cm below the surface.

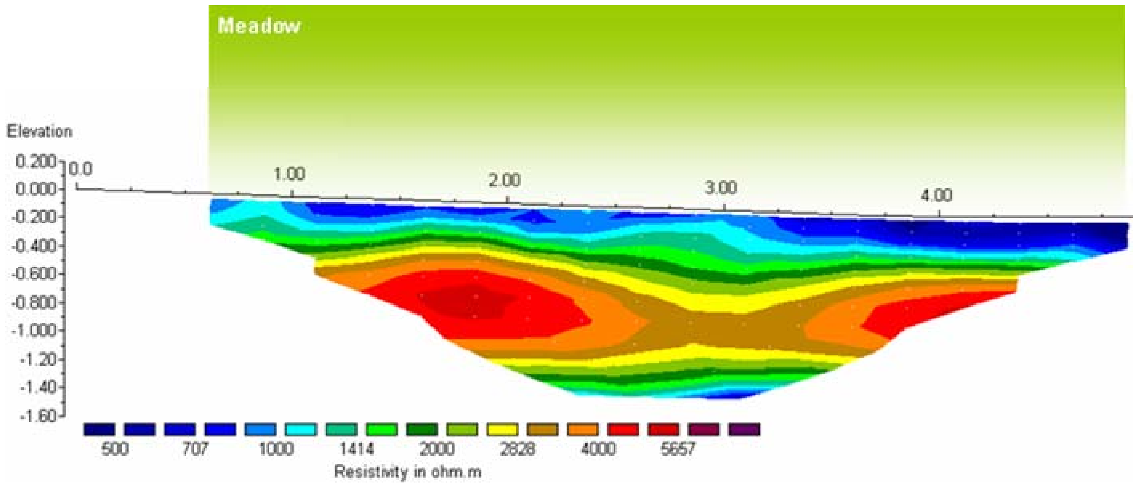

Figure 4.19: ERT *4f* (dipole – dipole | 0.5 m spacing | 12 electrodes | RMS error 2.2 % | 19.01.04) with surface facts.

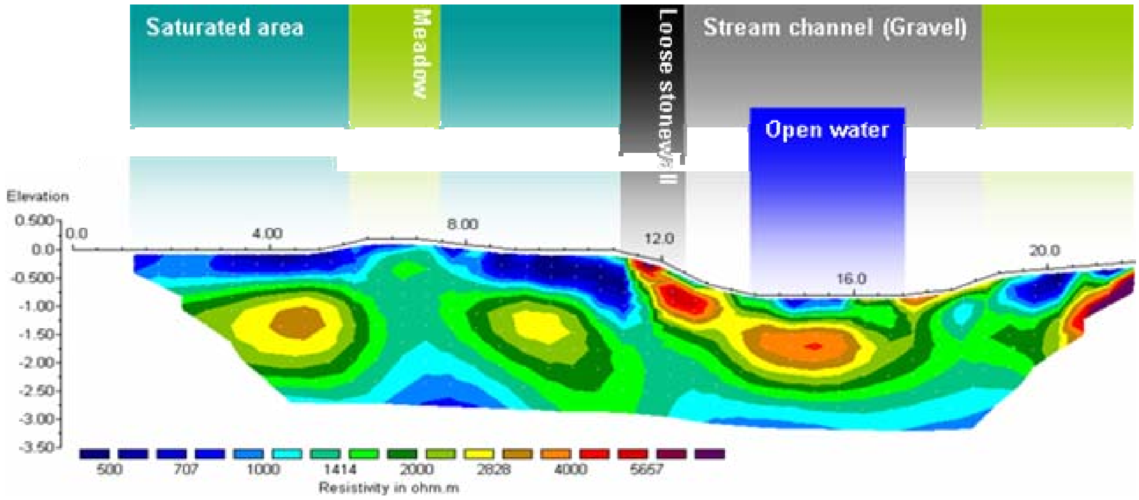

Figure 4.20: ERT *g* (dipole –dipole | 1 m spacing | 24 electrodes | RMS error 5.9 % | 12.12.03) with surface facts.

Variation from 500 Ωm up to 7500 Ωm is monitored in ERT 1 under the use of dipole – dipole array with 1 m spacing (see Figure 4.20). Values below 1200 Ωm were recorded at depths of more than 1.8 m as well as in regions close to the surface. These surface regions are interrupted by zones of higher resistivity at the loose stonewall as well as in the stream channel to both sides of the open water. Values lower than 1200 Ωm reach depth of 20 cm in the channel, over 50 cm at the saturated areas and up to 130 cm in depth are shown in vicinity to the loose stonewall.

Resistivity greater than 6000 Ωm only appears in the first centimetres beneath the stonewall and at the right margin of the profile in deepness of 20 - 100 cm. In general, values from 1500 to 6000 Ωm are found at a 2 m band in a depth from 50 cm to 250 cm. Exceptions are at x = 10 m, where higher resistivity reaches depth of 300 cm and in the stream channel where high resistivity gets to the surface.

4.3.2 Spatial resolution: wide spacing (= penetration depth < 20 m)

Together with a shift in knowledge about the hydrological processes areas hill slope valley bottom and terrace – saturated area interface, a comprehensive picture of the contribution of previously suspected layers in the valley bottom was desired. Thus a set of surveys was executed with properties described in Table 4.2.

The transformation from hill slope flow to flow in the valley bottom’s filling is of major interest for process hydrology. The significance of interlocking of slope sediments with valley deposits remains fairly unknown although being a key section for changes in processes determining further transport of water. Enclosing of slope and valley bottom through a single 260 m roll-along measurement with five meter spacing was performed and the benefit from such a two dimensional sight on this important interface was qualified.

The hillslope electrical resistivity profile as well as the transversal profile, mapped in Figure 4.21, were both monitored during dry conditions. The slope profile cuts an anticipated flowpath down the hill towards the valley bottom until it reaches areas with gentler incline from the saturated area downwards. From here on the transversal profile is more likely to correspond to an imaginary pathway along the valley bottom though still most probably not matching reality.

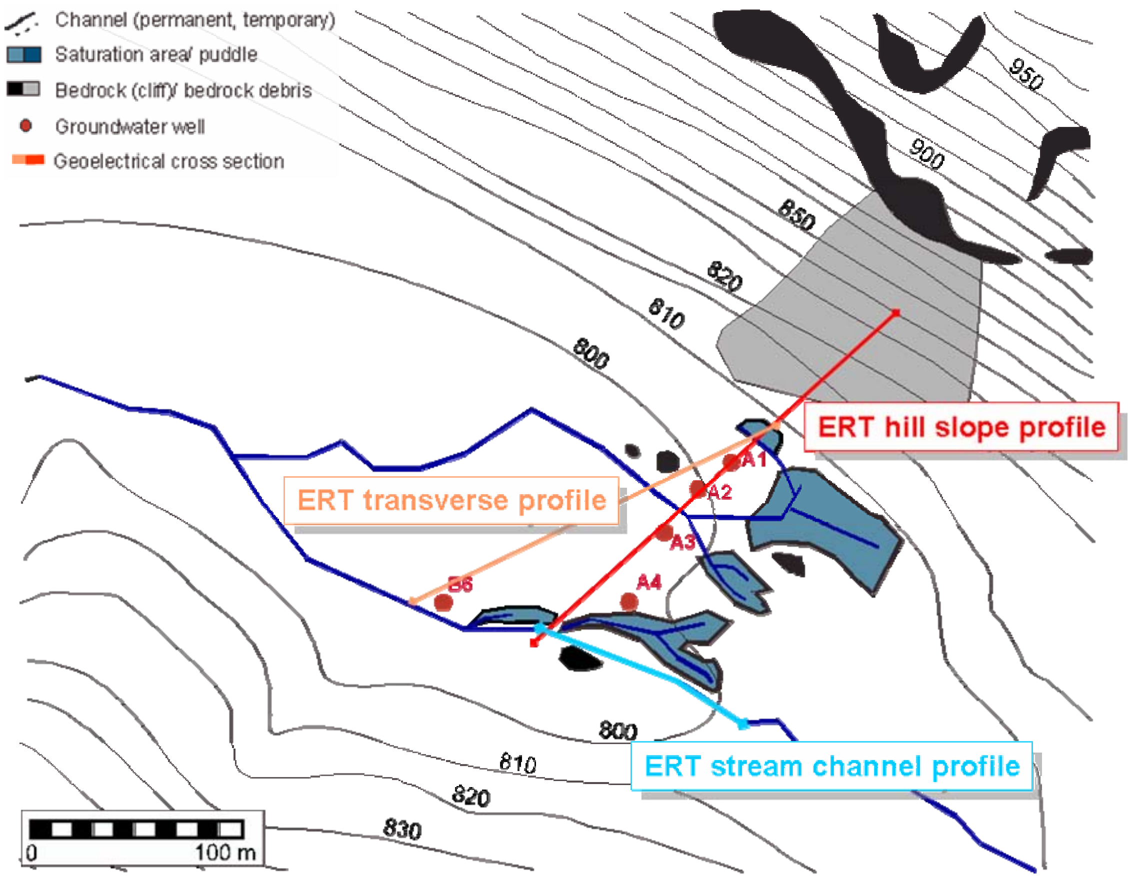

Figure 4.21: Location of conducted electrical resistivity tomographies.

With the use of natural tracers, Wenninger (2002) proved drainage trenches on the research site to be perched. The stream being perched as well was doubted but remained a question to further research. Unfortunately, for electrical resistivity tomography only few transects along the stream channel are suited to educe connection of the aquifer with the river bed, for the placement of electrodes is mostly limited by a paved road to one site of the channel. However, with regards to the heterogeneities in this area, numerous cross-sections are essential to any serious statements on the stream bed – aquifer interface. Being not able to place more than one cross-section actually crossing the stream, a profile was placed directly in the channel itself (see Figure 4.21 for location) to estimate up and down stream comparability of the results obtained from the one profile which intersected the stream bed (Figure 4.20). The second profile was measured without the use of steel electrodes, because cables were directly placed in the stream water. Therefore, default spacing is five meters, given by the distance between the not insulated parts of the cables.

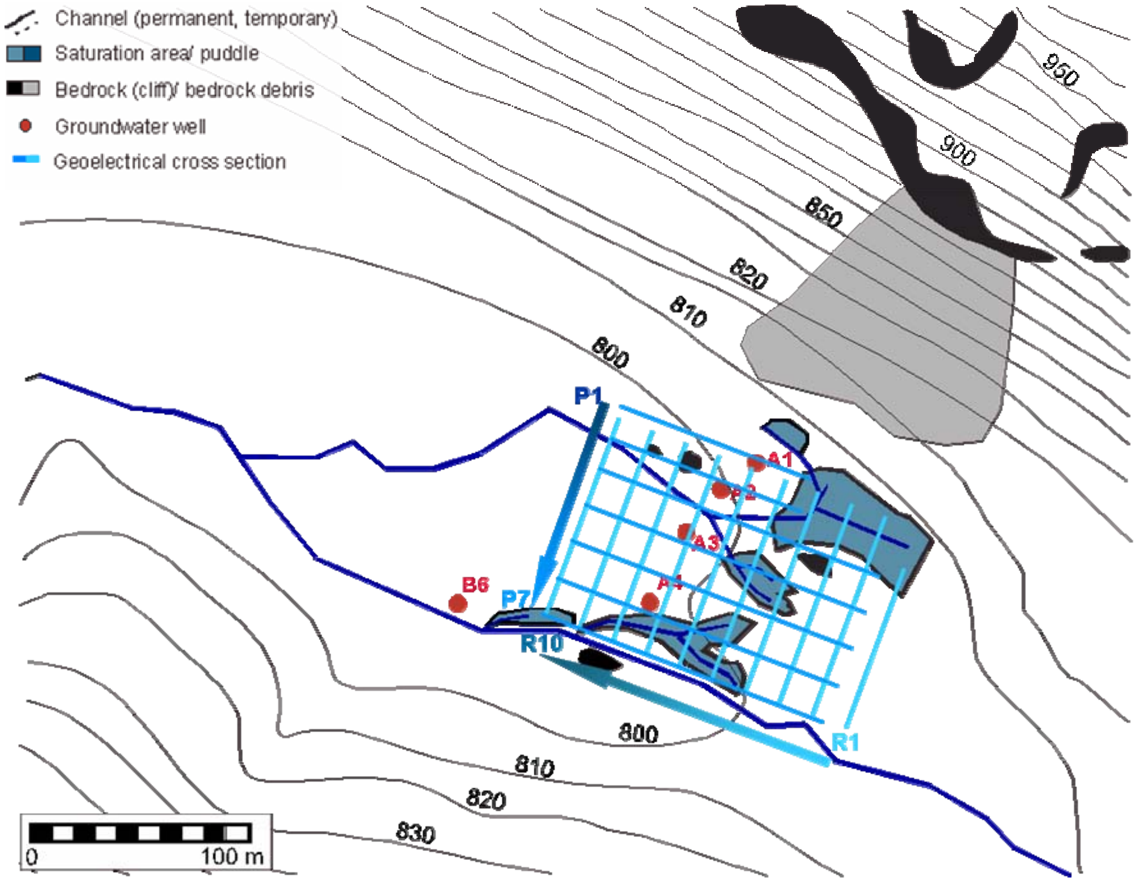

Figure 4.22: Location of conducted electrical resistivity tomographies.

In order of good spatial resolution a raster survey was conducted. The number of conducted profiles in connection with their extend is a compromise between desired resolution, penetration depth and time frame available to ensure steady conditions during the recording of the raster survey. The raster grid displayed in Figure 4.22 features 17 cross-sections separated by a distance of 15 m from one to another. Measuring was conducted at three consecutive days during a dry period. Thus subsurface structures were recorded in resembling moisture condition and consequently differences in profiles could be related to differences in material.The spacing of four meters between electrodes was chosen due to the good penetration depth and the fact that its main disadvantage, the lack of resolving the first decimetres of soil close to surface, was not of importance for the survey's topic. To specify, earlier electrical resistivity tomographies with smaller spacing showed that under dry conditions it is not possible to identify the top layer as it shows resistivity similar to the upper layer.

The interest was further focused on groundwater bearing layers and their spatial distribution as described in the previous paragraph. Moreover, the spatial distribution of the layer at the very surface was recorded via soil probing by WENNINGER (2002) and did not show any larger gaps. However, the soil probing did not cover the whole grid area and is a source of punctual data; therefore it lacks good comparability to two dimensional electrical resistivity imaging.

Table 4.2: Properties of conducted electrical resistivity tomographies.

ERT	Array type	Spacing *(profile length)*	Number of electrodes	RMS error	Date
Hill slope profile	Wenner	5 m *(265 m)*	54	4.5 %	10.12.03
Transverse profile	dipole – dipole	4 m *(172 m)*	44	15.9 %	26.4.04
Stream channel profile	dipole – dipole	5 m *(115 m)*	23	10.5 %	20.4.04
R1	dipole – dipole	4 m *(76 m)*	20	6.4 %	30.3.04
R2	dipole – dipole	4 m *(92 m)*	24	2.3 %	30.3.04
R3	dipole – dipole	4 m *(92 m)*	24	3.5 %	30.3.04
R4	dipole – dipole	4 m *(92 m)*	24	2.8 %	30.3.04
R5	dipole – dipole	4 m *(92 m)*	24	3.1 %	30.3.04
R6	dipole – dipole	4 m *(92 m)*	24	1.9 %	30.3.04
R7	dipole - dipole	4 m *(92 m)*	24	2.5 %	31.3.04
R8	dipole - dipole	4 m *(92 m)*	24	1.6 %	31.3.04
R9	dipole - dipole	4 m *(92 m)*	24	1.7 %	31.3.04
R10	dipole - dipole	4 m *(92 m)*	24	1.5 %	31.3.04
P1	dipole - dipole	4 m *(92 m)*	24	3.0 %	31.3.04
P2	dipole - dipole	4 m *(92 m)*	24	2.3 %	31.3.04
P3	dipole - dipole	4 m *(140 m)*	36	3.1 %	1.4.04
P4	dipole - dipole	4 m *(140 m)*	36	2.7 %	1.4.04
P5	dipole - dipole	4 m *(140 m)*	36	3.0 %	1.4.04
P6	dipole - dipole	4 m *(140 m)*	36	4.9 %	1.4.04
P7	dipole - dipole	4 m *(140 m)*	36	4.4 %	1.4.04

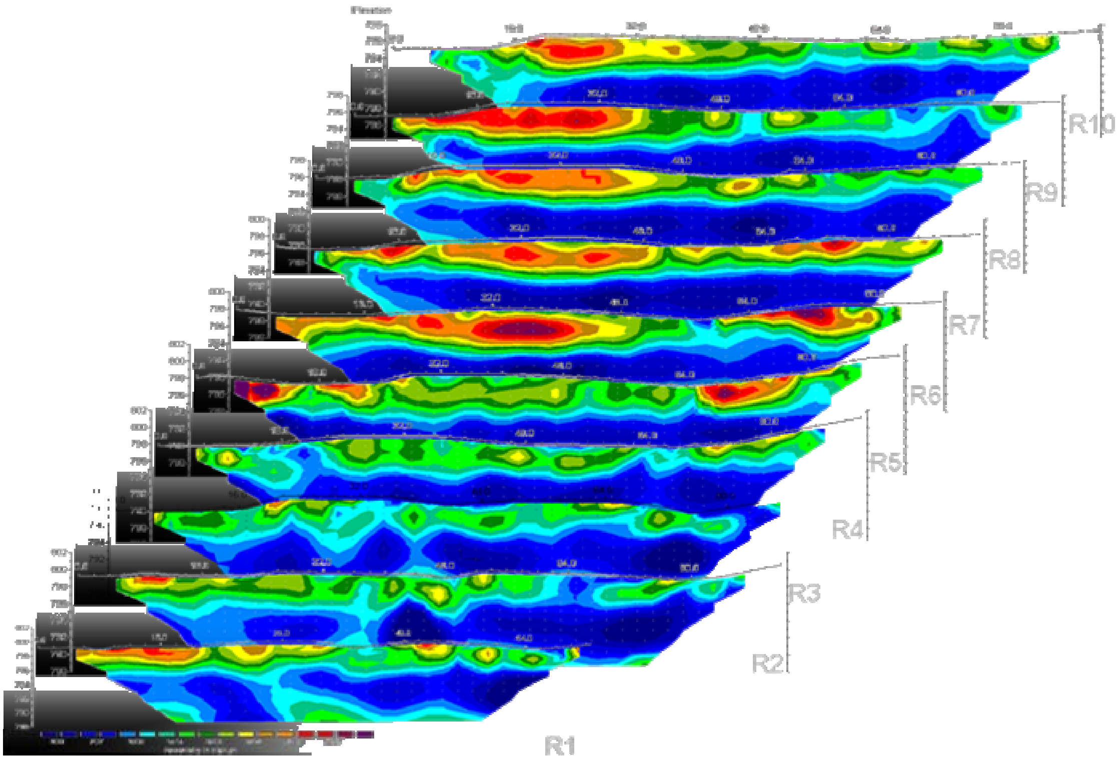

Figure 4.23: ERT raster profiles perpendicular to stream R1 – R10 (dipole - dipole | 4 m spacing | 20 - 24 electrodes | RMS error 1.5 – 6.4 %) [scale: dark blue = 500 Ωm, purple = 8000 Ωm].

The ten perpendicular and the seven profiles located parallel to the stream channel displayed in Figure 4.23 and Figure 4.24 show resistivities from about 500 to 8000 Ωm. The upper layer described in chapter 4.3.1 with resistivity higher than 1500 Ωm is consistent all over the raster grid except for view interruptions. Its thickness and the strength of electrical resistivity however do vary throughout the field site. A pattern in terms of spatial distribution of these variations can be depicted, as strong resistivity with values over 8000 Ωm prevails in the south-east quarter of the grid namely in transects R5 to R10 and P5 to P7. Other occurrences of resistivity values above 8000 Ωm are found in close vicinity to the adjacent hill slope in profile P1 and on the northern site of R5 to R7. For the remaining three quarters of the studied grid, the upper layer has been recorded and measures from 1500 to 3000 Ωm. In addition, these zones of the upper layer with less resistivity reach shallower depth with two to three meters instead of up to five meters of penetration of the upper layer in zones with resistivity beyond 4000 Ωm.

The limit between the described upper layer and the deeper layer with electrical resistivity values beneath 1200 Ωm ranges between five meters and the surface. Variations in depth are more abrupt in the eastern and northern halves of the grid space (profiles R1 – R5 and P1 – P4). Zones where low resistivity reaches the surface of measurement mainly coincide with the position of saturated areas in the field.

The deeper layer with typical resistivity values from 500 to 1200 Ωm fills the complete space underneath the upper layer and may reach to twelve meters of depth. Even though close to maximal penetration depth of the conducted measurements, the bottom border of this layer is characterised by rising resistivity which at some points may exceed 1500 Ωm. Although found at all individual profiles this observed layer shows zones of low resistivity in almost every displayed cross-section (see R1 and P7 as an example).

Electrical resistivity variations inside the layer of low electrical resistivity correspond to some degree to structures which are visible in more than one profile. As an example see the dark blue area with a diameter of six meters surrounded by zones of higher resistivity at the centre of P7 which shifts more and more eastwards until it reaches the right edge of the grid at P4 (Figure 4.24).

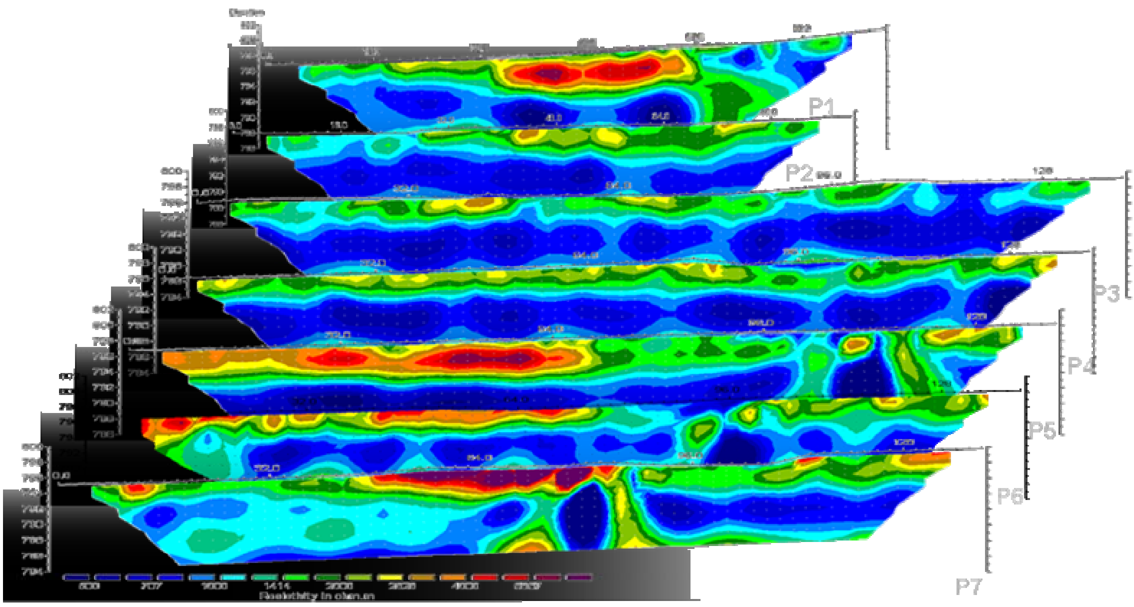

Figure 4.24: ERT raster profiles parallel to stream P1 – P7 (dipole - dipole | 4 m spacing | 24 - 36 electrodes | RMS error 2.3 – 4.9 %) [scale: dark blue = 500 Ωm, purple = 8000 Ωm].

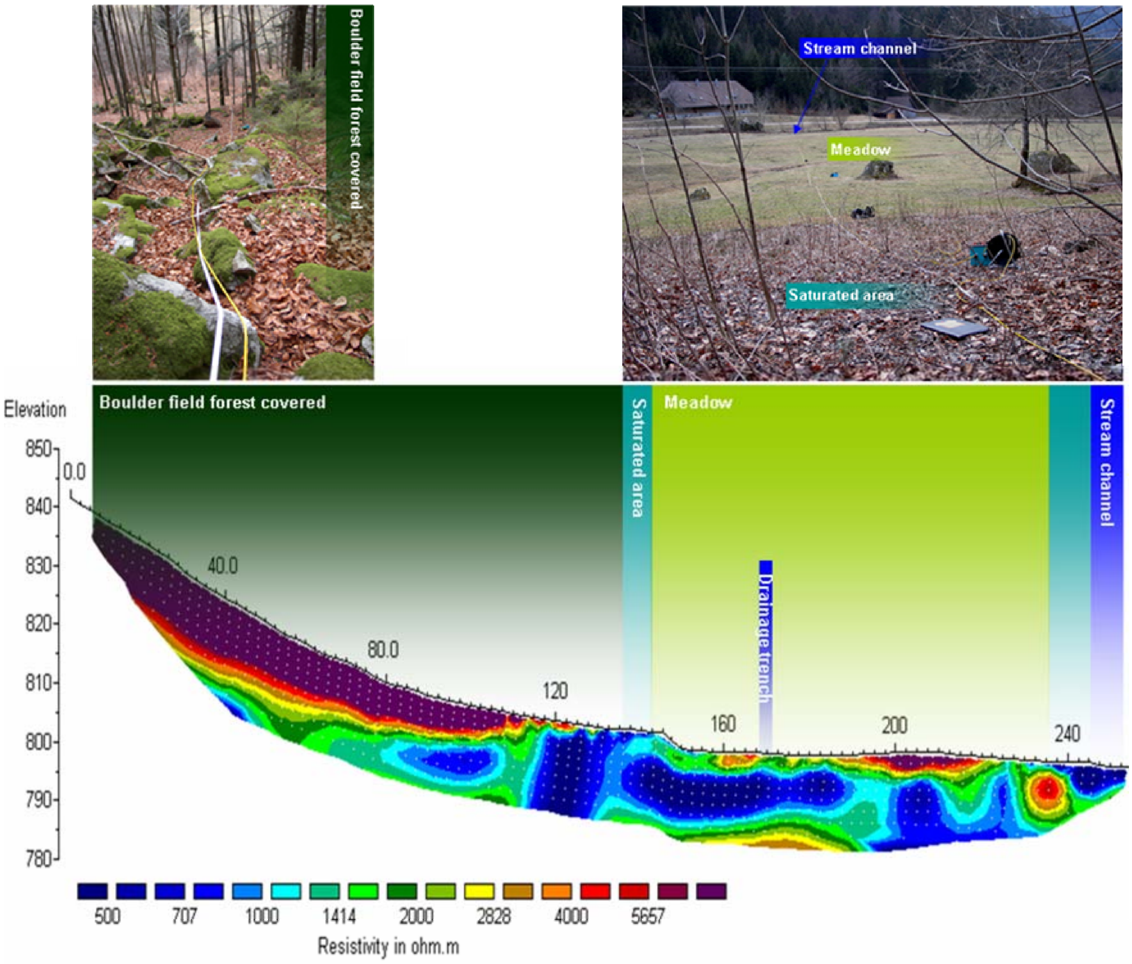

Figure 4.25: ERT slope profile (Wenner | 5 m spacing | 54 electrodes | RMS error 4.5 %) with surface facts.

The electrical resistivity tomography illustrated in Figure 4.25, shows the transition from hill slope to valley bottom. The hill slope part is dominated by high electrical resistivity largely exceeding the applied scale with electrical resistivity values of 20000 Ωm instead of about 8000 Ωm which are maximum values recorded with valley bottom materials. This highly resistive structure thins out towards x = 120 m. Its maximum depth recorded is 14 m at x = 35 m. Underneath this zone of resistivity above 5000 Ωm, electrical resistivity drops down to values of minimum 600 Ωm in depth of 20 m at x = 40 and in 10 m depth at x = 100. At x = 120 m weak resistivity with values between 350 to 600 Ωm prevails in all depths except for the very surface, where 6000 Ωm are recorded. This particular zone has contact to the surface around x = 140 m where a saturated area is located. In depth of about two meters beneath the saturated area a two meter thick zone of electrical resistivity above 1200 Ωm linked to the upper layer of the valley bottom's filling.

The valley bottom part of the profile from 140 m (saturated area) to 250 m (Stream channel) suits the description made in the results of the raster survey well. Regions not previously described are the crossing of stream channel and regions deeper than twelve meters. In vicinity of the stream, resistivity values displayed are to be regarded cautiously as in the settings it was marked in the settings that an additional twelve electrodes are connected from x = 240 m on when in reality there are five. All data connected to this defect was removed before further processing from raw data file. The effect on the remaining data from x = 240 to x = 260 m is not fully understood and thus this area is not part of any further discussion. All data from x = 0 to x = 240 m is not effected by these circumstances. In direct neighbourhood of the stream there is a circular form with approximately five meters in diameter showing resistivities of 3500 to 5500 Ωm. In depth of 15 to 17 m underneath the valley bottom's surface two zones with different properties according to electrical resistivity are drawn. On the right side from x = 190 to 230 m low resistivity with values between 500 and 800 Ωm have been recorded, while closer to the hill slope values from1500 to 3000 Ωm are shown.

General descriptions of results from the raster survey apply fully to the transversal profile represented in Figure 4.26. The zone between x = 0 and x = 32 m is not covered by previously described measurements. From x = 0 m on the upper layer's thickness decreases from depth of roughly four meters until at x = 28 m zones of weak resistivity almost reach the surface where different vegetation can be observed.

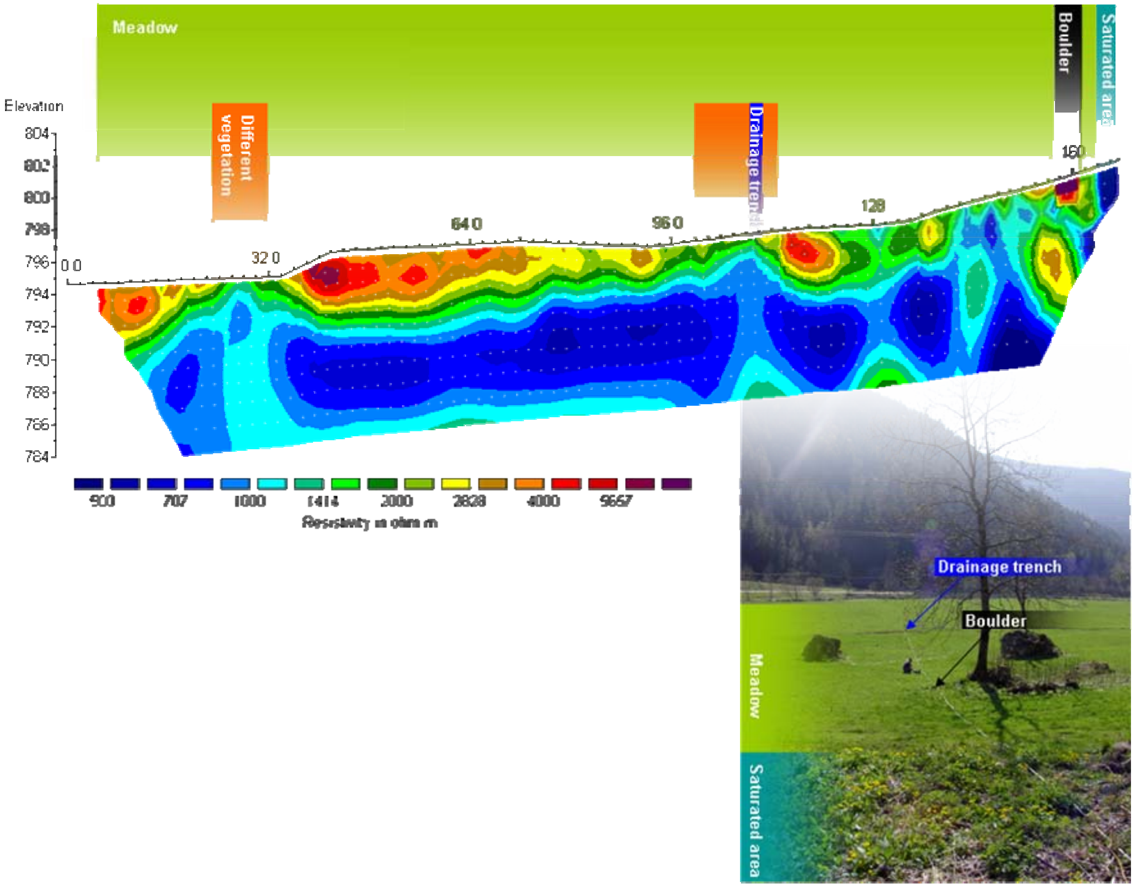

Figure 4.26: ERT transversal profile (dipole - dipole | 4 m spacing | 44 electrodes | RMS error 15.9 %) with surface facts.

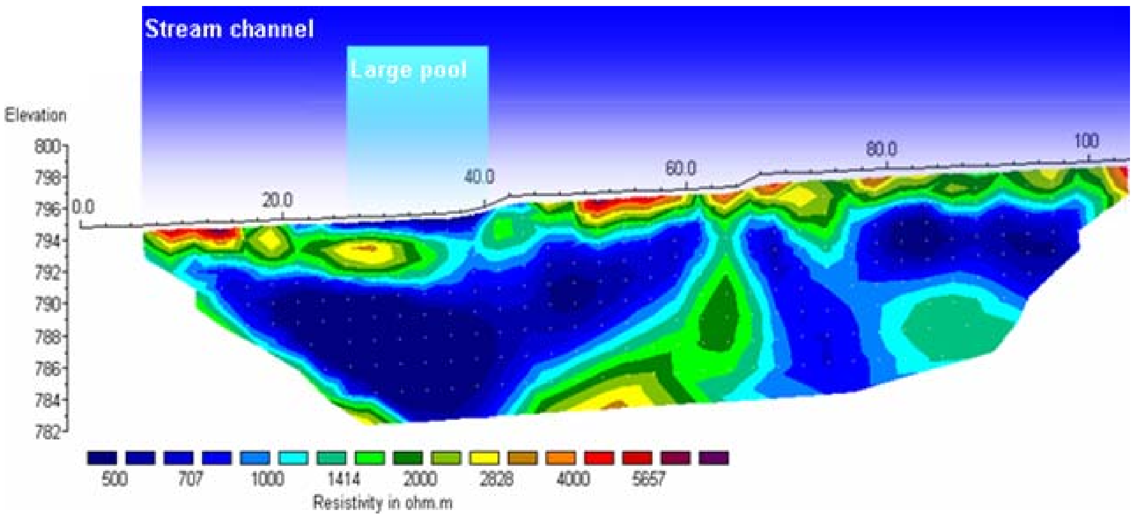

Figure 4.27: ERT stream channel (dipole –dipole | 5 m spacing | 23 electrodes | RMS error 10.5 %) with surface facts.

In Figure 4.27 strong electrical resistivity prevails in areas close to surface of the ERT results and may attain values up to 7500 Ωm. Weakest electrical resistivity (200 Ωm) is encountered 8.5 m beneath a large pool which is at the surface at x = 30 m. Though all electrodes are placed in open water in the stream channel, low resistivity values at the surface are only recorded between x = 30 and x = 40 m, where a large pool is located with a maximum depth of one meter at the time the measurement was conducted. As described in chapter 3.5 wide spacing (in this case five meters) cannot provide information on the top structures with depth smaller than circa half a meter. In this profile, low resistivity with values from 500 Ωm to 1200 Ωm is mainly distributed inside an upper boundary of maximum 1.5 m and a lower edge of 12 m, which corresponds in some places to the maximum penetration depth achieved at this transect. It is disturbed by zones with 2000 Ωm at x = 62.5 m, eight meters deep and 1400 Ωm at x = 85 m, ten meters underneath the surface. Other areas with an electrical resistivity from 1200 Ωm to 2900 Ωm are shown along the left rim from four to twelve meters in depth as well as in twelve meters depth in the middle of the transect at x = 52.5 m.

4.3.3 Temporal resolution

To retrieve information on groundwater dynamics and different soil moisture conditions, measurements of exactly the same transect need to be repeatable to minimize sources of error. Therefore two transects were equipped with electrodes. One transect from December the 12th until January the 24th with 1 m spacing. An additional half meter spacing set up was used at the same profile, from 11th until 24th of January. A second half meter spacing configuration, also from the 14th to the 24th of January, was made up directly crossing the soil-moisture measurement profile (chapter 3.3) in order of comparison. The tomographies were later offset against each other to calculate the change in resistivity related to depth from one time-step to another.

The observation of moisture content in the vadose zone as well as a shift of the saturated zone throughout an event may offer an important opportunity for understanding processes. The comparison of two tomographies of the same profile provides a relative image of the chosen transect. Not the specific electrical resistivity properties of the individual solid subsurface structures are pictured but the properties of the liquid phase transported through them.

A survey of the same transect in different conditions (throughout an event) yields information about process dynamics and the differences between two time steps are of interest.

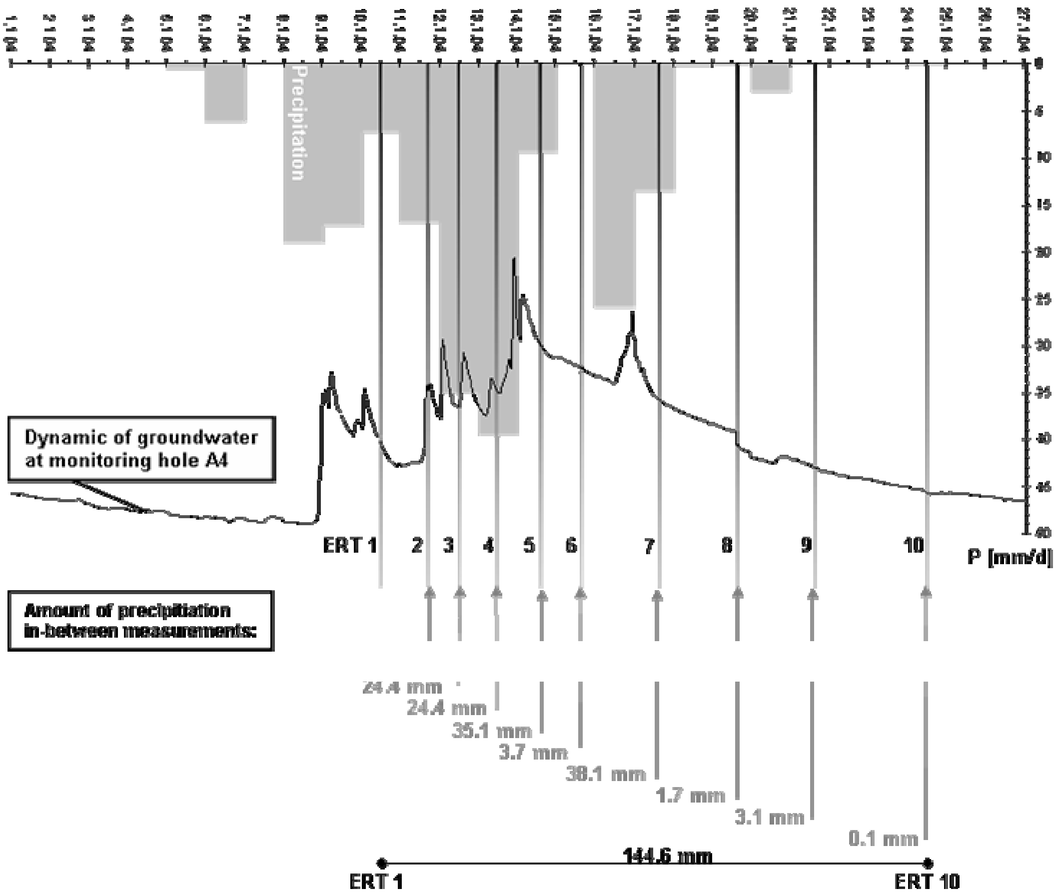

Figure 4.28: Exact point in time of ERT 1 to 10 in combination with the amount of rainfall between the individual time steps.

Table 4.3: Properties of conducted electrical resistivity tomographies.

ERT	Array type	Spacing *(profile length)*	Number of electrodes	RMS error	Date
1	Wenner	1 m *(24 m)*	24	%	11h40 10.1.04
2	Wenner	1 m *(24 m)*	24	%	17h10 11.1.04
2b	Wenner	1 m *(24 m)*	24	--	19h00 11.1.04
2c	Wenner	1 m *(24 m)*	24	--	21h30 11.1.04
3	Wenner	1 m *(24 m)*	24	%	12h10 12.1.04
3b	Wenner	1 m *(24 m)*	24	--	16h30 12.1.04
4	Wenner	1 m *(24 m)*	24	%	11h40 13.1.04
4b	Wenner	1 m *(24 m)*	24	--	13h20 13.1.04
5	Wenner	1 m *(24 m)*	24	%	14h20 14.1.04
6	Wenner	1 m *(24 m)*	24	%	15h00 15.1.04
7	Wenner	1 m *(24 m)*	24	%	15h10 17.1.04
8	Wenner	1 m *(24 m)*	24	%	15h20 19.1.04
9	Wenner	1 m *(24 m)*	24	%	14h40 21.1.04
10	Wenner	1 m *(24 m)*	24	%	11h40 24.1.04

The inversion software Res2Dinv holds several options to calculate the inversion models for each time-step recorded. Changes in resistivity between different time-steps may be the result of a true change in resistivity from one time-step to another, but may also be caused by inaccuracy of the measurement. To minimize the effect of failures in measured resistivity, the software features options where the different time-steps are “constrained” from calculation. However, as each particular time-step showed accurate results, it was preferred to choose no constrain between the time steps and let the programme calculate the inversion for each time-step independently and afterwards subtract the tomographies to achieve as a result the differences in resistivity from one time step to another.

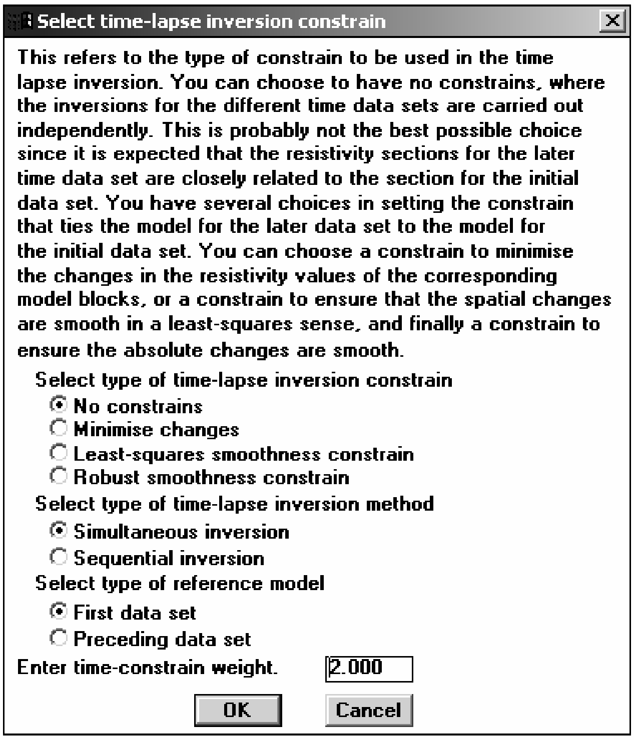

Figure 4.29: Screenshot from Res2Dinv programme, time-lapse configurations.

Regarding the results from examining the different types of constrain between the individual time-steps (Figure 4.29) it was found that the actual type of inversion constrain was not a sensitive parameter as each setting showed well comparable results. Constrains between the time-steps are meant to reduce the effect of possible high signal-to-noise-ratio or other differences between the measurement not caused by changes in moisture conditions (LOKE 1999). The programme however, does not know about the reason for an eventual change in resistivity and therefore might even-out true moisture changes. Another parameter with little sensitivity was the type of reference model. Choosing “preceding data set“ is recommended to balance large discrepancies between individual time-steps, as they might add up if “first data set” is chosen as configuration. No such inconsistency of the data set seemed existent. The third parameter of little influence to the later results was the “time-constrain weight”, which sets the relative importance of similarity between a time-step model and its reference model. Nevertheless, large differences were recorded choosing either “Simultaneous inversion” or “Sequential inversion” as time-lapse inversion method. Using “simultaneous inversion”, each iteration step of one time-step is followed by the calculation of the same iteration step at the consecutive time-step. In contrast with the use of “sequential inversion”, each time-step’s iteration steps are completed before the following time-step’s iteration is calculated. In the software’s documentation it is recommended to select the “sequential inversion” method in case of large resistivity contrasts, which do appear in the calculated data set. However, large discrepancies in the results of the two alternative inversion methods showed. These differences were related to a different ratio of change in resistivity, but to some degree also showed varieties in special distribution of zones with rising electrical resistivity values compared to zones with weaker electrical resistivity values. A comparison of these methods with inversions which were carried out for each time step individually showed that the sequential method results were less matching the individual inversion results than the results from “simultaneous inversion”. Thus the sequential results are not part of the further discussion, but can be found in Figure A 9.

Figure 4.30 shows the results of the time-lapse electrical resistivity experiment conducted at the ERT *a* profile. The electrical resistivity tomography result from the 10th of January is displayed on top of the figure. A detailed description of this cross-section is given in chapter 4.3.1. Consecutive time-steps are displayed below the initial measurement and the colour scheme used does not monitor the true electrical resistivity values as shown from the source time-step, but their electrical resistivity ratio calculated from their dissimilarity towards this base time-step from the 10th of January. In contrast, the values of precipitation monitored at the right side of the figure give the volume of rain between two consecutive time-steps, as the time units are in the order of one to three days and precipitation is split to several events (Figure 4.28).

The border between the regions coloured in dark green and olive green equals no change in resistivity from the displayed time-step to the 10^{th} of January. Maximal changes do not exceed 17.5 % lower (blue), as well as 12.5 % higher (red) electrical resistivity than recorded January the 10^{th}. In the course of the time-lapse experiment no regions were monitored where electrical resistivity constantly weakens. During the first days of the event electrical resistivity in the first meter of the cross-section is generally decreasing, but showing wavering from one time-step to another.

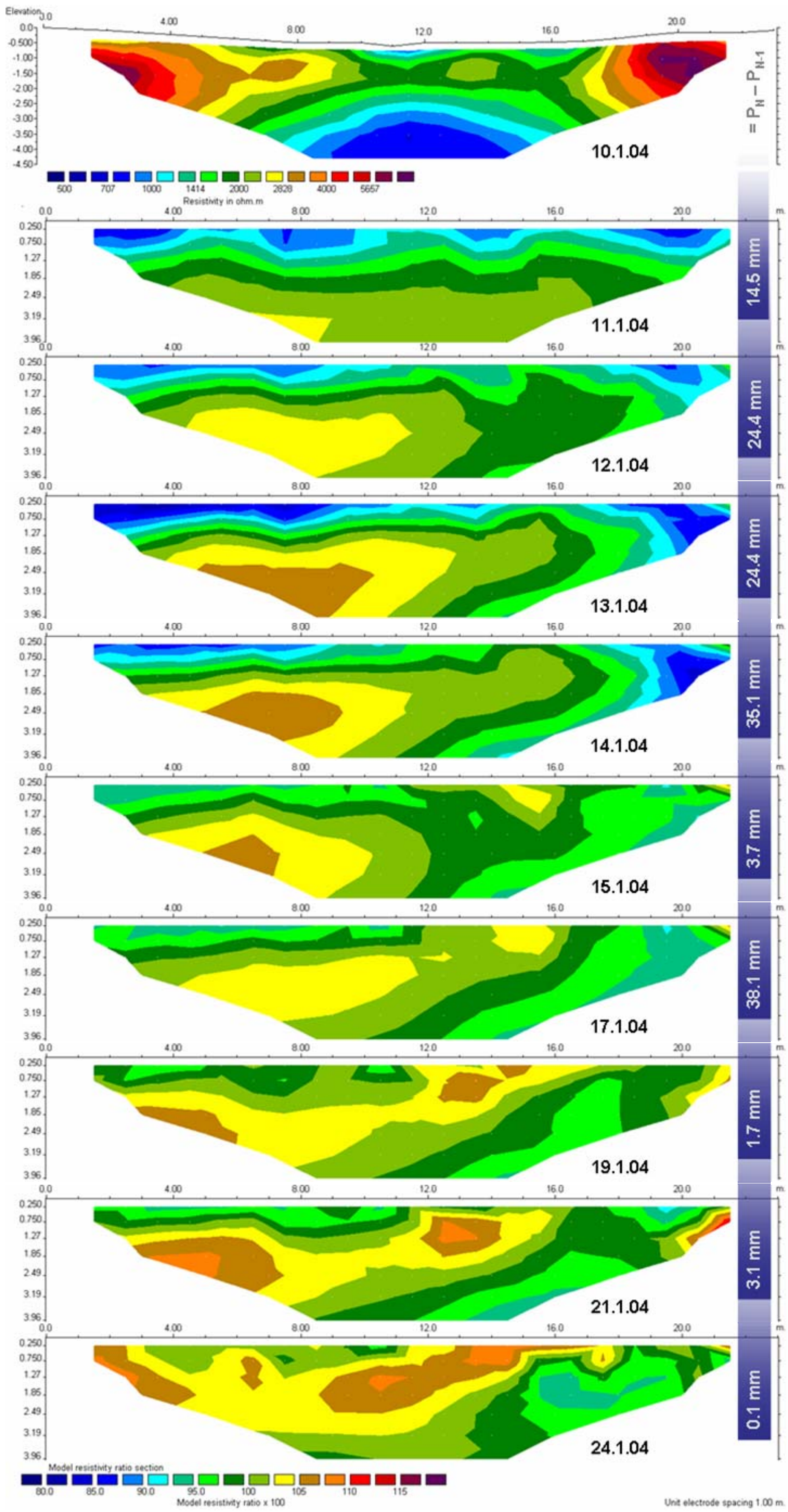

Figure 4.30: Time-lapse model calculated with the simultaneous inversion method.

Lower electrical resistivity values show maximal spread on the 11th and the 13th of January. An additional drop of resistivity is recorded from the 15th to the 17th though from a higher basis. A region with particularly strong changes in resistivity is located at the right side of the profile at x = 20. Values down to 85 % of the initial resistivity are recorded and their centre continuously shifts downwards from the 11th to the 14th and finally reaching the initial level on the 17th of January. Also at the right border of the profile but in depths of more than 2.5 m, electrical resistivity values shrink until January the 21st. Although continuously declining, values do not drop beneath 92.5 % of the base value. In general, electrical resistivity in depths greater than 2.5 m does not show changes of more than 5 % from values of the 10th January. An exception is the 13th and the two consecutive days, where values rise to almost 107.5 % of the base values. Here it is possible to depict tendencies of rising electrical resistivity until the 13th which then declines until the 17th of January. The 13th of January is also the day with the highest contrasts in the development of resistivity between the weakening resistivity at the surface and the rising electrical resistivity at the left bottom of the profile. Electrical resistivity rising to values of 107.5 to 110 % is only observed on January the 21st and 24th in zones between 2.5 m and 0.75 m at the 21st and 0.25 m at the 24th of January. Horizontal lines, persistent over the whole profile are more or less monitored on the 11th of January, but are less obvious and finally disappear towards the end of the time-lapse experiment.

5 Discussion

5.1 Comparison of dipole – dipole and Wenner array

The choice of dipole-dipole or Wenner switch depends on the researcher's interest on the outcome of a particular measurement. Factors on decision making are time, quality aspired, horizontal or vertical heterogeneity of the subsurface and penetration depth. The dipole-dipole array measurement consists of about double the datum points the Wenner array does. This is due to its geometrical concept on which the array's mathematical formulation, used to calculate true depth and resistivity, is based.

The Wenner array's geometrical concept is shown in Figure 5.1. The distance a is defined equal between all four electrodes (current electrodes and potential electrodes). This is the limiting factor on possible switches on the basis of (in our case) 24 electrodes. In case of the Dipole-dipole array (Figure 5.2) only the distance in between the two current electrodes as well as the distance in between potential electrodes is fixed. The spacing between current electrode pair and potential electrode pair is modified in order to measure the profile. Thus there are more combinations switching between the 24 strung electrodes.

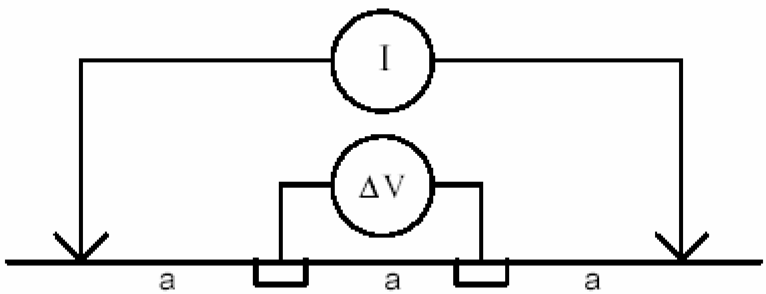

Figure 5.1: Geometry of the Wenner array. The depth of sounding is controlled by distance a (CARDIMONA 2002).

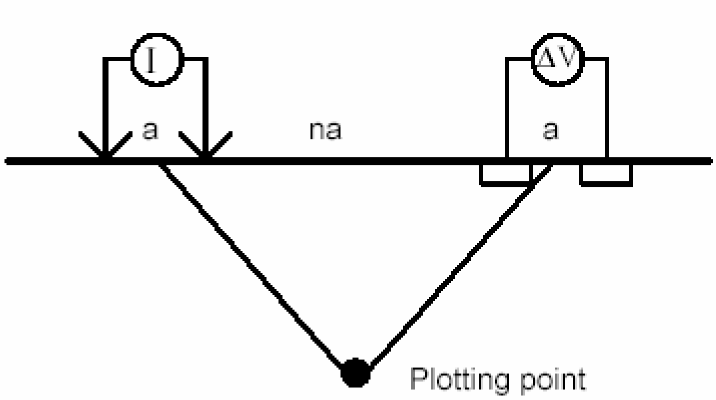

Figure 5.2: Geometry of the dipole-dipole array. The depth of sounding mainly depends on the distance na, as distance a is fixed throughout a 2D survey (CARDIMONA 2002).

Apart from the number of measurements per profile, other factors on spatial resolution might play a role but remain difficult to assess. Eventual influence caused by the difference in alignment is for example shown in the signal to noise ratio of the two arrays. Due to the potential electrode pair's position in the center of the current electrode pair, the signal received is rather strong (ZHOU 2002; ZHOU 2000) compared to dipole-dipole array, where the potential electrode pair is either located left or right of the current electrode pair. Thus a higher deviation is recorded and the latter inversion will be defined less accurately. However, the accuracy of the Wenner array's electrical resistivity tomographies is based on fewer measurements.

Another advantage of the Wenner array is its deeper penetration depth. Though, due to its pyramid structure of plotting points (Figure 5.3), it bares less and less reliable information reaching deep subsurface. The deepest level of penetration is represented solely through one measurement. The dipole-dipole array as well looses consistence with depth, but each depth level is mapped according to several measurements (Figure 5.4).

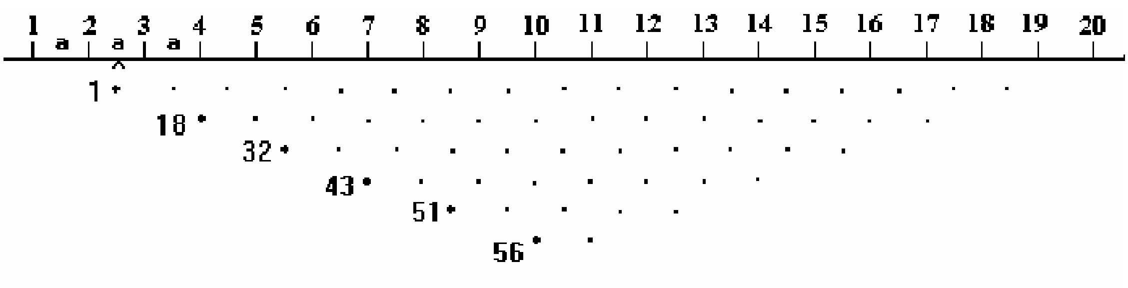

Figure 5.3: Wenner switch plotting points beneath the electrodes (1-20) (LOKE 2000).

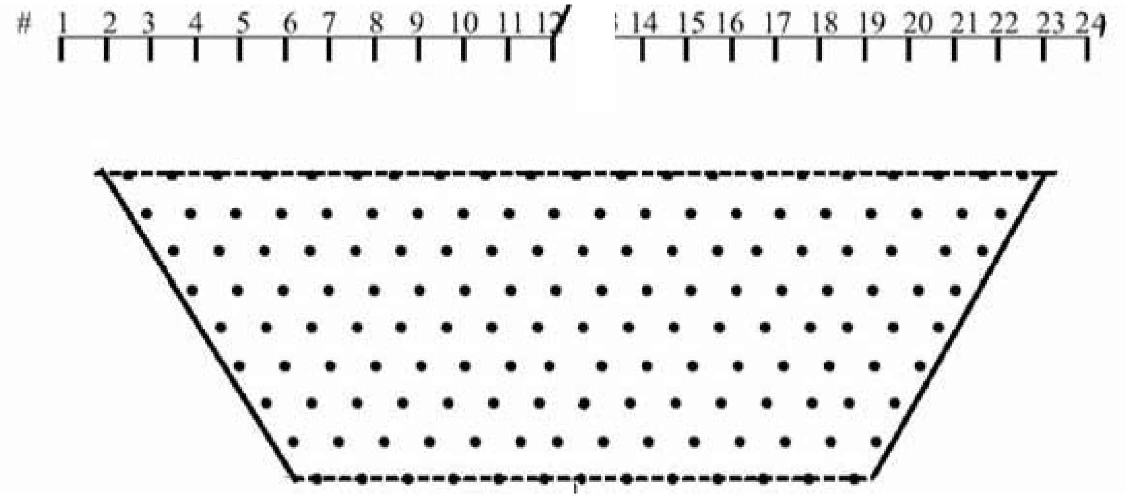

Figure 5.4: Dipole-dipole switch plotting points beneath the electrodes (1-24) (Syscal Kid operating manual, 2001).

5.1.1 Conclusion

Overall, the dipole-dipole array is the better geometrical concept to cover information on a transect under unknown conditions. One is able to detect anomalies applying dipole-dipole electrical resistivity tomography which are averaged out in Wenner electrical resistivity tomography as a result of the smaller amount of data collected at each profile. If possible however, both arrays should be applied and compared. When the attained results match the researcher's requirements on a particular site and subject the Wenner array's benefits lie in its being less time and data intensive. During a field campaign for example, this enables to cover a larger area with additional profiles or achieving better temporal resolution in studying groundwater dynamics.

5.2 Soft information

Relatively moist conditions from previous rainfall supported the formation of overland flow during the heavy storm event in mid-January. However, water table in groundwater monitoring holes was relatively low at its starting point. Different hydrological processes can be identified as a source for overland flow which even occurred days after rainfall stopped. Infiltration (at compacted soils) and saturation excess (at saturated areas as well as micro-topographical sinks) was observed. Overland flow produced by water which comes out of the soil might be either due to subsurface stormflow transformed to return flow or up-welling from pre-event water forced by piston flow effects. Dependent from the prevailing conditions and location of a zone where water emerges, the one or the other hypothesises might characterise the dominant flowpath. Return flow might be associated to the leakage of water at the edge of the boulder field which after traversing the surface of the valley supplies the pond (e.g. Figure 4.1). While the up-welling of groundwater could be the better explanation for water coming from macropores (e.g. molehills) as well as directly from the soil (e.g. Figure 4.3). The latter hypothesis is supported by different indications. First, their location, in some cases a 100 m away from the hillslope itself (e.g. Figure 4.4) in areas with relatively little incline does not exclude return flow but makes it less probable. Second, even after days with snow cover and air temperatures below zero (Figure A 2) these sources were still active (chapter 4.1). The difference of starting and end point between macropore sources and water emerging from regular pores might add to the idea of strong influence of groundwater under pressure. As friction is relatively stronger in smaller pores the effect of the pressure gradient on rising of the water is less distinct. Thus in pores with larger diameter, a smaller gradient of pressure is sufficient for the water to reach the surface.

This effect could also be observed in vicinity to an artesian source during dry conditions. In that case the surface was only moist until an artificial macropore was formed through the use of a stake of two centimetre diameter, which made a pathway available for water to get to the surface.

5.3 Subsurface structures

Shallow and intermediate aquifer parts

The top layer might be described as a horizon of more than 20 cm thickness well spread throughout the valley bottom. It possesses high content of biological matter (soil probing by WENNINGER (2002) and personal observation) and shows relatively good hydraulic conductivity. At some regions it is possibly followed by well sorted alluvial sedimentation associated with higher hydraulic conductivity. Depth of 80 cm could be concluded from Figure 4.14 and Figure 4.16 as well as the time-lapse results (see Figure 4.30) and the electrical resistivity cross-section of the stream channel (Figure 4.20). Accordingly, high amounts of gravel in little depth detected whilst placing the steel electrodes for the stream channel survey could be an artefact of an ancient stream bed where maybe a pool was located in this area. The possible alluvial sediments, which are sorted in contrast to the mixed glacial sediments found in their neighbourhood, would show good hydraulic conductivity and function as drainage. The weak resistivity at the left from the loose stonewall is possibly through human influence as a result of the construction of the wall, also possibly more sorted.

The subsequent 20 to ~250 cm (at some places depth 500 cm occur) show a massive proportion (~80 %) of gravel up to boulder size. This upper layer's pores are filled with material of all kinds of smaller grain sizes down to loamy, sometimes clayey material. Thus the regular properties of gravel aquifers (good hydraulic conductivity due to large pores) are neglected. The existing pore volume between gravel is filled with sand, silt and loam. Where loam may imprint its hydraulic conductivity properties on the whole layer (compare to Figure 5.5), the volume of water which may be transported in this type of mixed material is of low quantity (the normally high pore volume of pure loam is reduced with every piece of gravel see Figure 5.6).

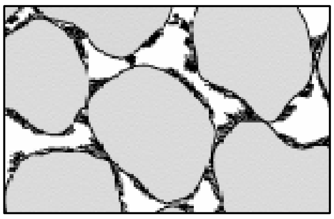

Figure 5.5: Schematic sketch of clay minerals clogging gravel pore-space (after BORUS 1999).

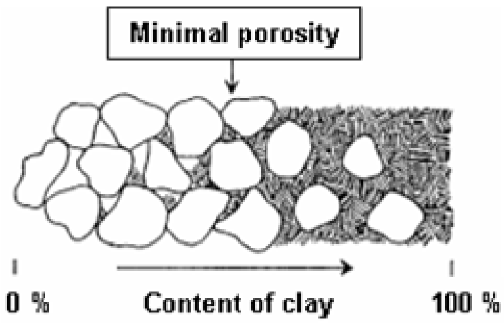

Figure 5.6: Mixture of sand and clay with increasing content of clay and decreasing content of sand (after MARION 1992).

The smaller ohmic resistance of the third, deeper layer may be described through two alternative hypothesises. While the origin of all material filling the valley bottom is assumed similar (see chapter 2.3) in terms of their resistivity properties and the upper, more resistant layer is no less saturated (water level is constantly recorded at depth not exceeding 130 cm), a higher percentage of water filled pore volume possibly explains the better electrical conductivity. Thus the discrepancy between the second and third layer may be either through decrease in the fraction of gravel to the benefit of grains with smaller diameter or the absence of small (e.g. loamy) particles. Both eventualities result in larger pore volume responsible for better hydraulic as well as electric conductivity. The options presented are not to be seen independently but most likely connected, each in parts responsible for the overall change. According to a drilling conducted on the 7th of July 2004, the less resistive layer mainly consists of sandy material with fractions of smaller gravel as well as a less significant amount of cohesive matter.

Two main structures and their transition zones are described in the results of the raster survey. The idea of two aquifer parts may be introduced and their hydrological properties addressed. Based on the raster survey it is possible to describe the layers spatial distribution as well as each layer’s specific heterogeneity. The upper layer clearly shows variation in thickness and state. The thought of associating strong electrical resistivity to poor hydrological conductivity in case of the upper layer is supported by observations on the field’s surface. In regions where the upper layer is relatively thin and electrical resistivity of less than 1500 Ωm are recorded, plants dominate which otherwise may be found in proximity of saturated areas. Zones of electrical resistivity lower than 700 Ωm reaching surface often correlate with saturated areas. For example almost every saturated area crossed by one of the electrical resistivity profiles is connected to the deeper aquifer by a band of low resistivity.

It can be stated that this connection does not simply display higher degrees of saturation of the more resistive layer as it has been shown that this layer only has little sensitivity towards change in moisture (see chapter 4.3.3). Thus presence of different materials with better hydrologic conductivity can be assumed. However, this conclusion does not provide information about the direction of flow in these linkages between the surface and deeper aquifer. Therefore additional information is needed to discuss whether there exists a deep, at least partly confined aquifer which supplies the saturated areas or whether these areas are laterally fed and water percolates to depth by the means of this pathway.

If one neglects the possibility that a confined deeper aquifer can supply water to the saturated areas at the surface due to its pressure, it is necessary to have other supplying sources. From electrical resistivity tomography it is known that there is no water supplying layer other than the top layer possible. Anyhow, this layer is shallow and therefore may often dry out completely. Existing small preferential flowpaths or thin layers might not be covered by electrical resistivity tomography even with the use of half meter spacing and need to be discussed. However, it is difficult to associate these small structures with almost constant water supply to saturated zones throughout the year. A steady source though is needed to create a saturated area at the research site where water is drained through trenches. Moreover, if one follows the idea that no groundwater under pressure supplies the saturated areas, the zones of low resistivity beneath the saturated zones should feature impermeability instead of the assumed permeability to hinder loss of water towards groundwater. This would mean that there must be a structure with even less hydrologic conductivity than the discussed upper layer which seems only possible if pore space between the approved proportions of gravel is filled with clay instead of loam or larger grains. Only small amounts of clay clogging the pores of a structure similar to the upper layer would not produce such a change in resistivity. Pores between the gravel completely filled with clay might be able to produce the recorded drop in electrical resistivity. However, a mixture of almost pure gravel and pure clay seems nearly impossible to imagine with the existing knowledge of the study area. To explain a massive difference in electrical resistivity compared to the known mixture of gravel with all kinds of grain-sizes in the upper layer only having the information that gravel is also existent in this structure, can be only done through a reduced proportion of other grain-sizes filling the gravel’s pores. This would result in better hydrologic conductivity compared to the upper layer.

The saturated area at the hill slope valley bottom interface needs to be considered separately. Addressing the slope's electrical resistivity is based on several assumptions as additional data for interpretation is limited to the knowledge about the visible surface and general information about the regions geology.

Known structures impose that the high electrical resistivity close to the surface is caused by huge boulders with relatively large gaps in-between, which are filled with loose material and air. It is not known to which depth this structure may reach. At the bottom of the survey, weak resistivity allows the assumption that bedrock is not detected within this tomography. The third known fact is that the low resistivity values at x = 140 m are associated with a saturated structure underneath a saturated area, where we do know about the presence of gravel as also described for other saturated areas. The difference here is the saturated area's position on top of a small hill in connection to the adjacent hill slope. From the slope profile (Figure 4.25) it is interpreted that the confining upper layer from the valley bottom's filling is not existent beneath this saturated area. However, it is not known whether the confining layer continues up the slope framed by the boulder field on its top and the zone with lower resistivity underneath. Abstracting away from the possibility of potential other layers with different electrical resistivity signature than the ones previously described enables to establish a concrete concept of the hill slope which is presented in chapter 6. Anyhow, a layer with little permeability underneath the boulder field and no transitional layer in-between damping the discrepancies of the two systems would result in a horizon of sources at the impermeable layer's outcrop along the slope during bigger events. No such observation was made neither any clear traces of such have been recorded above this saturated area. Observation period might have been to short in order to solve this issue, though one event with extreme conditions was witnessed (see chapter 4.1).

According to the band of low resistivity illustrated in Figure 4.25, one could suppose that the deeper layer of the valley bottom continues up the slope. Hence, the upper border of the low resistivity values might be interpreted first as the layers upper edge or second a level of high moisture content (maybe groundwater) inside the layer.

The deeper layers variations in its electrical resistivity pattern possibly illustrate its heterogenic character. The variation in resistivity values is either due to changing electrical conductivity properties of the material and/or changing properties of the water. Another possible factor could be possible inaccuracy of the measurements.

Inaccuracy of measurement is difficult to asses, as no facts on the deeper layer were available. However, supported by several indications imprecision is not assumed to be the determining factor for these anomalies. First, the anomalies could be discovered using dipole – dipole as well as Wenner array (compare for example the slope profile (Wenner array) and raster grid (dipole – dipole array)). Second, a possible influence from the upper layer's existing diversity on deeper regions of the measurement is calculated as described in chapter 3.5. Thus the presented images are free of influence from divergence in upper horizons. Third, anomalies can be depicted in multiple cross-sections and because of the spatial resolution obtained by the raster survey patterns (instead of chaotic variation) can be depicted.

Hence, these variations in electrical resistivity do signify subsurface changes in material or water quality. A regional difference in conductivity of water however, must be coupled to changes in the aquifers hydraulic properties. These changes can be found throughout the entire set of ERT with wide spacing.

Figure 5.7 shows the spatial distribution of these structures, where the most accentuated structure is marked in red, while slighter variations in the subsurface are coloured blue. Due to the distance of fifteen meters inbetween cross-sections a concrete mapping of structures was not feasible, as several options of associating one profile to another are possible. As an example green flashes indicated alternative links from one profile to another in Figure 5.7. Moreover, similarity between tomographies may also be identified through special arrangement of zones with lower and higher resistivity. These are indicated by circles and crosses in the excerpt at the bottom of the figure.

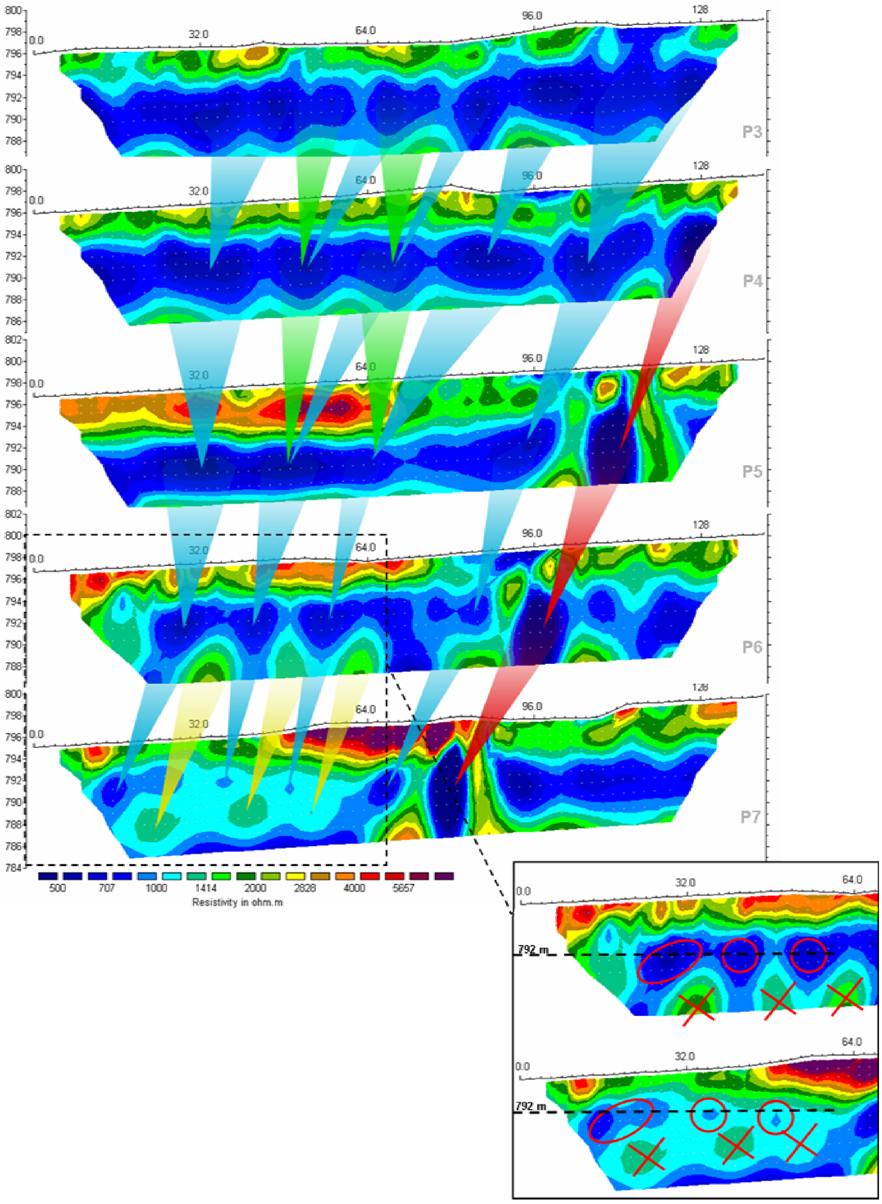

Figure 5.7: Repeating structures in the deeper layer.

The studied electrical resistivity tomographies indicate that water flow is not only at variance horizontally (in depth) but also vertically, inside a single layer. Consequently, the deeper layer can be envisioned as a region where the proportions of different grain sizes are not evenly distributed. But however, regions with similar hydraulic conductivity appear to be linked to each other.

Stream water – groundwater interface

The channel profile reviewed in Figure 4.20 shows that the stream is encircled by regions of strong resistivity. With regards to electrical resistivity only directly underneath the river bed this image is confirmed by Figure 4.27 for the next 100 m upstream. The zone of weaker resistivity beneath the labelled pool in

Figure 4.27 is an exception to this observation and is considered separately. In regions with well sorted sediments, high resistivity implicates the presence of a gravel layer with its typical good hydraulic conductivity. However, in the research area these well sorted gravel layers are not common. Instead a gravel layer with its pores filled with small grained material as described above might be more probable. Still this supposition must not be correct as the ERT alone does not prove either one of the interpretations.

Nevertheless, assuming well sorted gravel (which does exist in the stream bed at the very surface) also as interface material to the groundwater body is doubtful. Indication to this doubt is provided by electrical resistivity tomography, artesian sources as well as stream- and groundwater data.
First of all structures clearly identified as gravel mixed with smaller grain sizes down to loam are visualized through the use of ERT in the test field, seem to continue in the river bed at same level (though thinned out to some degree (Figure 4.27)). The presence of an artesian source 4 m from the 80 cm deeper situated stream bed (see chapter 4.1) with an electrical conductivity of 92 µS/cm shows that the pressure of the groundwater is not fully released by the channel which is in its close vicinity. In case of a good coupling via a gravel interface between stream and groundwater, no such discrepancies in the level of pressure appear likely.

Considering environmental tracers, the characteristics of stream and groundwater data imply influence of deeper groundwater to the stream due to high silica values. At the same time very low values of electric conductivity and large fluctuations of stream water temperature during base flow might be a sign for strong influence from shallow aquifers.
However, the paradox of high silica values in combination with extremely low electrical conductivity possibly even supports the assumption that deep groundwater is stream water's main source, as sources of deep and old water presumably from fractured bedrock aquifers in the research area show similar chemical patterns with little alkaline cations and relatively much silica (UHLENBROOK, personal communication 2004, UHLENBROOK (1999), KIENZLER (2001)). In line with high silica values, high values of electric conductivity may

also show longer residence times, but are assumed to mainly relate to processes in zones of very active weathering of rocks and soils rich on basic cations instead of deep fractured bedrock zones already exposed to weathering for a long time. The better electric conductivity of the upper groundwater monitored at the test site fits these general remarks and supports the hypothesis of a perched stream channel in the studied area. A concept of a stream channel which is primarily fed by sources of deep groundwater in the upper catchment and which is not influenced by diffuse inflow of groundwater monitored at the test site itself is furthered by the stream water's temperature time variation curve. Even-tempered groundwater does not balance the air temperature's influence for strong stream temperature oscillations have been monitored (chapter 4.2.2, Figure 4.11). These data cannot give much information on the amount of stream water feeding the groundwater body. Thus, statements on this issue remain uncertain until further investigations have been accomplished. However, it can be assumed that there truly is poor coupling as it is described which surely has limiting effect on effluent flow. The possible influence from stream on groundwater is imagined to be only punctual, as an extensive contribution would presumably result in a severe reduction of discharge while passing the examined field site during conditions of low groundwater level.

5.4 Monitored groundwater

Competing theories were considered about the origin of water mainly responsible for water height in the groundwater monitoring holes. Before ERT was applied, one "continuously heterogenic" valley bottom aquifer underneath a thin confining horizon was more or less assumed and data recorded was interpreted as the true hydraulic head of it. But images of subsurface electrical resistivity showed that the poorly conductive layer confining it may reach depth of three to five meters whilst groundwater monitoring holes are maximally two meters deep. Therefore, it is prone to think that water height in the monitoring holes is not well coupled with the deeper aquifer and does not show its actual hydraulic head. Smaller pore diameters in an aquifer influence water velocity and friction, while these two factors again modify the affect of pressure. Thus the recorded water height data depends on the distance between the bottom of the monitoring hole and the deep aquifer with its wider pores (VOGEL, 1995, 115pp). Yet, considering the monitored heterogeneity at the research site, this has not been proven and some or all monitoring holes might have a good hydraulic connection to the deep aquifer. An exact detection of the position with ERT of groundwater monitoring holes in the subsurface is not possible due to the disturbing influence of their metal construction.

Another possibility is the parallel existence of two clearly separated aquifers with individual piezometric heads. Evidence or further indication for either one of the theories might be obtained by samples of deep groundwater.

Overall, fast and strong response may be generated by two factors. At first, the extremely small pore volume is quickly saturated and thus a few millimetres of rainfall create centimetres of phreatic rise. Capillary forces possibly accelerate transport through the vadose zone of an almost impermeable zone due to its small pore space and possibly create *capillary fall*. Secondly, strong and quick response can be generated by a rise in pressure. Water from more conductive deeper aquifer part is forced into the upper aquifer part due to the deeper layers connection to the hillslope.

The experience off the snowmelt event (Figure A 2) shows that the water table in the groundwater monitoring holes may rise quickly after infiltration begins and does so in a significant manner. If assumptions that snowmelt can be seen as a local source contributing to the groundwater are correct, it can be stated that the recorded quick response is not necessarily due to pressure transmission. Thus local infiltration might be, at least to some extend, the responsible factor which can explain most of the recorded hydrometric data. The changes in the hydrograph can be caused by actual transport of event water molecules. This hypothesis is supported by the finding that tracer data collected during two events (WENNINGER (2002), SCHEIDLER (2002)) does show dilution which is in agreement with water table rise instead of being delayed. In contrast a water table rise purely evoked by piston flow, would be free from changes in water chemistry. However, many sections of the groundwater monitoring holes hydrographs remain poorly understood dealing with the data and process understanding at hand.

Though the existing set of groundwater monitoring holes does not provide proof of piston flow processes, many indications provided in chapter 4 sustain the assumption that groundwater at the test site is confined. The fact that this is not clearly visible from studying the observation wells can be explained by the small depth of less than 200 cm of the holes which is often not enough to fully penetrate the upper more impervious layer (see chapter 4.3). An alternative explication is the heterogeneity not only of the upper layers thickness but also of the conditions inside the deeper layer (chapter 4.3.2). Pure piston flow might be only proven in distinct zones of the subsurface and is otherwise more or less masked, or diminished by mixing with non piston flow processes.

Comparing the specific time variation curves from each groundwater monitoring hole, it is shown that identical events may produce different quality of response and different character of recession. The knowledge that groundwater monitoring holes mirror hydrologic properties of their filter zone, gives us a hint on heterogeneity inside the monitored aquifer at the test site. The recorded differences however, do not accord to the monitoring holes distance to the hill slope (A4 & A2 act similar, where A3 seems to semblance more to A1). This can be referred to inhomogeneity on the one hand, on the other hand it should be marked that monitoring holes are not located along the same flow path.

It was found through comparison of time duration curves from ground- and stream water that pressure gradient is always directed from the stream towards groundwater (see Figure 4.12). This however, can not be transferred to the entire stream bank as subsurface water pressure-head was observed to also rise well above stream water level at locations some 50 m upstream from the monitoring hole B6 (see chapter 4.1).

5.5 Temporal resolution

No change according to a rise of groundwater table can be depicted from the differences between the displayed time steps in Figure 4.30. The groundwater table measured at groundwater monitoring hole A4 varies around depth of 70 cm which is inside the upper layer with strong electrical resistivity. A small pore volume is associated with this layer. Consequently, changes in moisture content have only small impact on the overall resistivity. In addition, the measured electrical conductivity of water in groundwater monitoring holes is relatively low (regularly beneath 150 µS / cm in winter) and thus does have a less significant influence on the subsurface electrical resistivity than in regions with higher electrical conductivity. Another factor probably making it not possible to identify the groundwater table is the heterogeneity of the material resulting in zones with different moisture content due to varying pore sizes.

However, general influence of moisture is visible as the top regions react rather quickly to the changing conditions between the different time steps which correspond to the general perception of the top layer described in previous paragraphs. Another point fitting the previously made assumptions is the relatively small degree of changes in resistivity of the deeper layer, which is assumed to be permanently saturated. Changes of resistivity in saturated materials can be either provoked by changes in temperature or by changing electrical resistivity of water. As temperature changes are of minor importance with the conditions at hand, it might be less conductive water which provokes a small rise in electrical resistivity at the profile. However, an experimental set-up to improve evaluation of the measurements accuracy is needed to know whether monitored data can be further interpreted or it is simply an artefact from the calculated inversion.

5.6 Conclusions

Data from groundwater monitoring holes (hydrometric and tracer data) does not show evidence of the piston flow effect. However, subsurface structures do provide the structural background for pressure transmission. Proof for one confined flowpath is given through the existence of an artesian spring. Additionally, indication for more than one pathway being confined is provided by several artesian springs ascending from macropores as well as directly from grass covered soil during and after a strong storm event. Under the influence of the strong event, the stream channel was not draining the aquifer sufficiently to counter surface flow evoking from groundwater upwelling even in its close vicinity and after rainfall was over. At least at one point of the study area the stream water level is constantly above groundwater level. Overall, the stream is possibly embedded in the more impervious layer and thus does not show an effective coupling with the valley's aquifer.

The more impervious layer is perceived as hindering the flux between the deeper aquifer part and the topsoil layer which show better hydraulic conductivity. The top layer is the first zone of contact for precipitation input. In case of high precipitation input it is drained by multiple drainage trenches when the more impervious layer underneath is saturated.

Direct communication between the top and the deeper layer is only possible at certain areas which are often related to saturated areas occurring at the surface. Water of the deeper aquifer part is assumed to be mainly supplied by hillslope sediment layers and to an unknown portion by deep aquifer parts (bedrock). Material characteristics are not only differing from one layer to another but also at the inside of the deeper layer, which makes flowpaths of different transmissivity available.

However, the fact that due to the upper layers characteristics the water table cannot rise to the surface in the way a free water table would do may indicate, that the water table measured in the upper layer may correspond to changes of pressure gradient in the deeper aquifer part. In combination with subsurface heterogeneity it can be concluded that the true water table's surface might show for example wavy variations. Illustrating the true water table's surface via ERT is not possible most probably because of the upper layer's composition. Water table measured in the groundwater monitoring holes represents the piezometric head of groundwater in the perforated zone instead of the true distance from zones to the surface under saturated conditions. Consequently, water table can be underestimated (or correct, however) when the influence of pressure from underneath is little and water from the surface plays a bigger role, whereas water table might be overestimated in cases where influence of water pressing upward is strong, as the effect of pressure is more damped by the upper layer in for example a depth of 50 cm instead of 200 cm.

6 Hydrological concept

The idea of an almost free exchange between groundwater and stream water is visualized in the stream bank concept (Figure 6.1). If the groundwater level is higher than the stream's water table, conditions are influent. Vice versa, effluent conditions prevail, when stream water table is higher than the groundwater table. Equilibrium rarely exists, but is attained when there is no difference in pressure heads between ground- and stream water level. Part of this concept is the idea that the stream is centre of all water flow in the catchment, transferring water from some upstream storage to local groundwater during dry conditions and draining the catchment when the groundwater level is high.

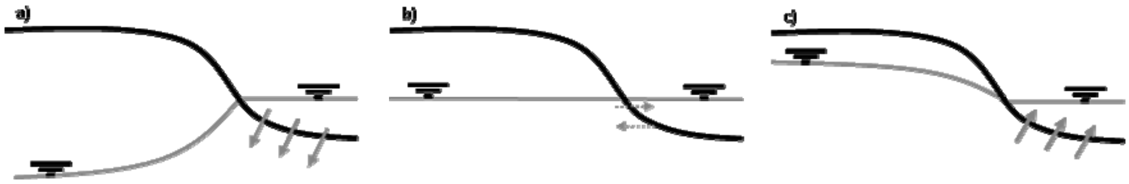

Figure 6.1: Stream bank concept: a) groundwater level < stream water level b) groundwater level = stream water level c) groundwater level > stream water level.

Differences in the water table height at a specific point along the course of a river are caused by the different hydrological properties of the two systems groundwater and stream water. For example a signal, like rainfall from a convective cell on a certain spot in the upper catchment, is modified not only by the distance it travels but also by the materials it passes through. The signal's modification can be monitored with help of the hydrograph recorded in that stream and at a nearby groundwater monitoring hole. These remarks exemplify the probable origin of differences in water level. According to laws of physics, the imbalances between the two systems need to be adjusted. This happens through the interface hyporheic zone. Consequently, the characteristics of the hyporheic zone determine the dynamics of the balancing discrepancies between the two structures. In the research area, this subsurface interface is probably of little importance for the total amount of water moved in the entire aquifer.

Another important factor for the exchange between ground– and stream water is the general hydrologic situation, i.e. whether stream water constantly supplies to groundwater or whether base flow is generated via local groundwater. An examination of the results obtained at the research site, promoted the view that the conditions which define if the stream contributes to groundwater or vice versa seem to vary in local reality (chapter 5.3).

From the interpretation of the ERT slope profile the concept of stream water – groundwater interaction in this area can be derived (Figure 6.2). Due to the assumption that only small volumes of water are exchanged between the two systems, the question, whether influent or effluent conditions prevail seems not significant. Instead of diffuse inflow of groundwater all over the streambed, the stream water level is possibly controlled by sources connected to the main channel via smaller channels which correspond to an increased pressure gradient in the aquifer with higher yield. Fast lateral flowpaths in shallow depths supply event water to the stream. The groundwater table may still be below the stream water table and due to higher stream water level more, but still little stream water may infiltrate (Figure 6.2 b)). In zones with a thin or non-existent confining layer, the confined groundwater body may evacuate pressure towards the stream channel (Figure 6.2 c)).

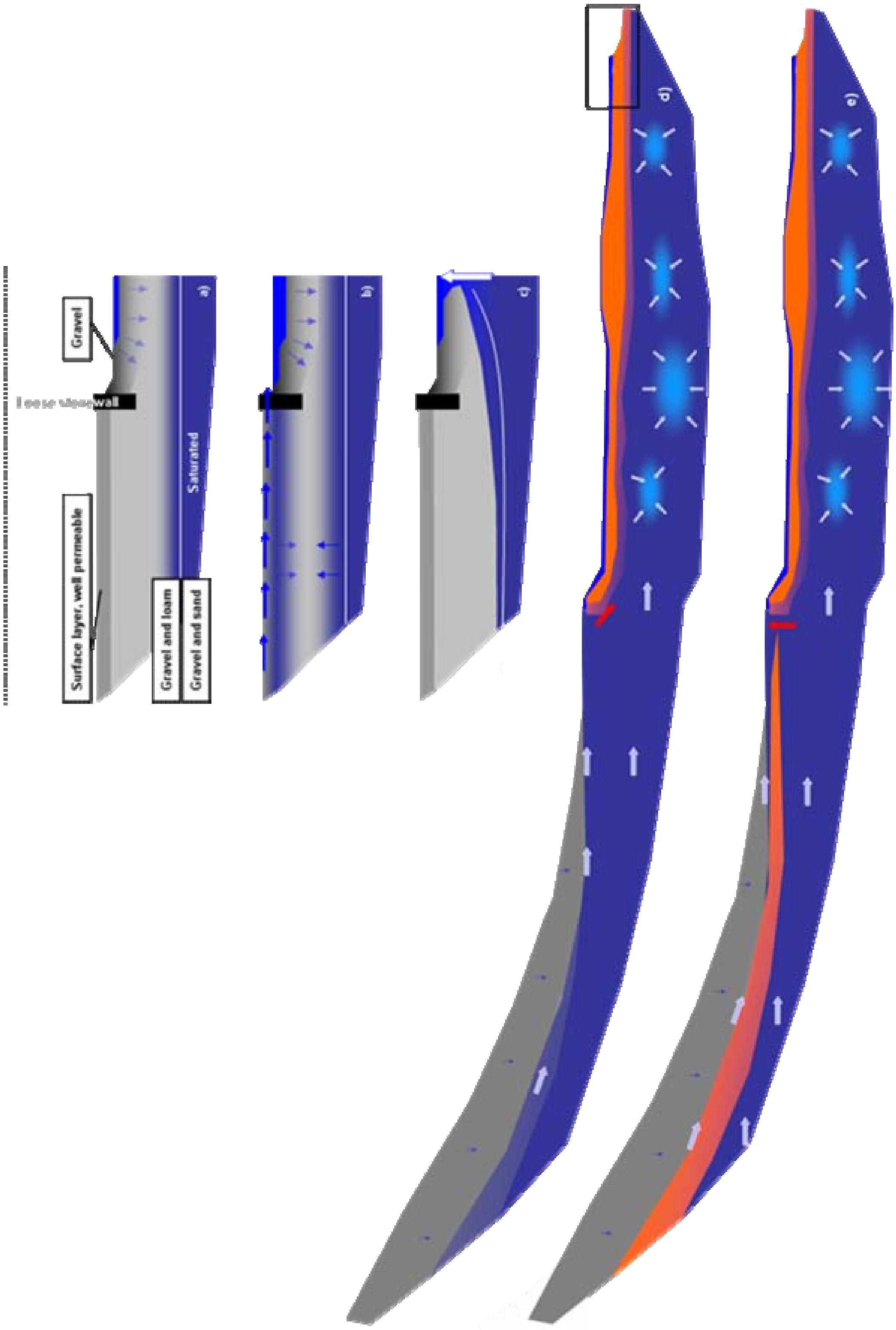

Figure 6.2: Hillslope concept based on ERT results together with the concept of possible stream – groundwater interaction in the research area. a) Dry conditions. b) Wet conditions. c) Dry conditions. The confining gravel and loam layer has a weak spot d) Groundwater is not confined at the hillslope but becomes confined at the interface to the valley bottom's filling. e) The more impervious layer reaches over the whole profile length, confining the deeper aquifer with a weak spot at the slope – valley bottom interface.

Two processes could account for the fact that the stream – groundwater interface is not notably coupled. Firstly, the stream possibly eroded into a layer of poor hydraulic conductivity and therefore only small amounts of water may be exchanged. Secondly, particles transported in the water could clog pore space in the hyporheic zone. This effect can be compared to the clogging observed at artificial drainage pipes and is more likely to occur when shifts in the direction of the flow in or out of the stream are rare.

Both theories are probable and may exist in parallel, although the second one describes a more dynamic situation where conditions may change in the cause of extreme events or in the case of changes in solute transport (e.g. deforestation).

The two hillslope concepts displayed in Figure 6.2 d) and e) show two possible interpretations of the hillslope. Figure 6.2 d) shows a slope in which water can quickly infiltrate through the boulder field (grey), and then reaches the unconfined aquifer. In contrast, Figure 6.2 e) shows the confining layer spread over the total length of the profile but disturbed at the slope – valley bottom interface. Consequently, in d) water at the saturated area on top of the interface is not under pressure, whereas in the concept shown in e) water may be confined along the entire hillslope according to the prevailing conditions. Thus the saturated area would be fed by up-welling of groundwater under pressure supplied by deeper slope sediments or the fractured bedrock aquifer. During storm events additional water might be supplied from subsurface stormflow on top of the confining layer.

At the valley bottom, the water transported in the thin top layer (bright blue) comes almost exclusively from local precipitation (i.e. rare influence of deeper (pre-event water)). The upper layer (orange) almost always contains the borderline of the saturated zone and is influenced by local infiltration and deeper groundwater pressing upward from the deeper layer (dark blue). This deeper layer features better hydraulic conductivity and is the main water transporting structure in this concept. This determining part of the aquifer is characterised by a strong heterogeneity. Zones with possible higher transport capacities (light blue) drain the surrounding subsurface. In these structures, the

flow is directed straight down the valley and may stay under the surface until a barrier is reached or the structures transport capacity is exceeded.
If these structures prove to be connected over longer distances, they form an efficient subsurface drainage network fulfilling a function comparable to that of the stream network at the surface. The strong mixing of grains with different sizes in the study area might support a natural formation of such a subsurface network. Compared to well-sorted alluvial sediments, a displacement of single elements in the aquifer material is more probable. Another factor that makes space subsurface available (which is needed for any movement of particles) is the freezing and melting of water in the soil. This was the case during the Pleistocene.

The remarks about the hillslope concept promote the hypothesis that every catchment has a *core zone* in which more water is transported than anywhere else in the catchment, and which is the basins most important drainage. In process hydrology, only the river network is regarded as possible focus for the confluence of flowpaths. For example this is the case for hillslope concepts as introduced by DUNNE 1970a,b; KIRKBY 1978; BEVEN, 1986 and ANDERSON 1990, more or less transferred in other texts until today (BONELL, personal communication 2004). An exception is hydrology of Karst areas where other important drainage is recognized. However, the perched stream channel and the possible existence of a subsurface drainage system in the study area necessitate a re-evaluation of the general idea that the stream channel system is always the *core zone* of a region. A *core zone* could be more or less defined and show varying hydraulic properties; and thus it does not necessarily have to be the flowpath with a relatively free water movement like in a river. Properties may vary from one catchment to another as well as throughout a single catchment.

Applying this concept to the study site, the *core zone* would be the deeper aquifer part, in particular the natural drainage network. The stream channel at this site may more likely function as drainage to backwater from the actual *core zone* during big events, in addition to its constant base flow sources.

7 Final remarks and outlook

Throughout the study the site's groundwater table could not be identified. Reasons for this were the poor electrical conductivity of the groundwater and the small pore space in the layer in which the transition line between phreatic and vadose zone oscillates. Another focus of the study was the transformation from water at the hillslope to water in the valley bottom's aquifer. As the penetration depth of the electrical resistivity device (~16 to 22 m) was not sufficient to detect bedrock, only incomplete interpretation was possible. Knowledge about this lower limit would have provided the exact thickness of the sediments at the slope. However, the results give helpful information for further interpretation.

Connection among monitored variations in the subsurface material in a few meters depth could not be proven. However, a comprehensive picture of these apparent pathways could probably be obtained by increasing the ERT raster grid resolution from the applied 15 m to a much smaller distance between the individual profiles. Afterwards, with help of precise electrical resistivity images, piezometers could be placed both into and next to a possible drainage network. By this, possible effects on groundwater dynamics in these zones may be monitored.

The strong indication leading towards the idea of a perched stream at the research site needs to be studied upstream and downstream for possible confirmation. However, changes from influent to effluent conditions and vice versa could be explained with the varying incline of the stream channel (pools and riffles) as opposed to a rather continuous descent of the groundwater level. The low hydraulic conductivity of the interface stream water – groundwater seems to be more related to the genesis of the valley. Due to the fact that the stream is using a valley that was previously formed by glaciers, the stream is not in close contact with the bedrock surface, but flowing on top of the glacial sediments. A comparison the stream, which is two to three meters wide and roughly 20 cm deep, with the valley bottom's filling, which is 150 m wide at the surface and an assumed to be 25 m deep in its middle, gives rise to the assumption that groundwater could be capable of transporting most of the basin's water down the valley in more or less distinct flowpaths. A comparative study in catchments of different morphology (concave and convex valleys) might show a general connection between the role a stream is playing in a catchment's hydrology and the way the basin's form developed.

Although choosing the correct of several possible interpretations of the electrical resistivity imagery was difficult and remains unproved in some cases due to missing information about any material deeper than two meters, the hydrological perception of the research site advanced greatly. It could be shown that the use of ERT is not necessarily bound to availability of other geophysical or borehole data. Instead, a broad geological and hydrological background of an area may already bring about interesting results. The combination with tracer methods may even provide proof of some assumptions and supply additional temporal (e.g. residence times) and spatial (e.g. probable flowpath) information. Using ERT and tracer data technology enables to gain information on an area's hydrology without disturbing the subsurface. Thus, both are valuable instruments for learning about contexts in nature. Additionally, the applied techniques do not require comprehensive time-series on runoff and precipitation or similar. Of course, geological borehole data and an extensive observational network facilitate the accurate description of the encountered hydrology and geology. Further, each supplementary technique yields its own benefits and adds to a detailed picture of the hydrological processes.
However, depending on the prevailing conditions and general geological assessment of a region, a single field campaign with tracer methods and electrical resistivity tomography complementing one another can greatly enhance the understanding of a basin's hydrology. In particular, this means that possible links between different hydrological structures (e.g. subsurface layers, stream channels, saturated areas and possible natural drainage) can be assessed more easily. This contributes to the capabilities of process-oriented modeling – even in ungauged catchments.

References

ANDERSON, M. G. and BURT, T. P., 1990. *Process Sudies in Hillslope Hydrology.* Wiley, Chichester, UK. 539pp.

BEVEN, K. J., 1986. Runoff production and flood frequency in catchments of order n: an alternative approach. In: *Scales Problems in Hydrology*, V.K. Gupta, I. Rodriguez-Iturbe and E. F. Wood (eds), Reidel, Dordrecht, The Netherlands. 107–131.

BONELL, M., 2004a. Runoff generation in tropical Forests. In*: Forests, Water and People in the Humid Tropics*, M. Bonell and L. A. Bruijnzeel (eds), UNESCO-Cambridge University Press, Cambridge, UK.

BONELL, M., 2004b. personal communication, UNESCO, Paris, France.

BORUS, H., 1999. *Einsatz geophysikalischer Meßverfahren zur Abschätzung der hydraulischen Durchlässigkeit tonhaltiger Sedimente - ein Beitrag zum Grundwasserschutz.* Dissertation zur Erlangung des Doktorgrades an der Mathematisch-Naturwissenschaftlichen Fakultät der Christian-Albrechts-Universität Kiel.

CARDIMONA, S., 2002. *Electrical resistivity techniques for subsurface investigation.* Department of Geology and Geophysics, University of Missouri-Rolla, Rolla, MO, U.S.A..

CHORLEY, R. J., 1978. Glossary of terms. In: *Hillslope Hydrology*, M. J. Kirkby (ed.), Wiley, Chichester, UK. 365–375.

DAMIATA, B., 2001. Assessment of the Skagafjörjur Archaeological Settlement Survey. Cotsen Institute of Archaeology, UCLA, CA, U.S.A.. http://sass.ioa.ucla.edu /2001.

DUNNE, T. and BLACK, R. D., 1970a. An experimental investigation of runoff production in permeable soils. *Wat. Resour. Res.,* 6: 179–191.

DUNNE, T. and BLACK, R. D., 1970b. Partial area contributions to storm runoff in a small New England watershed. *Wat. Resour. Res.*, 6: 1269–1311.

FRIEG, B., 1987. *Hydrologie und Grundwasserhydraulic des Einzugsgebietes des Wasserwerkes Freiburg-Ebnet.* Heidelberg, Univ., Diss., 1987.

HERMAN, R., 2001. An introduction to electrical resistivity in geophysics, *Am. J. Phys.* 69 (9): 943-952.

HORTON, R. E., 1933. The role of infiltration in the hydrological cycle. *Trans. Amer. Geophys. Union* 14: 446–460.

HORTON, R. E., 1945. Erosional development of streams and their drainage basins: Hydrological approach to quantitative morphology. *Bull. Geol. Soc. Amer.,* 56: 275–370.

KIENZLER, P. M., 2001. *Experimentelle Untersuchungen zur chemischen Zusammensetzung oberflächennaher unterirdischer Abflusskomponenten im Bruggaeinzugsgebiet.* Diplomarbeit am Institut für Hydrologie der Universität Freiburg i. Br. (unveröffentlicht).

KIRKBY, M. J. (ed.), 1978. *Hillslope Hydrology*. Wiley, Chichester, UK. 389pp.

KOCH, W., 2004. personal communication, KOSOLCO, Dinkelsbühl, Germany.

LOKE, M. H., 2000. Electrical imaging surveys for environmental and engineering studies - A practical guide to 2-D and 3-D surveys. www.geoelctrical.com.

MARION, D., NUR, A., YIN, H., and HAN, D., 1992. Compressional velocity and porosity in sand-clay mixtures. *Geophysics*, 57, 554–563.

REKLIP, 1995. *Klimaatlas Oberrhein Mitte-Süd, Atlas Climatique du Fossé Rhénana Méridional*. Zürich-Offenbach-Strasbourg.

SCHACHTSCHABEL, P., *et al.,* 2002. *Lehrbuch der Bodenkunde*. Spektrum Akademischer Verlag, Heidelberg, Berlin.

SCHEIDLER, S., 2002. *Experimentelle Untersuchung zur Grundwasserdynamik im Hang-/Talaquifer-System des St.Wilhelmer Talbachs (Südschwarzwald).* Diplomarbeit am Institut für Hydrologie der Universität Freiburg i. Br. (unveröffentlicht).

UHLENBROOK S., und LEIBUNDGUT, Ch., 1997. *Abflussbildung bei Hochwasser*. Wasser und Boden, 9, 13-22.

UHLENBROOK, S., 1999. *Untersuchung und Modellierung der Abflussbildung in einem mesoskaligen Einzugsgebiet* (Investigating and modelling of the runoff generation in a mesoscaled catchment; in German). Freiburger Schriften zur Hydrologie, Band 10, Institute of Hydrology, University of Freiburg, Germany.

UHLENBROOK, S., 2004. personal communication, Institute of Hydrology, University of Freiburg, Germany.

VOGEL, H., 1995. *Gerthsen Physik*. Springer Verlag, Berlin, Heidelberg.

WENNINGER, J., 2002. *Experimentelle Untersuchung zur Dynamik von Hanggrundwasser und dessen Übertritt in die Talaue und den Vorfluter im Bruggaeinzugsgebiet* (Experimental investigation of hillslope groundwater and its flow into a floodplain and the channel at the Brugga basin; in Germany). Diploma thesis, Universität Freiburg i. Br., Institute of Hydrology, Freiburg i.Br., Germany (unpublished).

ZHOU, W., BECK, B. F. and STEPHENSON, J. B., 2000. *Reliability of dipol-dipol electrical resistivity tomography for defining depth to bedrock in covered karst terranes*.Environmental Geology Springer Verlag, 39 (7).

ZHOU, W., BECK, B. F. and ADAMS, A. L., 2002. *Effective electrode array in mapping karst hazards in electrical resistivity tomography.* Environmental Geology Springer Verlag, 42: 922-928.

Appendix

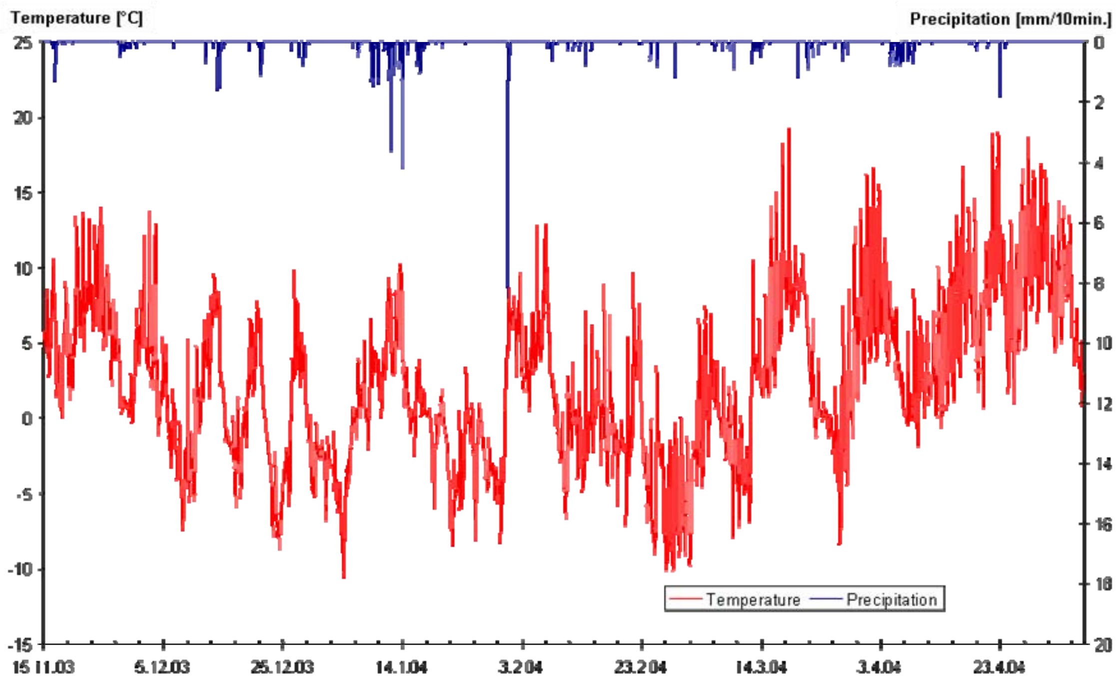

Figure A 1: Temperature and precipitation data from the *Katzensteig* meteorologic station.

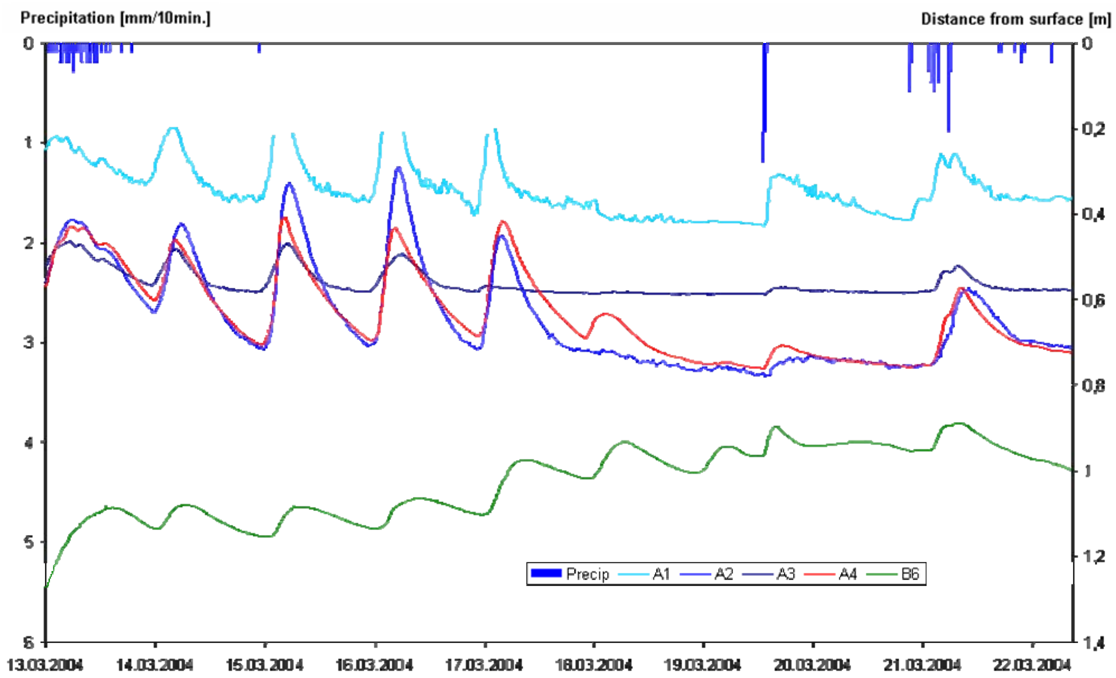

Figure A 2: Reaction in groundwater monitoring holes to a snowmelt event in March 2004.

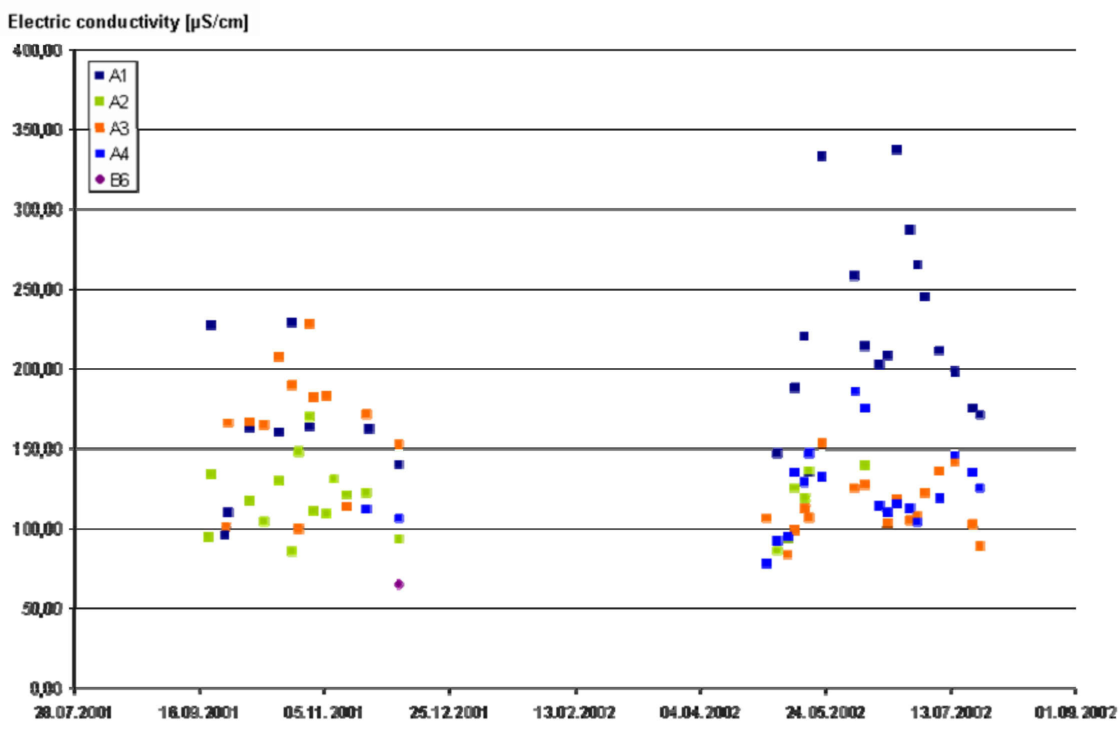

Figure A 3: Electrical conductivity in the groundwater monitoring holes recorded by WENNINGER (2002) and SCHEIDLER (2002).

SYSCAL Kid *Switch-24*

MAJOR BENEFITS

- Attractive output parameters:
  - 200 V maximum voltage,
  - 25 W maximum power,
  - 500 mA maximum current
- Automatic fixing of the output voltage in relation with the level of the measured signal.
- Accuracy on resistivity: 1%.
- Quality control of the measurement through standard deviation and number of stacks.
- Display of measured voltage, intensity of current, apparent resistivity, and self potential.
- Serial link for transfer to PC.

ELECTRODE STRING

Made of heavy duty cable, the 12 take-out string cables are available with standard 1 or 3 meters electrode spacings. The 3 meters version is 40 m long and weights 2.5 kg. Other configuration can be made on request.

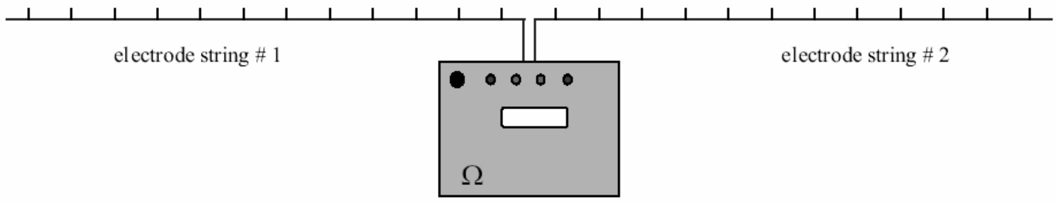

Supported arrays: pole-pole, pole-dipole, dipole-dipole and Wenner profiling

GENERAL SPECIFICATIONS

specifications subject to change

- LCD display: 4 lines of 20 characters
- Keypad: 6 functions keys
- Operating temperature range: -10 to +50 °C
- Internal rechargeable battery: 12V, 6.5 Ah with autonomy of 3000 readings typical.
- Internal memory for 1400 stations with full readings: self-potential, voltage, current, resistivity
- Dimensions: 23 x 18 x 23 cm
- Weight: 4.8 kg

TRANSMITTER

- Automatic current setting
- Output voltage: up to 200 V
- Output current: up to 500 mA
- Output power: up to 25 W
- Optional external 12V battery input
- Cycle time: 0.5, 1 or 2 s

RECEIVER

- Resistivity computation
- Automatic ranging
- SP compensation including linear drift
- Digital stacking for noise reduction
- Input voltage: protection up to 200 V, range from - 2.5 V to +2.5 V
- Input impedance: 22 MΩ
- Resistivity range: 10^{-3} to 10^{+5} Ω.m
- Resistivity precision: 1 % typical

IRIS instruments

IRIS Instruments - 1 avenue Buffon, B.P. 6007, 45060 Orléans Cedex 2, France
Phone: + 33 (0) 2 38 63 81 00 - Fax: + 33 (0) 2 38 63 81 82 - E-mail: irisins@attglobal.net
Web site: www.iris-instruments.com

Figure A 4: Technical data sheet of the electrical resistivity measuring device used in the study.

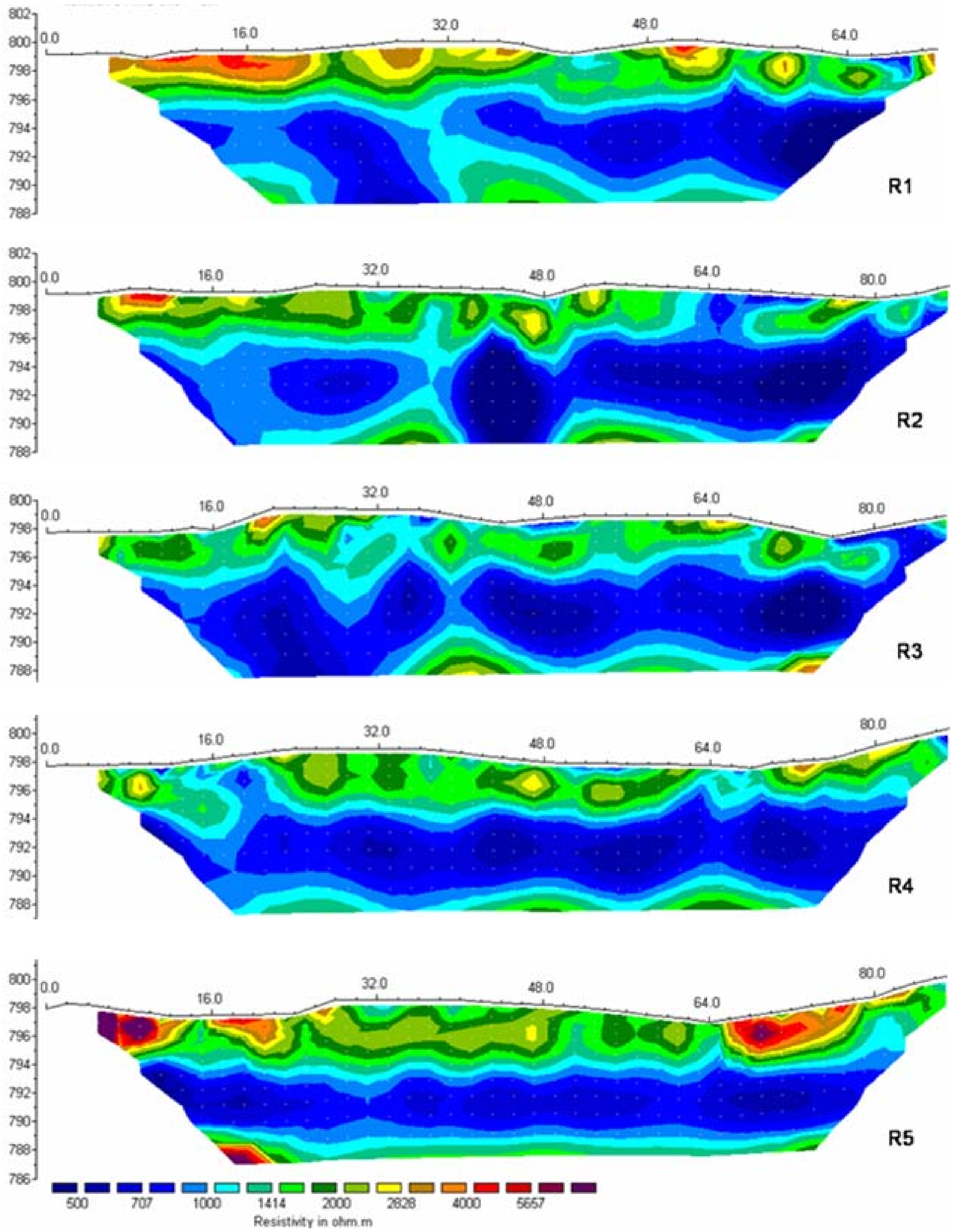

Figure A 5: Electrical resistivity images from the raster survey (R1 – R5).

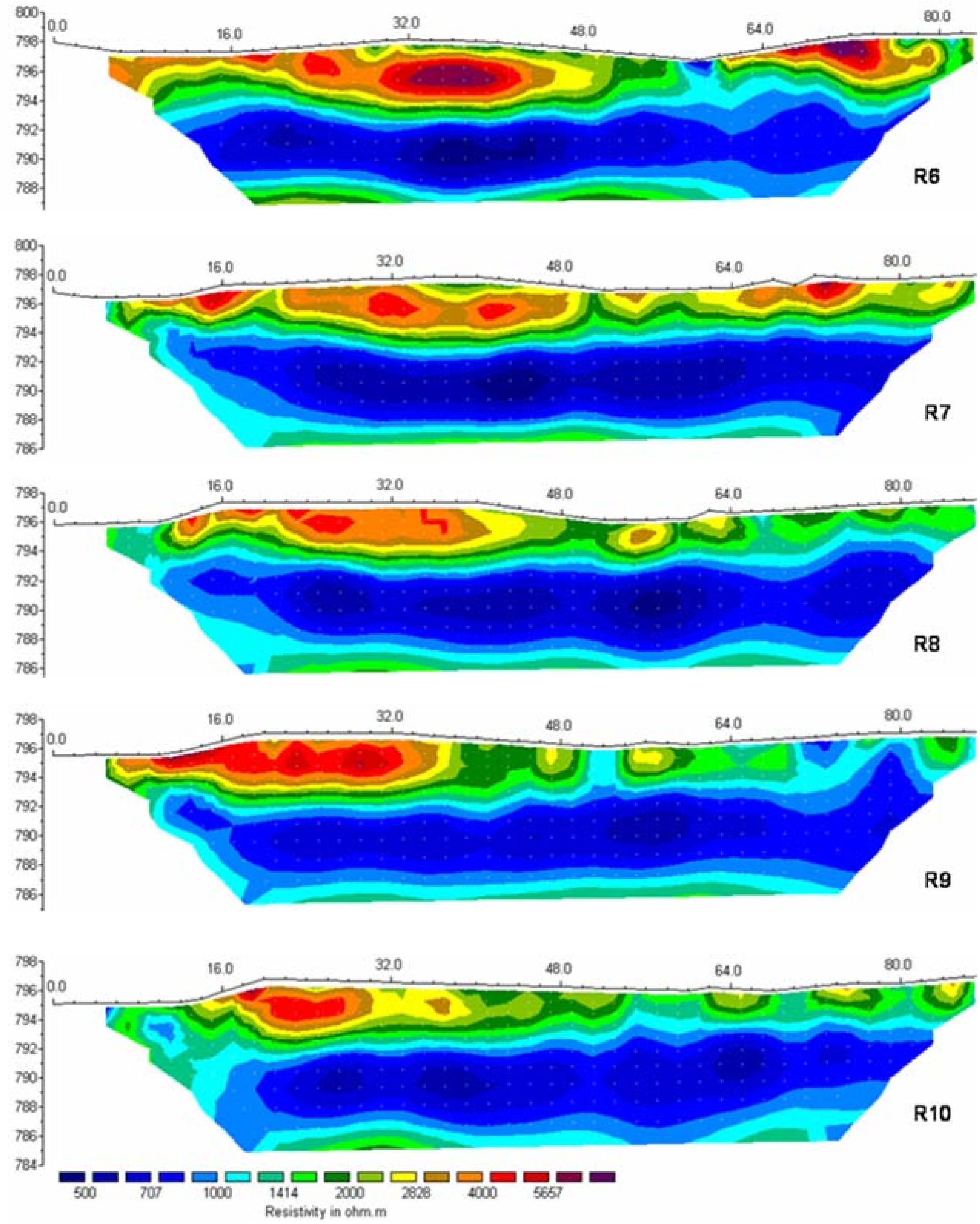

Figure A 6: Electrical resistivity images from the raster survey (R6 – R10).

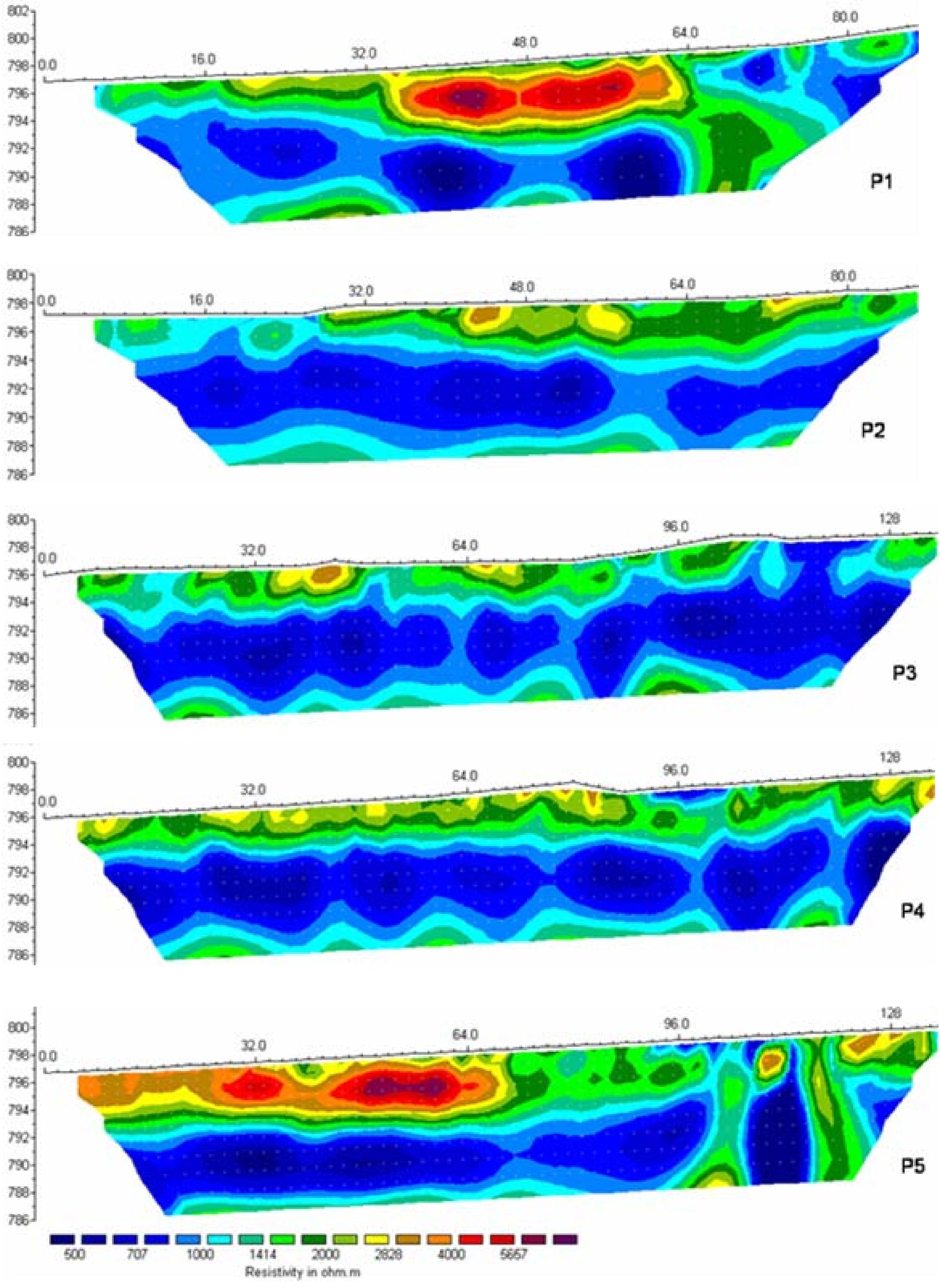

Figure A 7: Electrical resistivity images from the raster survey (P1 – P5).

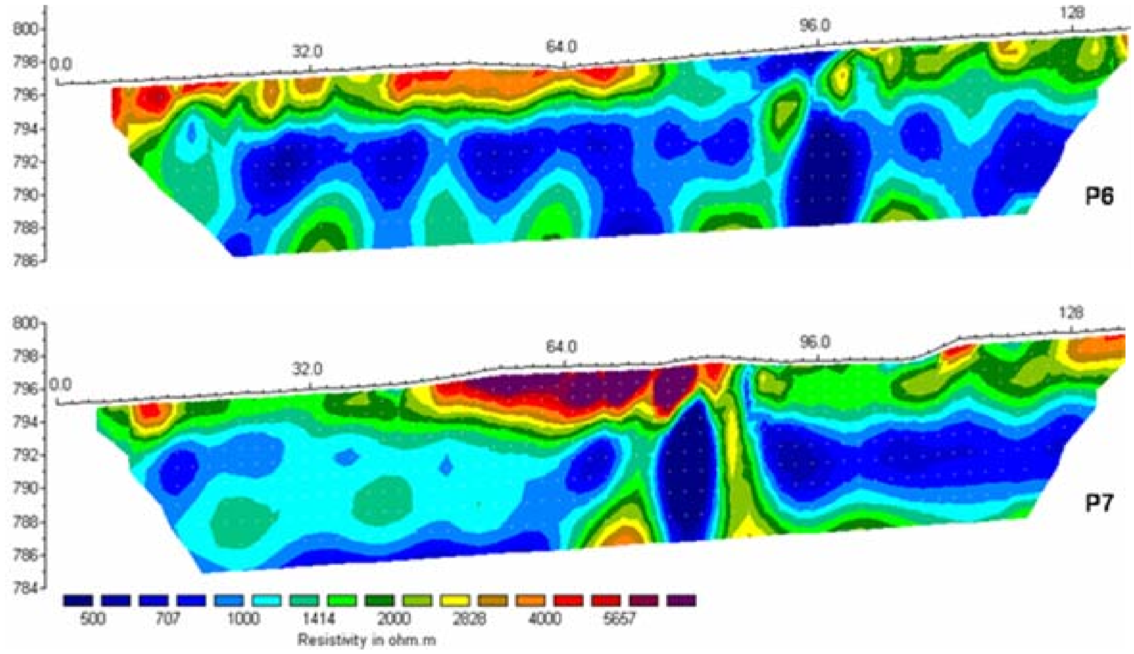

Figure A 8: Electrical resistivity images from the raster survey (P6, P7).

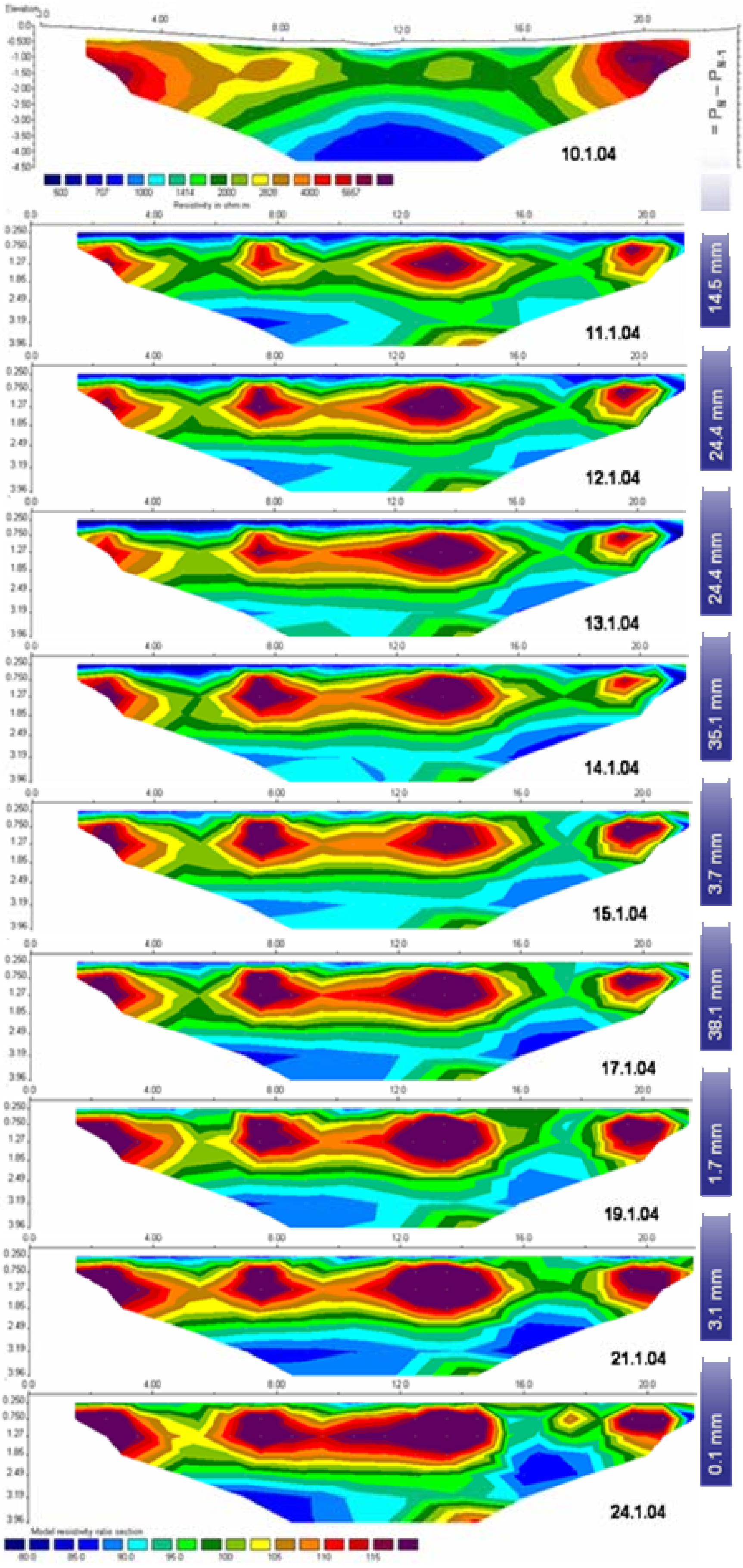

Figure A 9: Time-lapse model calculated with the sequential inversion method.